Theoretical analysis of spin current induced in cold atoms with artificial spin-orbit coupling

人工スピン軌道相互作用を持つ冷却原子系で誘起されるスピン流に対する理論的解析

Department of Physics,
Graduate School of Science and Engineering,
Tokyo Metropolitan University

Ryohei Sakamoto

2019

Abstract

Atomtronics, a technique to control atoms for an application of devices, has been studied in recent years. The purpose of this thesis is to propose a novel method to control atoms for the application to the atomtronics. To achieve this purpose, we use a spin current in a spin-orbit (SO) coupled cold atoms. The spin current, that is a counterflow of particles with different spins, has attracted attention as a method to control electrons. On the other hand, the artificial SO coupled cold atoms were experimentally realized in 2011 and have been studied theoretically and experimentally. We can expect that a spin current can be formed in the SO coupled cold atoms because the SO coupling is known to induce a spin current and controlled because the cold atoms have various experimentally controllable parameters. However, little has been studied so far on the spin current in the cold atom. Therefore, we studied novel controllability of the spin current in the SO coupled cold atom.

An SO coupled Bose-Einstein condensate (BEC) was experimentally realized in 2011 and then an SO coupled degenerate fermions became available in 2012. In these systems, since the SO coupling was engineered in a neutral atom by dressing two atomic spin states with a pair of Raman lasers and an external magnetic field, it is called artificial SO coupling. In addition, some parameters such as intensity of the SO coupling can be experimentally tuned by the lasers and the external magnetic field in the artificial SO coupled cold atoms. Therefore, by investigating parameter dependence of the spin currents, we reveal controllability of the atoms in the artificial SO coupled Bose and Fermi systems. As a result, in the SO coupled Bose system, the spin current changes discontinuously and non-smoothly across the phase boundaries, while in the SO coupled Fermi system, the spin current changes continuously and smoothly at zero temperature.

On the other hand, Bose-Fermi mixture was experimentally realized and have been studied from different viewpoints. Therefore, we can expect to realize an artificial SO coupled Bose-Fermi mixture in near future. In this system, since atoms of different quantum statistics coexist under an influence of the SO coupling, novel phenomena can be expected. Based on these ideas, we investigate a ground state and a spin current in a mixture of fermions and SO coupled bosons. The ground states are calculated in the SO coupled Bose-Fermi mixture with high density or low density of the atoms by using a variational method and some approximations such as tight-binding approximation. For the high density, the fermions have a large influence on the Bose system, while, for the low density, the fermions have little influence although the relative amounts of the bosons and the fermions are comparable in the two cases. In addition, we show that the spin current of the

fermions changes discontinuously and non-smoothly across the phase boundaries of the bosons.

Contents

Chapter 1

Introduction

Atoms trapped and cooled in ultra-low temperature is called cold atom. Cold atom can be experimentally realized and exhibit a variety of quantum phenomena. One of useful features of the cold atoms is controllability of physical parameters including interaction strength between the atoms[1, 2]. Taking advantage of the features, we can create various interesting atom systems. Particularly, in 2011, a spin-orbit (SO) coupled Bose-Einstein condensate (BEC) was experimentally realized[3] and then an SO coupled degenerate fermions became available[4, 5]. In these experiments, SO coupling was engineered in a neutral atom by dressing two atomic spin states with a pair of lasers and it is called artificial SO coupling. To explore rich properties of SO coupled BECs and degenerate Fermi gases, the SO coupled cold atoms have been studied theoretically and experimentally[6, 7, 8, 9, 10, 11, 12, 13, 14, 15, 16, 17, 18, 19, 20, 21, 22, 23, 24, 25, 26, 27]. In addition, another effort was made for simultaneous cooling of bosonic and fermionic atoms[28, 29]. The mixture systems where atoms of different quantum statistics coexist could have a variety of aspects and have been studied from different viewpoints[30, 31, 32, 33, 34].

On the other hand, atomtronics, the study of atomic transport phenomena for the application to devices, has attracted attention[35, 36, 37, 38]. In the atomtronics, a realization of a novel device unlike electronics can be expected because electrons, that is used in electronics, are Fermi particles with charge whereas atoms, that is used in atomtronics, are neutral Fermi or Bose particles. In our study, to propose a novel method to control atoms, we focus on a spin current. Spin current is generally defined as a counterflow of particles with different spins and various methods to induce and control a spin current, that is called spintronics, have been proposed[39, 40, 41, 42, 43, 44, 45, 46, 47, 48, 49, 50]. Since it is known that spin current is induced by SO coupling, we can expect that atoms can be controlled by spin current in the SO coupled cold atoms.

In this thesis, we investigate the ground state and the spin current in the three types of artificial SO coupled cold atoms. The original results are to show the ground state phase diagram in the SO coupled Bose-Fermi mixture and the controllability

of the spin current in the SO coupled cold atoms. In the following chapters, we first derive the definition of a spin current and review the experimental method to realize the artificial SO coupled cold atom. Afterwards, we show the ground states and spin currents in the artificial SO coupled Bose system, the artificial SO coupled Fermi system, and the artificial SO coupled Bose-Fermi mixture, respectively. The details are shown in the followings.

As a ready to analyze a spin current, in Chap. 2, we show the properties of particle and spin currents in the system with an arbitrary magnetic field and SO coupling. To define particle and spin currents, we first derive the conservation laws of particle and spin from U(1) and SU(2) symmetry. Next, we consider the effect of a magnetic field and SO coupling on the currents. In the latter half, the relation between the currents and an unitary transformation and the condition to induce currents are shown.

In order to experimentally create SO coupling in a cold atom, it is necessary to tune parameters in the cold atom with artificial gauge field[51]. Therefore, in Chap. 3, we review the experimental method to realize the cold atoms with artificial gauge field and artificial SO coupling, respectively. In addition, we show that the intensities of the SO coupling and effective magnetic field can be controlled by the external lasers and magnetic field in the artificial SO coupled cold atoms.

Based on the above chapters, in Chaps. 4, we discuss an artificial SO coupled Bose system. As a first step, we analyze a non-interacting Bose system where all the bosons behave as a single-particle. The ground state of the interacting Bose system have been investigated in the previous studies by using a variational method[8, 9, 10, 11, 15]. Therefore, we review the method to obtain the ground state phase diagram and show the ground state phase diagram and the spin current of the bosons.

In the next chapter, we show the ground state and the spin current in the artificial SO coupled Fermi system without the interaction. As a result, we can see that the ground state is classified by the difference of Fermi sphere and that the spin current of the fermions has a characteristic property unlike that of the bosons. In addition, we investigate the effect of the weak interaction on the Fermi system and show that it is negligible.

In Chap. 6, we consider the mixture of fermions and SO coupled bosons and show the ground state phase diagram and the spin current of the fermions. Since the SO coupled Bose-Fermi mixture is a novel system that had not been studied, all results in this chapter are original. We analyze the ground states of the bosons in the Bose-Fermi mixture without and with Bose-Fermi spin interaction by using the variational method same as in Chap. 4 and some approximations. In addition, the spin current of the fermions can be calculated in the same way as in Chap. 5 in the Bose-Fermi mixture with Bose-Fermi spin interaction. Finally, in Chap. 7, we conclude above results.

Chapter 2

Spin current

Spin current is a counterflow of particles with different spins. Recently, spintronics, the study of spin-dependent electron transport phenomena in solid-state materials, has attracted attention[39, 40, 41, 42, 43] and various methods to induce and control a spin current have been proposed[44, 45, 46, 47, 48, 49, 50].

In this chapter, as a ready for the following chapters, we discuss the properties of currents induced in the system of spin-1/2 particles with a magnetic field (Zeeman effect) and spin-orbit (SO) coupling. By using the invariance of Lagrangian, in Sec. 2.1, we derive the conservation law of particle and show the effect of a magnetic field and SO coupling on the conservation law. In the next section, we derive the (non-)conservation law of spin in the same way and define the spin current. Since the definitions of the particle and spin currents are changed by a unitary transformation of the wave function, we show the relation between the currents and the unitary transformation in Sec. 2.3. Finally, in Sec. 2.4, we analyze the properties of particle and spin currents and show the conditions that the currents are induced.

2.1 Conservation law of particle and particle current

Let us consider the system of spin-1/2 particles with a magnetic field (Zeeman effect) and SO coupling. The Lagrangian is given by

$$
\begin{aligned}
L &= L_0 + L_B + L_{\rm so}, && (2.1)\\
L_0 &= \int d\boldsymbol{r} \left\{ \psi^\dagger(\boldsymbol{r},t) \left[i\hbar\frac{\partial}{\partial t} - \frac{\hbar^2\nabla^2}{2m} + \mu \right] \psi(\boldsymbol{r},t) \right\}, && (2.2)\\
L_B &= \int d\boldsymbol{r} \left\{ \psi^\dagger(\boldsymbol{r},t) \left[\boldsymbol{B}(\boldsymbol{r}) \cdot \boldsymbol{\sigma} \right] \psi(\boldsymbol{r},t) \right\}, && (2.3)\\
L_{\rm so} &= \int d\boldsymbol{r} \left\{ \psi^\dagger(\boldsymbol{r},t) \left[\boldsymbol{B}_{\rm so} \cdot \boldsymbol{\sigma} \right] \psi(\boldsymbol{r},t) \right\}, && (2.4)
\end{aligned}
$$

where $\psi(\boldsymbol{r},t)$ is the field operator, m is the mass of particles, $\boldsymbol{\sigma} = (\sigma_x, \sigma_y, \sigma_z)$ is 2×2 Pauli matrix, and ∇ indicates the gradient with respect to $\boldsymbol{r}$. In Eqs. (2.3)

and (2.4), $\boldsymbol{B}(\boldsymbol{r})$ is an arbitrary magnetic field and $\boldsymbol{B}_{\rm so} = (B_{{\rm so},x}, B_{{\rm so},y}, B_{{\rm so},z})$, where $B_{{\rm so},j} = \boldsymbol{a}_j \cdot (-i\hbar\nabla)$ and $\boldsymbol{a}_j = (a_{xj}, a_{yj}, a_{zj})$ is an arbitrary vector corresponding to a strength of SO coupling [1)]. In the following, we will derive the conservation law of particle from the rotational symmetry in the phase factor of the wave function of the system[43, 49].

2.1.1 Conservation law of particle

Firstly, we analyze the system without the magnetic field and SO coupling described by Eq. (2.2). Using scalar quantity $\varphi(\boldsymbol{r}, t)$ that is dependent on space-time, we consider the phase transformation of field operator

$$\psi(\boldsymbol{r}, t) \to e^{i\varphi(\boldsymbol{r},t)}\psi(\boldsymbol{r}, t), \quad \psi^\dagger(\boldsymbol{r}, t) \to \psi^\dagger(\boldsymbol{r}, t)e^{-i\varphi(\boldsymbol{r},t)}. \tag{2.5}$$

By substituting this field operator into Eq. (2.2), the Lagrangian is converted into

$$\begin{aligned} L_0 \to L_0 + \int d\boldsymbol{r} \Bigg\{ & \psi^\dagger \left[-\hbar \frac{\partial \varphi}{\partial t} \right] \psi \\ & + \frac{i\hbar^2}{2m} \Big(\left[\left(\nabla \psi^\dagger \right) \psi - \psi^\dagger \left(\nabla \psi \right) \right] \cdot \left(\nabla \varphi \right) + \psi^\dagger \psi \left(\nabla \varphi \right)^2 \Big) \Bigg\}. \end{aligned} \tag{2.6}$$

When the phase φ is differentiable and a single-valued function of space-time, the original Lagrangian and the converted Lagrangian must describe the same physical phenomenon. Therefore, the first-order term of φ in Eq. (2.6) must be zero. This means that the variation of the action $\delta S_0 = \delta \int_{-\infty}^{\infty} dt L_0$ satisfies the following equation:

$$\begin{aligned} \delta S_0 &= \int_{-\infty}^{\infty} dt \int d\boldsymbol{r} \left\{ -\hbar \psi^\dagger \left[\frac{\partial \varphi}{\partial t} \right] \psi + \frac{i\hbar^2}{2m} \Big(\left[\left(\nabla \psi^\dagger \right) \psi - \psi^\dagger \left(\nabla \psi \right) \right] \cdot \left(\nabla \varphi \right) \Big) \right\} \\ &= \hbar \int_{-\infty}^{\infty} dt \int d\boldsymbol{r} \left\{ \left[\frac{\partial \left(\psi^\dagger \psi \right)}{\partial t} - \nabla \cdot \frac{i\hbar}{2m} \left[\left(\nabla \psi^\dagger \right) \psi - \psi^\dagger \left(\nabla \psi \right) \right] \right] \varphi \right\} \\ &= \hbar \int_{-\infty}^{\infty} dt \int d\boldsymbol{r} \left\{ \left[\frac{\partial \rho}{\partial t} + \nabla \cdot \boldsymbol{j} \right] \varphi \right\} = 0. \end{aligned} \tag{2.7}$$

From this equation, we can obtain the conservation law of particle

$$\frac{\partial \rho}{\partial t} + \nabla \cdot \boldsymbol{j} = 0, \tag{2.8}$$

[1)] The SO coupling term in Eq. (2.4) can be written as

$$\boldsymbol{B}_{\rm so} \cdot \boldsymbol{\sigma} = \begin{pmatrix} p_x & p_y & p_z \end{pmatrix} \begin{pmatrix} a_{xx} & a_{xy} & a_{xz} \\ a_{yx} & a_{yy} & a_{yz} \\ a_{zx} & a_{zy} & a_{zz} \end{pmatrix} \begin{pmatrix} \sigma_x \\ \sigma_y \\ \sigma_z \end{pmatrix},$$

where $\boldsymbol{p} = -i\hbar\nabla$.

where

$$\rho = \psi^\dagger \psi \quad \text{and} \quad \boldsymbol{j} = -\frac{i\hbar}{2m}\left[\left(\nabla\psi^\dagger\right)\psi - \psi^\dagger\left(\nabla\psi\right)\right] \tag{2.9}$$

are the number density of particle and the particle current density, respectively.

2.1.2 Particle current in the system with a magnetic field and SO coupling

Calculating the variation of the actions obtained from Eqs. (2.3) and (2.4) under the phase transformation (2.5), we analyze the effect of the magnetic field and SO coupling on the conservation law of particle (2.8).

Firstly, since the magnetic field term $\boldsymbol{B}(\boldsymbol{r})\cdot\boldsymbol{\sigma}$ in Eq. (2.3) commute the scalar quantity $\varphi(\boldsymbol{r},t)$ in the phase transformation, the magnetic field does not affect the conservation law of particle.

Secondly, by using the phase transformation (2.5), Eq. (2.4) is converted into

$$L_{\rm so} \to L_{\rm so} + \int d\boldsymbol{r}\left\{\psi^\dagger\left[\sum_{i,j=x,y,z} a_{ij}\left(\hbar\partial_i\varphi\right)\sigma_j\right]\psi\right\}, \tag{2.10}$$

where we use the relation $e^{-i\varphi}p_i e^{i\varphi} = p_i + \hbar\partial_i\varphi$. Thus, the variation of the action of the SO coupling term can be written as

$$\begin{aligned}
\delta S_{\rm so} &= \hbar\int_{-\infty}^{\infty} dt\int d\boldsymbol{r}\left\{\psi^\dagger\left[\sum_{i,j=x,y,z} a_{ij}\left(\partial_i\varphi\right)\sigma_j\right]\psi\right\} \\
&= \hbar\int_{-\infty}^{\infty} dt\int d\boldsymbol{r}\left\{\nabla\cdot\left[-\sum_{i,j=x,y,z} a_{ij}\psi^\dagger\sigma_j\psi\boldsymbol{e}_i\right]\varphi\right\}, \\
&= \hbar\int_{-\infty}^{\infty} dt\int d\boldsymbol{r}\left[\left(\nabla\cdot\boldsymbol{j}_{\rm so}\right)\varphi\right],
\end{aligned} \tag{2.11}$$

where $\boldsymbol{e}_i$ is the unit vector in the direction i and we used integration by parts. Consequently, from Eqs. (2.7) and (2.11), we can obtain the modified conservation law

$$\frac{\partial\rho}{\partial t} + \nabla\cdot\left(\boldsymbol{j} + \boldsymbol{j}_{\rm so}\right) = 0, \tag{2.12}$$

$$\rho = \psi^\dagger\psi, \quad \boldsymbol{j} = -\frac{i\hbar}{2m}\left[\left(\nabla\psi^\dagger\right)\psi - \psi^\dagger\left(\nabla\psi\right)\right], \quad \boldsymbol{j}_{\rm so} = -\sum_{i=x,y,z}\boldsymbol{e}_i(\boldsymbol{a}_i\cdot\boldsymbol{s}), \tag{2.13}$$

where $\boldsymbol{s} = \psi^\dagger\boldsymbol{\sigma}\psi$ is the spin density. Equation (2.12) shows that SO coupling induces the particle current $\boldsymbol{j}_{\rm so}$ and the total particle current $\boldsymbol{j}+\boldsymbol{j}_{\rm so}$ is a conservative quantity.

2.2 Conservation law of spin and spin current

In the above section, we derived the conservation law of particle by using the phase transformation (2.5) with the scalar quantity $\varphi(\boldsymbol{r},t)$. In this section, we use the phase transformation with a three-component vector $\boldsymbol{\phi}(\boldsymbol{r},t)$

$$\psi(\boldsymbol{r},t)\to e^{i\boldsymbol{\phi}(\boldsymbol{r},t)\cdot\boldsymbol{\sigma}}\psi(\boldsymbol{r},t),\quad \psi^{\dagger}(\boldsymbol{r},t)\to\psi^{\dagger}(\boldsymbol{r},t)e^{-i\boldsymbol{\phi}(\boldsymbol{r},t)\cdot\boldsymbol{\sigma}}, \tag{2.14}$$

and derive the conservation law of spin and show that the magnetic field and the SO coupling break this conservation law.

2.2.1 Conservation law of spin

By using the phase transformation (2.14), the Lagrangian (2.2) is converted into

$$\begin{aligned} L_0\to L_0+\int d\boldsymbol{r}\Bigg\{&\psi^{\dagger}\left[-\hbar\frac{\partial\left(\boldsymbol{\phi}\cdot\boldsymbol{\sigma}\right)}{\partial t}\right]\psi \\ &+\frac{i\hbar^2}{2m}\Big(\left[\left(\nabla\psi^{\dagger}\right)\cdot\left(\nabla\boldsymbol{\phi}\cdot\boldsymbol{\sigma}\right)\psi-\psi^{\dagger}\left(\nabla\boldsymbol{\phi}\cdot\boldsymbol{\sigma}\right)\cdot\left(\nabla\psi\right)\right]+\psi^{\dagger}\left(\nabla\boldsymbol{\phi}\cdot\boldsymbol{\sigma}\right)^2\psi\Big)\Bigg\}, \end{aligned} \tag{2.15}$$

When the phase $\boldsymbol{\phi}(\boldsymbol{r},t)$ is differentiable and a single-valued function of space-time, the variation of the action can be written as

$$\begin{aligned} \delta S_0 &= \hbar\int_{-\infty}^{\infty}dt\int d\boldsymbol{r} \\ &\quad\times\left\{-\psi^{\dagger}\left[\frac{\partial\left(\boldsymbol{\phi}\cdot\boldsymbol{\sigma}\right)}{\partial t}\right]\psi+\frac{i\hbar}{2m}\Big(\left[\left(\nabla\psi^{\dagger}\right)\cdot\left(\nabla\boldsymbol{\phi}\cdot\boldsymbol{\sigma}\right)\psi-\psi^{\dagger}\left(\nabla\boldsymbol{\phi}\cdot\boldsymbol{\sigma}\right)\cdot\left(\nabla\psi\right)\right]\Big)\right\} \\ &= \hbar\int_{-\infty}^{\infty}dt\int d\boldsymbol{r}\sum_{\alpha=x,y,z}\left\{\left[\frac{\partial\left(\psi^{\dagger}\sigma_{\alpha}\psi\right)}{\partial t}-\nabla\cdot\frac{i\hbar}{2m}\left[\left(\nabla\psi^{\dagger}\right)\sigma_{\alpha}\psi-\psi^{\dagger}\sigma_{\alpha}\left(\nabla\psi\right)\right]\right]\phi_{\alpha}\right\} \\ &= \hbar\int_{-\infty}^{\infty}dt\int d\boldsymbol{r}\sum_{\alpha=x,y,z}\left\{\left[\frac{\partial\rho_s^{\alpha}}{\partial t}+\nabla\cdot\boldsymbol{j}_s^{\alpha}\right]\phi_{\alpha}\right\}=0. \end{aligned} \tag{2.16}$$

Therefore we can obtain the conservation law of spin

$$\frac{\partial s_{\alpha}}{\partial t}+\nabla\cdot\boldsymbol{j}_s^{\alpha}=0, \tag{2.17}$$

where

$$s_{\alpha}=\psi^{\dagger}\sigma_{\alpha}\psi\ \text{ and }\ \boldsymbol{j}_s^{\alpha}=-\frac{i\hbar}{2m}\left[\left(\nabla\psi^{\dagger}\right)\sigma_{\alpha}\psi-\psi^{\dagger}\sigma_{\alpha}\left(\nabla\psi\right)\right] \tag{2.18}$$

are the spin density and the spin current density with spin α, respectively.

2.2.2 Spin current in the system with a magnetic field and SO coupling

Next, we consider the effect of the magnetic field and SO coupling on the conservation law of spin (2.17). Firstly, under the phase transformation (2.14), Eq. (2.3) is converted into

$$L_B \to \int d\boldsymbol{r} \left\{ \psi^\dagger \left[e^{-i\boldsymbol{\phi}\cdot\boldsymbol{\sigma}} \left[\boldsymbol{B}(\boldsymbol{r}) \cdot \boldsymbol{\sigma} \right] e^{i\boldsymbol{\phi}\cdot\sigma} \right] \psi \right\}. \tag{2.19}$$

Here, we can find

$$e^{-i\boldsymbol{\phi}\cdot\boldsymbol{\sigma}} \left[\boldsymbol{B}(\boldsymbol{r}) \cdot \boldsymbol{\sigma} \right] e^{i\boldsymbol{\phi}\cdot\sigma} = \boldsymbol{B}(\boldsymbol{r}) \cdot \boldsymbol{\sigma} + 2\boldsymbol{\phi} \cdot (\boldsymbol{B}(\boldsymbol{r}) \times \boldsymbol{\sigma}) + O(\phi^2),$$

from the relations $[\sigma_i, \sigma_j] = 2i \sum_{k=x,y,z} \epsilon_{ijk}\sigma_k$, $A \times B \cdot C = A \cdot B \times C$,

$$[-i\boldsymbol{\phi} \cdot \boldsymbol{\sigma}, \boldsymbol{B}(\boldsymbol{r}) \cdot \boldsymbol{\sigma}] = -i \sum_{\alpha,\beta} \phi_\alpha B_\beta(\boldsymbol{r}) \left(2i \sum_\gamma \epsilon_{\alpha\beta\gamma}\sigma_\gamma \right) = 2 \left[\boldsymbol{\phi} \times \boldsymbol{B}(\boldsymbol{r}) \right] \cdot \boldsymbol{\sigma},$$

and Campbell-Baker-Hausdorff formula

$$e^A B e^{-A} = B + [A, B] + \frac{1}{2!} [A, [A, B]] + \frac{1}{3!} [A, [A, [A, B]]] + \cdots, \tag{2.20}$$

where ϵ_{ijk} is Levi-Civita symbol and A, B, and C are arbitrary operators. Therefore, we can rewrite Eq. (2.19) as

$$L_B \to L_B + 2 \int d\boldsymbol{r} \left\{ \psi^\dagger \left[(\boldsymbol{B}(\boldsymbol{r}) \times \boldsymbol{\sigma}) \cdot \boldsymbol{\phi} + O(\phi^2) \right] \psi \right\}, \tag{2.21}$$

and the variation of the action of the magnetic field term can be written as

$$\begin{aligned} \delta S_B &= \hbar \int_{-\infty}^{\infty} dt \int d\boldsymbol{r} \sum_{\alpha=x,y,z} \left\{ \left[\psi^\dagger \left(\frac{2}{\hbar} \left(\boldsymbol{B}(\boldsymbol{r}) \times \boldsymbol{\sigma} \right)_\alpha \right) \psi \right] \phi_\alpha \right\} \\ &= \hbar \int_{-\infty}^{\infty} dt \int d\boldsymbol{r} \sum_{\alpha=x,y,z} \left\{ -\mathcal{T}_B^\alpha \phi_\alpha \right\}. \end{aligned} \tag{2.22}$$

Secondly, under the phase transformation (2.14), Eq. (2.4) is converted into

$$\begin{aligned} L_{\rm so} &\to \int d\boldsymbol{r} \left\{ \psi^\dagger \left[e^{-i\boldsymbol{\phi}\cdot\boldsymbol{\sigma}} \left(\boldsymbol{B}_{\rm so} \cdot \boldsymbol{\sigma} \right) e^{i\boldsymbol{\phi}\cdot\sigma} \right] \psi \right\} \\ &= \int d\boldsymbol{r} \left\{ \psi^\dagger \left[e^{-i\boldsymbol{\phi}\cdot\boldsymbol{\sigma}} \left(\sum_{i,j} a_{ij} p_i \sigma_j \right) e^{i\boldsymbol{\phi}\cdot\sigma} \right] \psi \right\}, \end{aligned} \tag{2.23}$$

Here, we can find

$$e^{-i\boldsymbol{\phi}\cdot\boldsymbol{\sigma}} \left(p_i \sigma_j \right) e^{i\boldsymbol{\phi}\cdot\sigma} = p_i \sigma_j + 2i\hbar \sum_{\alpha,\beta} \epsilon_{\alpha\beta j} \phi_\alpha \sigma_\beta \partial_i + \hbar \sigma_j \sum_\alpha \partial_i \phi_\alpha \sigma_\alpha + O(\phi^2),$$

from the relation

$$[-i\boldsymbol{\phi}\cdot\boldsymbol{\sigma}, -i\hbar\partial_i\sigma_j] = -\hbar[\boldsymbol{\phi}\cdot\boldsymbol{\sigma}, \sigma_j]\partial_i + \hbar\sigma_j(\partial_i\boldsymbol{\phi}\cdot\boldsymbol{\sigma})$$
$$= -\hbar\sum_{\alpha,\beta}\epsilon_{\alpha\beta\gamma}(-\phi_\alpha)(2i\sigma_\beta)\partial_i + \hbar\sigma_j\left(\partial_i\sum_\alpha\phi_\alpha\sigma_\alpha\right), \quad (2.24)$$

and Campbell-Baker-Hausdorff formula (2.20). Therefore, we can rewrite Eq. (2.23) as

$$L_{\rm so} \to L_{\rm so} + \hbar\int d\boldsymbol{r}\left\{\psi^\dagger\sum_{i,j}a_{ij}\left[2i\sum_{\alpha,\beta}\epsilon_{\alpha\beta j}\phi_\alpha\sigma_\beta\partial_i + \sigma_j\sum_\alpha\partial_i\phi_\alpha\sigma_\alpha + O(\phi^2)\right]\psi\right\},$$

and the variation of the action of the SO coupling term can be written as

$$\begin{aligned}\delta S_{\rm so} &= \hbar\int_{-\infty}^{\infty}dt\int d\boldsymbol{r}\sum_\alpha\phi_\alpha\left\{2i\sum_{i,j,\beta}a_{ij}\epsilon_{\alpha\beta j}\psi^\dagger\sigma_\beta\partial_i\psi - \sum_{i,j}a_{ij}\partial_i\left(\psi^\dagger\sigma_j\sigma_\alpha\psi\right)\right\}\\ &= \hbar\int_{-\infty}^{\infty}dt\int d\boldsymbol{r}\sum_\alpha\phi_\alpha\left\{-\frac{2m}{\hbar}\sum_i\left(\boldsymbol{a}_i\times\boldsymbol{j}_{s,i}\right)_\alpha + \nabla\cdot\left(-\sum_i\boldsymbol{e}_i a_{i\alpha}\rho\right)\right\}\\ &= \hbar\int_{-\infty}^{\infty}dt\int d\boldsymbol{r}\sum_\alpha\left[(-\mathcal{T}^\alpha_{\rm so} + \nabla\cdot\boldsymbol{j}^\alpha_{\rm so})\right]\phi_\alpha, \end{aligned} \quad (2.25)$$

where we used Eqs. (2.9) and (2.18) and the relation $\sum_{\alpha,\beta,\gamma}\epsilon_{\alpha\beta\gamma}a_\beta b_\gamma = (\boldsymbol{a}\times\boldsymbol{b})_\alpha$. Finally, from Eqs. (2.16), (2.22), and (2.25), we can obtain the non-conservation law of spin

$$\frac{\partial s_\alpha}{\partial t} + \nabla\cdot(\boldsymbol{j}^\alpha_s + \boldsymbol{j}^\alpha_{\rm so}) = \mathcal{T}^\alpha_B + \mathcal{T}^\alpha_{\rm so}, \quad (2.26)$$

$$s_\alpha = \psi^\dagger\sigma_\alpha\psi, \quad \boldsymbol{j}^\alpha_s = -\frac{i\hbar}{2m}\left[\left(\nabla\psi^\dagger\right)\sigma_\alpha\psi - \psi^\dagger\sigma_\alpha\left(\nabla\psi\right)\right] \quad (2.27)$$

$$\mathcal{T}^\alpha_B = -\frac{2}{\hbar}(\boldsymbol{B}(\boldsymbol{r})\times\boldsymbol{s})_\alpha, \quad \boldsymbol{j}^\alpha_{\rm so} = -\sum_i\boldsymbol{e}_i a_{i\alpha}\rho, \quad \mathcal{T}^\alpha_{\rm so} = \frac{2m}{\hbar}\sum_{i,j,k}\epsilon_{\alpha jk}a_{ji}j^k_{s,i}, \quad (2.28)$$

Eq. (2.26) shows that the spin and the spin current are not conservative quantities when $\mathcal{T}^\alpha_B \neq 0$ or $\mathcal{T}^\alpha_{\rm so} \neq 0$. Note that above discussion is not valid when the strength of SO coupling a_{ij} has spatial variation from Eq. (2.24).

2.3 Unitary transformation

Unitary transformation is used well to simplify analysis. However, particle and spin current densities and a spin density are not invariant for the unitary transformation

having a spatial variation and spin dependent, respectively. Therefore, in this section, we show the relation between the unitary transformation and the currents or the spin.

Let us consider the unitary transformation

$$\psi(\boldsymbol{r}) = U^{\dagger}(\boldsymbol{r})\tilde{\psi}(\boldsymbol{r}), \tag{2.29}$$

where $\psi(\boldsymbol{r})$ is the field operator and $U(\boldsymbol{r})$ is the unitary matrix ($U^{\dagger}U = I$). Under this transformation, the number density of particle (2.9) dose not change obviously ($\rho = \psi^{\dagger}\psi = \tilde{\psi}^{\dagger}\tilde{\psi}$). On the other hand, the particle current density (2.9) is converted into

$$\begin{aligned} \boldsymbol{j} &= -\frac{i\hbar}{2m}\left[\left(\nabla\tilde{\psi}^{\dagger}\right)\tilde{\psi} - \tilde{\psi}^{\dagger}\left(\nabla\tilde{\psi}\right)\right] - \frac{i\hbar}{2m}\left\{\tilde{\psi}^{\dagger}\left[\left(\nabla U\right)U^{\dagger} - U\left(\nabla U^{\dagger}\right)\right]\tilde{\psi}\right\} \\ &= \tilde{\boldsymbol{j}} + \tilde{\boldsymbol{j}}_{U}. \end{aligned} \tag{2.30}$$

This equation shows that the unitary transformation having spatial variation causes the additional term $\tilde{\boldsymbol{j}}_{U}$. This is because the unitary transformation having spatial variation is equivalent with the coordinate transformation having spatial variation. Next, since the spin density (2.27) can be written as $\boldsymbol{s} = \psi^{\dagger}\boldsymbol{\sigma}\psi = \tilde{\psi}^{\dagger}U\boldsymbol{\sigma}U^{\dagger}\tilde{\psi}$, the direction of the spin changes like $\boldsymbol{\sigma} \to \tilde{\boldsymbol{\sigma}} = U\boldsymbol{\sigma}U^{\dagger}$. This comes from the rotation in the spin space by the unitary transformation. The spin current (2.27) is converted into

$$\begin{aligned} \boldsymbol{j}_{s}^{\alpha} &= -\frac{i\hbar}{2m}\left[\left(\nabla\psi^{\dagger}\right)\sigma_{\alpha}\psi - \psi^{\dagger}\sigma_{\alpha}\left(\nabla\psi\right)\right] \\ &= -\frac{i\hbar}{2m}\left[\left(\nabla\tilde{\psi}^{\dagger}\right)\tilde{\sigma}_{\alpha}\tilde{\psi} - \tilde{\psi}^{\dagger}\tilde{\sigma}_{\alpha}\left(\nabla\tilde{\psi}\right)\right] - \frac{i\hbar}{2m}\left\{\tilde{\psi}^{\dagger}\left[\left(\nabla U\right)\sigma_{\alpha}U^{\dagger} - U\sigma_{\alpha}\left(\nabla U^{\dagger}\right)\right]\tilde{\psi}\right\} \\ &= \tilde{\boldsymbol{j}}_{s}^{\alpha} + \tilde{\boldsymbol{j}}_{sU}^{\alpha}. \end{aligned} \tag{2.31}$$

This equation shows that the spin current is converted by the spatial variation and spin (Pauli matrix) dependence of U, respectively.

2.4 Properties of the currents

In this section, we consider the conditions that the particle and spin currents are induced. In the followings, firstly, we first analyze the relation between the spinor wave function and the currents[48, 52] and then show the force acting on a particle in the system with a magnetic field and SO coupling[49, 53].

Spinor wave function is given by

$$\psi_{1}(\boldsymbol{r}) = \sqrt{n_{1}(\boldsymbol{r})}\begin{pmatrix}\cos\frac{\gamma(\boldsymbol{r})}{2}e^{i\phi_{\uparrow}(\boldsymbol{r})} \\ \sin\frac{\gamma(\boldsymbol{r})}{2}e^{i\phi_{\downarrow}(\boldsymbol{r})}\end{pmatrix}, \tag{2.32}$$

where $n_1(\boldsymbol{r})$ is the density normalized to unity ($\int d\boldsymbol{r}\, n_1(\boldsymbol{r}) = 1$), γ is the parameter to determine the ratio between the two spinor components, and $\phi_\uparrow$ and $\phi_\downarrow$ are the phases of the components. Substituting Eq. (2.32) into Eq. (2.9), the particle current density is written as

$$\boldsymbol{j} = -\frac{\hbar n_1}{m}\left(\nabla\phi_\uparrow \cos^2\frac{\gamma}{2} + \nabla\phi_\downarrow \sin^2\frac{\gamma}{2}\right) = -\frac{\hbar n_1}{2m}\left(\nabla\phi + \nabla\phi_z\cos\gamma\right), \tag{2.33}$$

where we define $\phi = \phi_\uparrow + \phi_\downarrow$, $\phi_z = \phi_\downarrow - \phi_\uparrow$. In addition, from Eq. (2.18), we can obtain the spin density

$$\boldsymbol{s}_1 = \psi_1^\dagger \boldsymbol{\sigma}\psi_1 = n_1\left(\cos\phi_z \sin\gamma, -\sin\phi_z\sin\gamma, \cos\gamma\right) \tag{2.34}$$

and the spin current densities

$$\begin{aligned}
\boldsymbol{j}_s^x &= -\frac{\hbar n_1}{2m}\left[\nabla\phi\cos\phi_z\sin\gamma - \nabla\gamma\sin\phi_z\right], \\
\boldsymbol{j}_s^y &= -\frac{\hbar n_1}{2m}\left[\nabla\phi\sin\phi_z\sin\gamma - \nabla\gamma\cos\phi_z\right], \\
\boldsymbol{j}_s^z &= -\frac{\hbar n_1}{2m}\left[\nabla\phi\cos\gamma + \nabla\phi_z\right],
\end{aligned} \tag{2.35}$$

where we assume that the spin quantization axis is along the z axis. Equations (2.33) and (2.35) show that the spatial variation of $\phi_\uparrow$, $\phi_\downarrow$, or γ is necessary to induce the currents. In particular, when $\phi_z = \boldsymbol{k}\cdot\boldsymbol{r}$, the spin density (2.34) have a spiral spin structure in x-y and the z-spin current proportional to $|\boldsymbol{k}|$ is induced in the direction of $\boldsymbol{k}$, where $\boldsymbol{k}$ is a constant vector.

At last, we investigate the force induced by a effective magnetic field $\boldsymbol{B}(\boldsymbol{r}) + \boldsymbol{B}_{\rm so}$ in Eqs. (2.3) and (2.4)[49, 53]. When a single particle Hamiltonian is given by

$$h'_{\rm so} = -\frac{\hbar^2\nabla^2}{2m} + \left[\boldsymbol{B}(\boldsymbol{r}) + \boldsymbol{B}_{\rm so}\right]\cdot\boldsymbol{\sigma}, \tag{2.36}$$

from the equation of motion $\boldsymbol{f}(\boldsymbol{r}) = m\mathrm{d}^2\boldsymbol{r}/(\mathrm{d}t^2)$ and Heisenberg equation of motion $i\hbar\mathrm{d}\boldsymbol{r}/(\mathrm{d}t) = [\boldsymbol{r}, h'_{\rm so}]$, the force operator $\boldsymbol{f}(\boldsymbol{r})$ can be written as

$$\begin{aligned}
\boldsymbol{f}(\boldsymbol{r}) &= \frac{m}{(i\hbar)^2}\left[[\boldsymbol{r}, h'_{\rm so}], h'_{\rm so}\right] \\
&= \frac{m}{(i\hbar)^2}\left\{\frac{\hbar^2}{m}\nabla\left(\boldsymbol{B}(\boldsymbol{r})\cdot\boldsymbol{\sigma}\right) + i\hbar\left[\sum_{i,j} a_{ij}\boldsymbol{e}_i\sigma_j, \sum_\ell\left(B_\ell + a_{k\ell}p_k\right)\sigma_\ell\right]\right\} \\
&= -\nabla\left(\boldsymbol{B}(\boldsymbol{r})\cdot\boldsymbol{\sigma}\right) + \frac{2m}{\hbar}\sum_{i,j} a_{ij}\boldsymbol{e}_i\left[\left(\boldsymbol{B}(\boldsymbol{r}) + \sum_k \boldsymbol{a}_k p_k\right)\times\boldsymbol{\sigma}\right]_j,
\end{aligned} \tag{2.37}$$

where we used the commutation relations $[x_i, p_j] = i\hbar\delta_{ij}$ and $[\sigma_i, \sigma_j] = 2i\epsilon_{ijk}\sigma_k$. The first term in Eq. (2.37) shows that the force depending on the spin is induced

by a spatial variation of the magnetic field $\boldsymbol{B}$ without SO coupling. In addition, the second term in Eq. (2.37) show that the SO coupling induces the force if the magnetic field has not spatial variation.

We are interested in a counterflow of particles with different spins. Therefore, in the following chapters, we call z-spin current as a spin current and analyze only it.

Chapter 3

Artificial spin-orbit coupled cold atom

In 2009, NIST (National Institute of Standards and Technology) group create Bose-Einstein condensate (BEC) with vector potential, that is called artificial gauge field, by manipulating the Raman lasers and the external magnetic field[51]. On the basis of this technique, afterwards, artificial magnetic field, artificial electric field, and artificial spin-orbit (SO) coupling can be created in BECs[3, 54, 55]. Furthermore, this technique can be used in degenerate Fermi system and SO coupled Fermi system have been created[4, 5]. Since SO coupling is known to induce interesting phenomena such as topological insulator or spin-Hall effect[46, 56, 57] in the solid state physics, we can expect that SO coupled cold atom also induce interesting phenomena.

In this chapter, we show the method to experimentally create a cold atom with a magnetic field and SO coupling. At first, we discuss the BEC with the artificial gauge field and, next, show the method to create the artificial SO coupling in the BEC.

3.1 Artificial gauge field

In the beginning, we will examine how create the artificial gauge field in BEC. In the experiment of NIST[51], they used ^{87}Rb BEC in the $F = 1$ ground state and counterpropagated two Raman lasers(Fig. 3.1a). Here, ^{87}Rb in the external magnetic field has Zeeman splitted three hyper-fine states $|F = 1, m_z = -1\rangle$, $|F = 1, m_z = 0\rangle$, $|F = 1, m_z = +1\rangle$, where m is a magnetic quantum number. In addition, these states are coupled by two Raman lasers with a wave number k_0 and frequency ω_L and $\omega_L + \Delta\omega$, respectively. As a result, effective Hamiltonian is given by

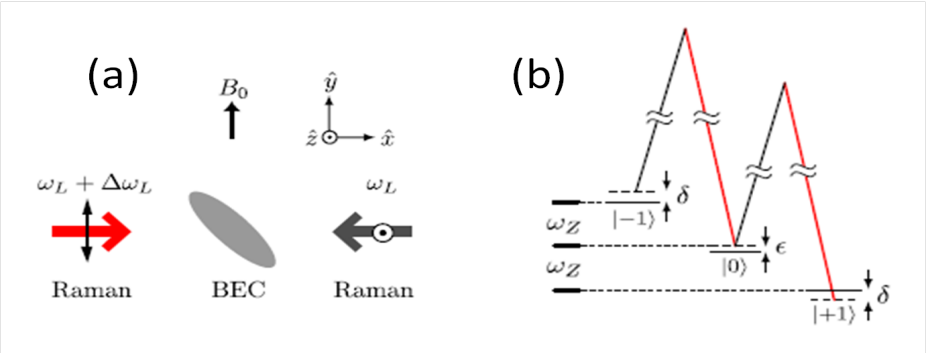

Figure 3.1: Experimental setup to create the artificial gauge field in BEC[51]. (a) The two Raman lasers with frequencies ω and $\omega + \Delta\omega$ and the external magnetic field with the strength B_0 are applied to ^{87}Rb BEC. (b) Level diagram of the Raman coupled $F = 1$ ground states detuned by the quadratic Zeeman shift $\epsilon(= \omega_q)$ and the Raman detuning δ.

$$h_3 = \begin{pmatrix} \dfrac{\boldsymbol{p}^2}{2m} - \hbar\omega_z & \dfrac{\hbar\Omega}{2}e^{-i\Theta} & 0 \\ \dfrac{\hbar\Omega}{2}e^{i\Theta} & \dfrac{\boldsymbol{p}^2}{2m} + \hbar\omega_q & \dfrac{\hbar\Omega}{2}e^{-i\Theta} \\ 0 & \dfrac{\hbar\Omega}{2}e^{i\Theta} & \dfrac{\boldsymbol{p}^2}{2m} + \hbar\omega_z \end{pmatrix}, \tag{3.1}$$

where $\boldsymbol{p}$ is momentum, $\hbar\omega_z$ and $\hbar\omega_q$ are first and quadratic Zeeman shift, and $\Theta = \Theta(x,t) = 2k_0x - \Delta\omega t$. The detail of the derivation of Eq. (3.1) is shown in appendix A.

To eliminate time-space dependence in Eq. (3.1), we use the following unitary matrix:

$$U_3(x,t) = \begin{pmatrix} e^{i\Theta} & 0 & 0 \\ 0 & 1 & 0 \\ 0 & 0 & e^{-i\Theta} \end{pmatrix}. \tag{3.2}$$

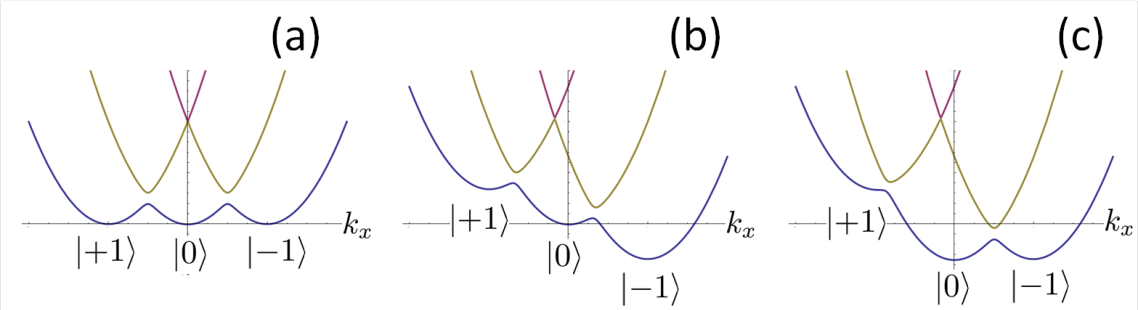

Figure 3.2: Dispersions provided from Eq. (3.3) for (a) $\delta_0 = \omega_q = 0$, (b) $\delta_0 > 0, \omega_q = 0$, and (c) $\delta_0 \simeq \omega_q$ (> 0). The number of minimum points can be tuned by the parameters.

Then, unitary transformed Hamiltonian is given by [1)]

$$\begin{aligned}\tilde{h}_3 &= U_3(x,t)h_3U_3^\dagger(x,t) - i\hbar U_3(x,t)\frac{\partial U_3^\dagger(x,t)}{\partial t} \\ &= \begin{pmatrix} \dfrac{(\boldsymbol{p}-2\hbar\boldsymbol{k}_0)^2}{2m} + \hbar\delta_0 & \dfrac{\hbar\Omega}{2} & 0 \\ \dfrac{\hbar\Omega}{2} & \dfrac{\boldsymbol{p}^2}{2m} - \hbar\omega_q & \dfrac{\hbar\Omega}{2} \\ 0 & \dfrac{\hbar\Omega}{2} & \dfrac{(\boldsymbol{p}+2\hbar\boldsymbol{k}_0)^2}{2m} - \hbar\delta_0 \end{pmatrix}, \end{aligned} \tag{3.3}$$

where $\boldsymbol{k}_0 = (k_0, 0, 0)$, $\delta_0 = \Delta\omega - \omega_z$ is detune, and we used the relation provided from Campbell-Baker-Hausdorff formula (2.20)

$$e^{\mp 2ik_0x}p_x^2e^{\pm 2ik_0x} = p_x^2 \pm 4\hbar k_0p_x + 4\hbar^2k_0^2 = (p_x \pm 2\hbar k_0)^2.$$

Fig. 3.2 is the dispersion provided from Eq. (3.3) and shows that the number of minimum points changes by tuning the parameters k_0, Ω, δ_0, and ω_q. At ultra-low temperature, when the dispersion has single minimum point $\boldsymbol{k}_{\min} = (k_{\min}, 0, 0)$, the effective single-particle Hamiltonian can be written as $h' \approx (\boldsymbol{p} - \hbar\boldsymbol{k}_{\min})^2/2m^*$, where m^* is the effective mass. By comparing this Hamiltonian with the one of the single electron with charge q and vector potential $\boldsymbol{A}$, we can see that these have the same form:

$$\frac{(\boldsymbol{p}-\hbar\boldsymbol{k}_{\min})^2}{2m^*} \quad \longleftrightarrow \quad \frac{(\boldsymbol{p}-q\boldsymbol{A})^2}{2m}. \tag{3.4}$$

Therefore, we can regard Eq. (3.3) as the system with the artificial vector potential (or artificial gauge field).

[1)] By substituting the unitary transformation of a wave function $\psi = U^\dagger\tilde{\psi}$ into Schrödinger equation $i\hbar\partial_t\psi = h\psi$, we can find that the Schrödinger equation for $\tilde{\psi}$ is given by $i\hbar\partial_t\tilde{\psi} = \left[UhU^\dagger - i\hbar U\left(\partial_tU^\dagger\right)\right]\tilde{\psi}$. In the same way, we can also obtain $h = U^\dagger\tilde{h}U + i\hbar\left(\partial_tU^\dagger\right)U$.

3.2 Artificial spin-orbit coupling

3.2.1 Method to create the artificial spin-orbit coupling

By tuning the parameters in BEC with artificial gauge field, we can create the SO coupled BEC[3]. Using the time dependent unitary matrix

$$U_3(t) = \begin{pmatrix} e^{-i\Delta\omega t} & 0 & 0 \\ 0 & 1 & 0 \\ 0 & 0 & e^{i\Delta\omega t} \end{pmatrix}, \tag{3.5}$$

and adding the constant term, Eq. (3.1) can be rewritten as

$$\begin{aligned} \bar{h}_3 &= U_3(t)h_3U_3^\dagger(t) - i\hbar U_3(t)\frac{\partial U_3^\dagger(t)}{\partial t} + \hbar\left(\frac{\delta_0+\omega_q}{2}\right) \\ &= \begin{pmatrix} \dfrac{\boldsymbol{p}^2}{2m} + \dfrac{3\hbar\delta_0+\hbar\omega_q}{2} & \dfrac{\hbar\Omega}{2}e^{-2ik_0x} & 0 \\ \dfrac{\hbar\Omega}{2}e^{2ik_0x} & \dfrac{\boldsymbol{p}^2}{2m} + \dfrac{\hbar\delta_0-\hbar\omega_q}{2} & \dfrac{\hbar\Omega}{2}e^{-2ik_0x} \\ 0 & \dfrac{\hbar\Omega}{2}e^{2ik_0x} & \dfrac{\boldsymbol{p}^2}{2m} - \dfrac{\hbar\delta_0-\hbar\omega_q}{2} \end{pmatrix}. \end{aligned} \tag{3.6}$$

From this equation, we can find that the energy of hyper-fine state $|1,+1\rangle$ is larger than other states when $\delta_0 \simeq \omega_q$ (Fig. 3.2c). In this case, if δ_0 is much larger than typical energy scale of the system $E_0 = \hbar^2k_0^2/(2m)$, hyper-fine states $|1,-1\rangle$ and $|1,0\rangle$ are energetically dominant and we can neglect the state $|1,+1\rangle$. Therefore, the effective Hamiltonian can be written as

$$\bar{h}_2 \simeq \begin{pmatrix} \dfrac{\boldsymbol{p}^2}{2m} + \dfrac{\hbar\delta}{2} & \dfrac{\hbar\Omega}{2}e^{-2ik_0x} \\ \dfrac{\hbar\Omega}{2}e^{2ik_0x} & \dfrac{\boldsymbol{p}^2}{2m} - \dfrac{\hbar\delta}{2} \end{pmatrix}, \tag{3.7}$$

where we define $\delta = \delta_0 - \omega_q$ ($\simeq 0$). By using the unitary matrix

$$U_2(x) = \begin{pmatrix} e^{ik_0x} & 0 \\ 0 & e^{-ik_0x} \end{pmatrix}, \tag{3.8}$$

we can find that Eq. (3.7) can be rewritten as

$$\begin{aligned} \tilde{h}_2 = U_2(x)\bar{h}_2U_2^\dagger(x) &= \begin{pmatrix} \dfrac{(\boldsymbol{p}-\hbar\boldsymbol{k}_0)^2}{2m} + \dfrac{\hbar\delta}{2} & \dfrac{\hbar\Omega}{2} \\ \dfrac{\hbar\Omega}{2} & \dfrac{(\boldsymbol{p}+\hbar\boldsymbol{k}_0)^2}{2m} - \dfrac{\hbar\delta}{2} \end{pmatrix} \\ &= \frac{\boldsymbol{p}^2}{2m} - \frac{\hbar k_0}{m}p_x\sigma_z + \frac{\hbar\Omega}{2}\sigma_x + \frac{\hbar\delta}{2}\sigma_z + E_0 \end{aligned} \tag{3.9}$$

In this Hamiltonian, the second term corresponds to the SO coupling term and the third and fourth terms correspond to Zeeman terms. One of useful features of this system is controllability of physical parameters. In fact, the intensities of the SO coupling and magnetic fields can be tuned by tuning the Raman lasers and external magnetic field[6, 58]. The details of the method to tune the parameters are shown in appendix B.

Since we are interested in the physical quantities in a laboratory frame but Eq. (3.9) is the Hamiltonian converted by the unitary transformation in the rotation frame, it is worth to mention Eq. (3.9) in a laboratory frame. By using the unitary matrix

$$U_2(x,t) = \begin{pmatrix} e^{i\frac{\Theta}{2}} & 0 \\ 0 & e^{-i\frac{\Theta}{2}} \end{pmatrix}, \tag{3.10}$$

Eq. (3.9) in the laboratory frame can be written as

$$\begin{aligned} h_2 &= U_2^\dagger(x,t)\tilde{h}_2 U_2(x,t) + i\hbar \left[\frac{\partial U_2^\dagger(x,t)}{\partial t}\right] U_2(x,t) \\ &= \begin{pmatrix} \dfrac{\boldsymbol{p}^2}{2m} - \dfrac{\hbar\omega_Z}{2} & \dfrac{\hbar\Omega}{2}e^{-i\Theta} \\ \dfrac{\hbar\Omega}{2}e^{i\Theta} & \dfrac{\boldsymbol{p}^2}{2m} + \dfrac{\hbar\omega_Z}{2} \end{pmatrix} \\ &= \frac{\boldsymbol{p}^2}{2m} + \boldsymbol{B}_{\text{eff}}(x,t)\cdot\boldsymbol{\sigma}, \end{aligned} \tag{3.11}$$

where

$$\boldsymbol{B}_{\text{eff}}(x,t) = \frac{\hbar}{2}\left(\Omega\cos\Theta, \Omega\sin\Theta, -\omega_Z\right) \tag{3.12}$$

is the effective magnetic field and $\omega_Z = \omega_z + \omega_q$ is the total Zeeman shift. This equation shows that the spiral magnetic field in x-y plane and the uniform magnetic field along z-axis act on the system.

In the above discussion, we consider only SO coupled BEC. However, SO coupled Fermi system has been realized by using a similar method[4, 5]. note that, the SO coupling in Eq. (3.9) is equivalent to that of an electronic system with equal contributions of Rashba ($\propto k_x\sigma_x + k_y\sigma_y$) [59] and Dresselhaus ($\propto k_x\sigma_x - k_y\sigma_y$) [60] couplings and, in a solid state physics, such a system can be created by using GaAs[61, 62]. Therefore, we can expect that SO coupled Fermi system described by Eq. (3.9) is used as a quantum simulater.

3.2.2 Experimental realization of the spin current

Let us finally mention the possibility of experimental realization of the spin current. When the spin of the particle $\boldsymbol{s}$ is aligned with the effective magnetic field, the spin

can be written as

$$\boldsymbol{s}(x,t) = (s_p \cos\Theta(x,t+\Delta t), s_p \sin\Theta(x,t+\Delta t), s_z)\,, \tag{3.13}$$

where Δt represents a time delay. Therefore, by using Eqs. (2.28) and (3.12), the spin dissipation can be written as

$$\mathcal{T}_B^z = -\frac{2}{\hbar}\left[\boldsymbol{B}_{\text{eff}}(x,t) \times \boldsymbol{s}(x,t)\right]_z = \frac{\hbar\Omega s_p}{2}\sin\left(\Delta\omega\Delta t\right),$$

This result shows that the spin current dissipate but, when the spin is well aligned to the effective magnetic field ($\Delta t \simeq 0$), the dissipation is negligibly small and we can regard the spin current as the dissipationless.

In a cold atom system, such a dissipationless spin current separates the up-spin component and the down-spin component from each other and results in spin accumulation. Therefore, we would be able to measure the spin current by investigating the spin accumulation using time-of-flight absorption imaging and Stern-Gerlach magnetic field.

Chapter 4

Artificial spin-orbit coupled Bose system

An spin-orbit (SO) coupled pseudo-spin-1/2 Bose system was realized in 2011[3]. Since this system has not been studied in a solid-state physics, it is expected that novel phenomena are presented. Therefore, in the past decade, a considerable number of theoretical and experimental studies of this system have been proposed [3, 6, 7, 8, 9, 10, 11, 12, 13, 14, 15, 16, 17, 18, 19, 20].

In this chapter, we show the ground state phase diagram of the artificial SO coupled Bose system with and without the interaction and the spin current. Firstly, we analyze the ground state of the SO coupled Bose system without the interaction in Sec. 4.1. Secondly, in Sec. 4.2, we show the ground state phase diagram of SO coupled Bose system with the interaction by using a variational method[8, 9, 10, 11, 15] and the parameter dependence of the spin current.

4.1 Ground state of the Bose system without interaction

When the interaction between atoms can be ignored in the Bose system at zero temperature, all the bosons are in the same ground state. Therefore, to investigate the SO coupled Bose system without the interaction, we analyze the property of a single-boson in the following.

Let us consider the single-particle Hamiltonian

$$\tilde{h}_{\rm so} = \frac{\boldsymbol{p}^2}{2m} - \frac{\hbar k_0}{m} p_x \sigma_z + \frac{\hbar\Omega}{2}\sigma_x + \frac{\hbar\delta}{2}\sigma_z + E_0. \tag{4.1}$$

Note that tilde indicates that the quantity is the unitary transformed one by Eq. (3.10). From this Hamiltonian, we can calculate the single-particle dispersion

$$\epsilon^{\pm}_{\rm so}(\boldsymbol{k}) = \frac{\hbar^2\boldsymbol{k}^2}{2m} + E_0 \pm \sqrt{\left(\frac{\hbar^2 k_0 k_x}{m} - \frac{\hbar\delta}{2}\right)^2 + \left(\frac{\hbar\Omega}{2}\right)^2}, \tag{4.2}$$

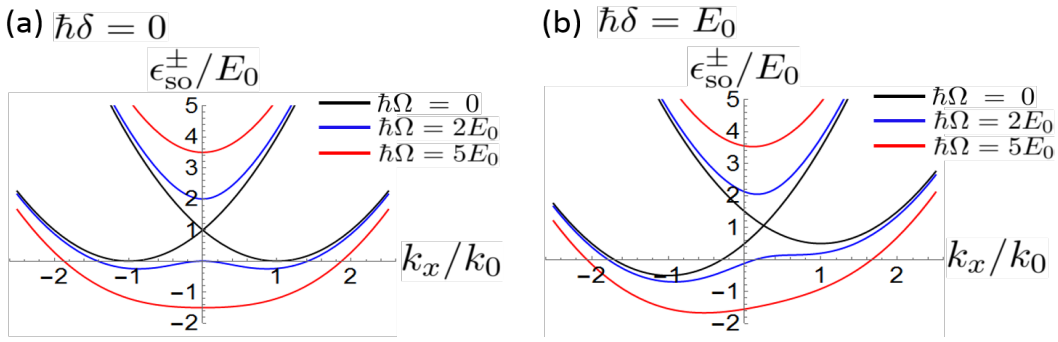

Figure 4.1: Dispersioins (4.2) in the k_x direction. The lines are for $\hbar\Omega = 0$ (black), $2E_0$ (Blue), and $5E_0$ (Red) with (a) $\hbar\delta = 0$ and (b) $\hbar\delta = E_0$. The black and blue lines in Fig. (a) show that the dispersion has two minima when $\delta = 0$ and $\hbar\Omega < 4E_0$.

and plot this dispersion as a function of k_x in Fig. 4.1. When $\delta = 0$, the ground state is doubly degenerated with nonzero momentum when $\Omega < 4E_0$ (black and blue lines in Fig. 4.1(a)) and has zero momentum with no degeneracy when $\Omega \geq 4E_0$ (red line in Fig. 4.1(a)), where these minima are given by

$$\pm\boldsymbol{k}^{\rm min}_{\delta=0} = (\pm k^{\rm min}_{\delta=0}, 0, 0), \quad k^{\rm min}_{\delta=0} = \begin{cases} k_0\sqrt{1-\left(\dfrac{\hbar\Omega}{4E_0}\right)^2} & (\hbar\Omega < 4E_0) \\ 0 & (\hbar\Omega \geq 4E_0) \end{cases}. \tag{4.3}$$

When $\delta \neq 0$, on the other hand, the ground state has nonzero momentum with no degeneracy, where the minimum is given by $\boldsymbol{k}^{\rm min}_{\delta\neq 0} = (k^{\rm min}_{\delta\neq 0}, 0, 0)$.

The eigen-state $\tilde{\psi}_{\pm,\boldsymbol{k}}$ satisfying $\tilde{h}_{\rm so}\tilde{\psi}_{\pm,\boldsymbol{k}} = \epsilon^{\pm}_{\rm so}(\boldsymbol{k})\tilde{\psi}_{\pm,\boldsymbol{k}}$ can be written as

$$\begin{pmatrix} \tilde{\psi}_{+,\boldsymbol{k}} \\ \tilde{\psi}_{-,\boldsymbol{k}} \end{pmatrix} = \begin{pmatrix} \cos\theta_{k_x} & \sin\theta_{k_x} \\ -\sin\theta_{k_x} & \cos\theta_{k_x} \end{pmatrix} \begin{pmatrix} \tilde{\psi}_{\uparrow,\boldsymbol{k}} \\ \tilde{\psi}_{\downarrow,\boldsymbol{k}} \end{pmatrix}, \tag{4.4}$$

$$\tan\theta_{k_x} = \frac{2}{\hbar\Omega}\left[\sqrt{\left(-\frac{\hbar^2 k_0 k_x}{m} + \frac{\hbar\delta}{2}\right)^2 + \left(\frac{\hbar\Omega}{2}\right)^2} - \frac{\hbar^2 k_0 k_x}{m} + \frac{\hbar\delta}{2}\right], \tag{4.5}$$

where $\tilde{\psi}_{\boldsymbol{k}} = (\tilde{\psi}_{\uparrow,\boldsymbol{k}}, \tilde{\psi}_{\downarrow,\boldsymbol{k}})^T$ is the wave function of the boson with the wave number $\boldsymbol{k}$ (T denotes transpose). When $\delta = 0$, since the ground state is doubly degenerated or is not degenerated, the ground state wave function in real space can be written as

$$\tilde{\psi}^{\delta=0}_{\rm g}(x) = e^{+ik^{\rm min}_{\delta=0}x}\tilde{\psi}_{-,+\boldsymbol{k}^{\rm min}_{\delta=0}} + e^{-ik^{\rm min}_{\delta=0}x}\tilde{\psi}_{-,-\boldsymbol{k}^{\rm min}_{\delta=0}}, \tag{4.6}$$

where we assume $\int d\boldsymbol{r}|\tilde{\psi}^{\delta=0}_{\rm g}(x)|^2 = 1$. Therefore, the ground state is classified in nonzero momentum phase where the wave function is expressed by two plane waves

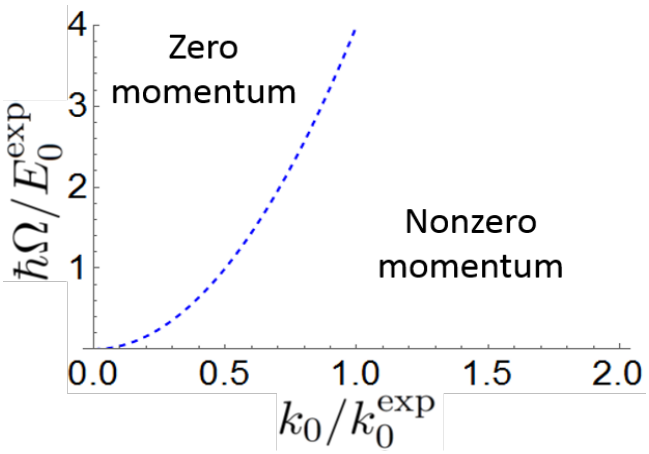

Figure 4.2: Phase diagram of SO coupled Bose system without the interaction. Dashed line indicates the second-order phase transition. The parameter is $m = 1.45 \times 10^{-25}$ and $k_0^{\rm exp} = 2\pi \sin(\pi/4)/(804.1){\rm nm}^{-1} \simeq 5.5\ \mu{\rm m}^{-1}$ and $E_0^{\rm exp} = (\hbar k_0^{\rm exp})^2/(2m)$ are experimental normalized parameters[3].

and zero momentum phase where the wave function is expressed by single plane wave.

When $\delta \neq 0$, as we mentioned above, the ground state has nonzero momentum $\boldsymbol{k}_{\delta\neq 0}^{\rm min}$ with no degeneracy. This mean that the ground state wave function is given by a single plane-wave form $\tilde{\psi}_{\rm g}^{\delta\neq 0}(x) = e^{ik_{\delta\neq 0}^{\rm min}x}\tilde{\psi}_{-,\boldsymbol{k}_{\delta\neq 0}^{\rm min}}$ and the probability amplitude is always uniform.

As we mentioned in the beginning of this section, all the bosons in the Bose system without the interaction are in the same state as the ground state of the single-particle. Therefore, we can write the many-body ground state wave function as $\psi_{\rm g}^{\rm b}(x) = \sqrt{n_{\rm b}}\psi_{\rm g}(x)$, where $n_{\rm b}$ is the mean number density of the bosons. In addition, when $\delta = 0$, the ground state can be classified in the nonzero momentum phase and the zero momentum phase as shown in Fig. 4.2, where the phase transition line is given by $\hbar\Omega = 4E_0$.

4.2 Bose system with weak interaction

Let us consider the SO coupled Bose system with weak interaction. The ground state of a spin-1/2 Bose gas of $N_{\rm b}$ particles enclosed in a volume V was investigated

in previous studies[9, 10, 11, 15]. The Hamiltonian is given by

$$H^{\rm b} = \sum_{j=1}^{N_{\rm b}} \tilde{h}^{\rm b}_{\rm so}(j) + \frac{1}{2} \sum_{\alpha,\beta=\uparrow,\downarrow} \int d\boldsymbol{r}\ u^{\rm bb}_{\alpha\beta} n^{\rm b}_{\alpha}(\boldsymbol{r}) n^{\rm b}_{\beta}(\boldsymbol{r}), \tag{4.7}$$

$$\tilde{h}^{\rm b}_{\rm so}(j) = \frac{\boldsymbol{p}_j}{2m} - \frac{\hbar k_0}{m} p_{j,x}\sigma_z + \frac{\hbar\Omega}{2}\sigma_x + \frac{\hbar\delta}{2}\sigma_z + E_0, \tag{4.8}$$

where $\boldsymbol{p}_j$ is the momentum of the boson labeled by j, α and $\beta(=\uparrow,\downarrow)$ are spin indicates, $u^{\rm bb}_{\alpha\beta}$ are the relevant coupling constants between the spin channels of the bosons, $n^{\rm b}_{\alpha}(\boldsymbol{r})$ is the number density of the bosons with the spin α at the position $\boldsymbol{r}$. For simplicity, in the following, we assume that $\delta = 0$, spin symmetric interaction $u^{\rm bb}_{\uparrow\uparrow} = u^{\rm bb}_{\downarrow\downarrow} = u^{\rm bb}_0$, and the interactions are much smaller than the typical energy scale of the system.

4.2.1 Ground state phase diagram

By using variational method, we analyze the ground state of the Bose system[8, 9, 10, 11, 15]. Since we assumed the weak interaction, it is expected that the properties of the single-particle discussed in Sec. 4.1 hardly change and that the bosons condense at one or two point(s) in the momentum space. Therefore, we can consider the following ansatz :

$$\tilde{\psi}^{\rm b}(x) = \begin{pmatrix} \tilde{\psi}^{\rm b}_{\uparrow}(x) \\ \tilde{\psi}^{\rm b}_{\downarrow}(x) \end{pmatrix} = \sqrt{n_{\rm b}} \left[C_+ \begin{pmatrix} \cos\theta \\ -\sin\theta \end{pmatrix} e^{ik_1 x} + C_- \begin{pmatrix} \sin\theta \\ -\cos\theta \end{pmatrix} e^{-ik_1 x} \right], \tag{4.9}$$

where $C_\pm$, θ, and k_1 are the variational parameters satisfying $|C_+|^2 + |C_-|^2 = 1$, $0 \le \theta \le \pi/4$, and $0 \le k_1$, respectively.

Substituting Eq. (4.9) into Eq. (4.7) with $\delta = 0$, we can obtain the energy per a boson as a function of the variational parameters:

$$\begin{aligned} \epsilon^{\rm b}(k_1,\beta,\theta) &= E_0 + \frac{\hbar^2}{2m}\left[k_1^2 - 2k_0 k_1 \cos(2\theta)\right] - \frac{\hbar\Omega}{2}\sin(2\theta) \\ &\quad + \left[1 + 2\beta^2\sin^2(2\theta)\right] U^{\rm bb}_1 + \cos^2(2\theta)(1-4\beta^2) U^{\rm bb}_2, \end{aligned} \tag{4.10}$$

where we define $\beta = |C_+||C_-|$ $(0 \le \beta \le 1/2)$, $U^{\rm bb}_1 = n_{\rm b}(u^{\rm bb}_0 + u^{\rm bb}_{\uparrow\downarrow})/4$, and $U^{\rm bb}_2 = n_{\rm b}(u^{\rm bb}_0 - u^{\rm bb}_{\uparrow\downarrow})/4$. Since Eq. (4.10) is a quadratic and convex downward function for k_1, we can easily find that the energy is minimized at $k_1 = k_0\cos(2\theta)$. By using this relation, Eq. (4.10) can be rewritten as

$$\epsilon^{\rm b}(k_1,\beta) = E_0 - \frac{\hbar\Omega}{2}\sqrt{1 - \frac{k_1^2}{k_0^2}} + \left(1 + 2\beta^2\right) U^{\rm bb}_1 - F(\beta)\frac{k_1^2}{k_0^2}, \tag{4.11}$$

where we define the function

$$F(\beta) = E_0 + 2\beta^2 U^{\rm bb}_1 - \left(1 - 4\beta^2\right) U^{\rm bb}_2.$$

The differential of Eq. (4.11) for β is given by

$$\frac{\partial \epsilon^{\mathrm{b}}(k_1,\beta)}{\partial \beta} = 4\beta\left[U_1^{\mathrm{bb}}\left(1-\frac{k_1^2}{k_0^2}\right) - 2U_2^{\mathrm{bb}}\frac{k_1^2}{k_0^2}\right]. \tag{4.12}$$

This equation shows that $\epsilon^{\mathrm{b}}(k_1,\beta)$ is a monotonous increasing or decreasing function of β. Hence, we can find that β minimized the energy is given by

$$\beta = \begin{cases} 0 & \left(U_1^{\mathrm{bb}}\left(1-\frac{k_1^2}{k_0^2}\right) > 2U_2^{\mathrm{bb}}\frac{k_1^2}{k_0^2}\right) \\ \frac{1}{2} & \left(U_1^{\mathrm{bb}}\left(1-\frac{k_1^2}{k_0^2}\right) < 2U_2^{\mathrm{bb}}\frac{k_1^2}{k_0^2}\right) \end{cases}. \tag{4.13}$$

When $u_{\uparrow\downarrow}^{\mathrm{bb}} > u_0^{\mathrm{bb}} > 0$, we can find that $(1-k_1^2/k_0^2)\,U_1^{\mathrm{bb}} > U_2^{\mathrm{bb}}$ and $\beta = 0$ because $U_1^{\mathrm{bb}} > 0$, $U_2^{\mathrm{bb}} < 0$, and $k_0 \geq k_1 \geq 0$. This mean that the ground state is always expressed by the single plane wave. Therefore, in the following, we assume that $u_0^{\mathrm{bb}} > u_{\uparrow\downarrow}^{\mathrm{bb}} > 0$ ($U_1^{\mathrm{bb}} > 0$ and $U_2^{\mathrm{bb}} > 0$) where the ground state can be doubly degenerated and it is expected to present rich phases. On the other hand, the differential of Eq. (4.11) for k_1 is given by

$$\frac{\partial \epsilon^{\mathrm{b}}(k_1,\beta)}{\partial k_1} = -\frac{k_1}{k_0^2}\left[\frac{\hbar\Omega}{2\sqrt{1-\frac{k_1^2}{k_0^2}}} + F(\beta)\right], \tag{4.14}$$

and we can find that k_1 minimized the energy is given by

$$k_1 = \begin{cases} k_0\sqrt{1-\left[\dfrac{\hbar\Omega}{4F(\beta)}\right]^2} & (\hbar\Omega \leq 4F(\beta)) \\ 0 & (\hbar\Omega > 4F(\beta)) \end{cases}. \tag{4.15}$$

Note that, since $F(\beta) = E_0$ when $u_0^{\mathrm{bb}} = u_{\uparrow\downarrow}^{\mathrm{bb}} = 0$, we can see that this result without the interaction agrees with Eq. (4.3).

In conclusion, by minimizing Eq. (4.11) with respect to the variational parameters, we can obtain the ground state phase diagram as shown in Fig. 4.3. Note that the phase transition lines in Fig. 4.3 are given by

$$\begin{aligned} \hbar\Omega_c^{(I-II)} &= 4\sqrt{\left(2E_0+U_1^{\mathrm{bb}}\right)\left(E_0-U_2^{\mathrm{bb}}\right)\frac{U_2^{\mathrm{bb}}}{U_1^{\mathrm{bb}}+2U_2^{\mathrm{bb}}}}, \\ \hbar\Omega_c^{(II-III)} &= 4\left(E_0-U_2^{\mathrm{bb}}\right), \\ \hbar\Omega_c^{(I-III)} &= 2\left(2E_0+U_1^{\mathrm{bb}}\right) - 2\sqrt{\left(2E_0+U_1^{\mathrm{bb}}\right)U_1^{\mathrm{bb}}}. \end{aligned} \tag{4.16}$$

Figure 4.3 shows that there are following three phases:

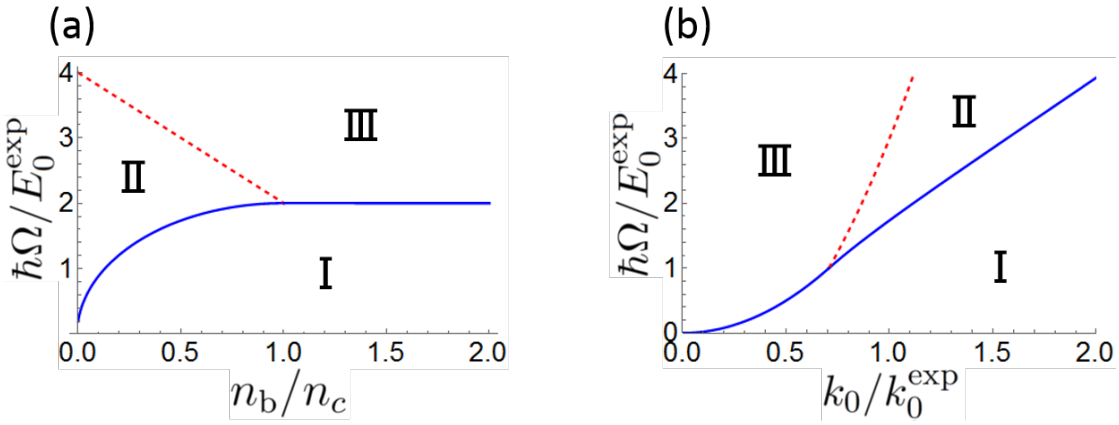

Figure 4.3: Phase diagram of SO coupled Bose system at zero temperature. The solid and dashed lines represent the first- and second-order phase boundaries, respectively. The parameters are $m = 1.45 \times 10^{-25}$ kg, $u_0^{\rm bb} = 4\pi\hbar^2(100a_B)/m$ J·m^3, $\gamma = U_2^{\rm bb}/U_1^{\rm bb} = 0.0012$, $G_2/G_1 = 0.0012$, (a) $k_0 = k_0^{\rm exp}$, and (b) $n_{\rm b} = 0.5n_c$, where $n_c = E_0^{\rm exp}/(\gamma u_0^{\rm bb})$ is the normalized parameter used in Ref. [10] and a_B is Bohr radius.

Phase I : Stripe phase ($\beta = 1/2, 0 < k_1 \le k_0, 0 \le \theta < \pi/4$)
The bosons condense in a superposition of the two plane wave states of the wave numbers $+k_1$ and $-k_1$ with the same weight. The density have a spatially stripe structure.

Phase II : Plane wave phase ($\beta = 0, 0 < k_1 \le k_0, 0 \le \theta < \pi/4$)
The bosons condense in a single plane wave state of the wave number $+k_1$ or $-k_1$. The density is uniform.

Phase III : Zero momentum phase ($\beta = 0, k_1 = 0, \theta = \pi/4$)
The bosons condense in a single plane wave state of zero wave number. The density is uniform.

Using Eq. (4.9), the number density and the spin density of the bosons are written as

$$n^{\rm b}(x) = |\tilde{\psi}^{\rm b}(x)|^2 = n_{\rm b}\left[1 + 2\beta\sin(2\theta)\cos(2k_1x + \phi)\right], \tag{4.17}$$

$$\tilde{\boldsymbol{S}}^{\rm b}(x) = \left(\tilde{\psi}^{\rm b}(x)\right)^\dagger \boldsymbol{\sigma}\tilde{\psi}^{\rm b}(x) = n_{\rm b}\begin{pmatrix} -\sin(2\theta) - 2\beta\cos(2k_1x + \phi) \\ 2\beta\cos(2\theta)\sin(2k_1x + \phi) \\ \pm\cos(2\theta)\sqrt{1 - 4\beta^2} \end{pmatrix}^T. \tag{4.18}$$

Equation (4.18) shows that the bosons have a spiral spin structure only in the phase I ($\beta \neq 0$, $0 < k_1$) and the z-spin density is finite only in the phase II ($\beta = 0$ and $\theta \neq \pi/4$).

By comparing Fig. 4.3 (b) with Fig. 4.2, we can find that the nonzero momentum phase in Fig. 4.2 changes to the phases I and II by the effect of the weak interaction.

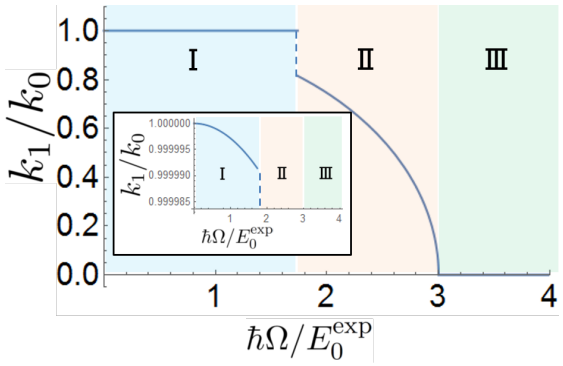

Figure 4.4: Variational parameter k_1/k_0 as a function of Ω for $k_0 = k_0^{\rm ex}$ and $n_{\rm b} = 0.5n_c$. The other parameters are the same as in Fig. 4.3. Inset is enlarged figures and shows that k_1 slight decreases in the phase I.

In the following, we will explain the reason to appear the new phases. Since we consider the case that $u_0^{\rm bb} > u_{\uparrow\downarrow}^{\rm bb}$, the interaction energy becomes smaller when the number of the bosons with up-spin and the one with down-spin are equal ($\tilde{S}_z^{\rm b} = 0$). However, this condition is not satisfied only in the phase II. On the other hand, in the phase I, the interaction energy increases because of the spatial variation of the density. Therefore, when the energy loss in the phase I is larger than that in the phase II, the phase transition from the phase I to II is occurred. In fact, we can see that, when Ω increases, the modulation amplitude of the density in the phase I ($\propto \sin(2\theta) = \sqrt{1-(k_1/k_0)^2}$) slight increases and $\tilde{S}_z^{\rm b}$ in the phase II ($\propto \cos(2\theta) = k_1/k_0$) decreases in Fig. 4.4. Note that the phase I vanishes when $u_0^{\rm bb} < u_{\uparrow\downarrow}^{\rm bb}$. This means that the ground state wave function is always expressed by single plane wave as mentioned before.

So far, we have analyzed the Bose system in the rotation frame transformed by the unitary matrix (3.10) from the laboratory frame, however, the spin density and the currents are changed by the unitary transformation. Therefore, we should discuss the physical quantities in the laboratory frame to consider the experimaental circumstance shown in Chap. 3. By using Eq. (3.10), the ansatz in the laboratory frame can be written as $\psi^{\rm b}(x,t) = U_2^\dagger(x,t)\tilde{\psi}^{\rm b}(x)$ and the spin density in the

laboratory frame is given by

$$\begin{aligned}\boldsymbol{S}^{\mathrm{b}}(x,t) &= \begin{pmatrix} \tilde{S}_x^{\mathrm{b}}\cos\Theta - \tilde{S}_y^{\mathrm{b}}\sin\Theta \\ \tilde{S}_x^{\mathrm{b}}\sin\Theta + \tilde{S}_y^{\mathrm{b}}\cos\Theta \\ \tilde{S}_z^{\mathrm{b}} \end{pmatrix}^T \\ &= n_{\mathrm{b}} \begin{pmatrix} -\sin(2\theta)\cos\Theta - 2\beta\left[\cos(2\theta)\sin\Theta\sin(2k_1x+\phi) + \cos\Theta\cos(2k_1x+\phi)\right] \\ -\sin(2\theta)\sin\Theta + 2\beta\left[\cos(2\theta)\cos\Theta\sin(2k_1x+\phi) - \sin\Theta\cos(2k_1x+\phi)\right] \\ \cos(2\theta)\alpha \end{pmatrix}^T, \end{aligned} \tag{4.19}$$

where we defined $\Theta = \Theta(x,t) = 2k_0x - \Delta\omega t$. From Eq. (4.19) and relation $\cos(2\theta) = k_1/k_0$, we can find that the spin density in the laboratory frame is uniform only when $k_1 = k_0$. We can find that these conditions correspond to the case of $\Omega = 0$ from Eq. (4.15). However, since Ω corresponds to the intensity of the Raman lasers to create SO coupling in the experiment, the spin density always has a spatial variation in the artificial SO coupled Bose system. In addition, we can see that the magnitude of the spatial variation of the spin is maximum in the phase III.

4.2.2 Spin current

At the end of this chapter, we analyze the particle and spin currents in the ground state of the SO coupled Bose system. In the beginning, we will analyze the particle current in the laboratory frame. From Eq. (2.30), the particle current is given by

$$\begin{aligned} \boldsymbol{j} &= \tilde{\boldsymbol{j}} + \tilde{\boldsymbol{j}}_U, \\ \tilde{\boldsymbol{j}} &= -\frac{i\hbar}{2m}\left[\left(\nabla\tilde{\psi}^\dagger\right)\tilde{\psi} - \tilde{\psi}^\dagger\left(\nabla\tilde{\psi}\right)\right], \\ \tilde{\boldsymbol{j}}_U &= -\frac{i\hbar}{2m}\left\{\tilde{\psi}^\dagger\left[\left(\nabla U\right)U^\dagger - U\left(\nabla U^\dagger\right)\right]\tilde{\psi}\right\}, \end{aligned}$$

where $\tilde{\boldsymbol{j}}$ is the particle current in the unitary tranformed frame and $\tilde{\boldsymbol{j}}_U$ is the additional term by the unitary transformation. Substituting Eqs. (4.9) and (3.10) into this equation, we can obtain the x-component of the particle current

$$\tilde{j}_x^{\mathrm{b}} = \frac{\hbar k_1}{m}\left(|C_-|^2 - |C_+|^2\right)n_{\mathrm{b}}, \quad \tilde{j}_{U,x} = -\frac{\hbar k_0\cos(2\theta)}{m}\left(|C_-|^2 - |C_+|^2\right)n_{\mathrm{b}}. \tag{4.20}$$

Note that the y- and z-components are zero because y- and z-components$\nabla\tilde{\psi}(x)$ and $\nabla U_2(x,t)$ vanish. However, by using the relation $\cos(2\theta) = k_1/k_0$, we can find that $\boldsymbol{j} = \tilde{\boldsymbol{j}} + \tilde{\boldsymbol{j}}_U = 0$. Therefore, the particle current is induced in the rotation frame but vanishs in the laboratory frame.

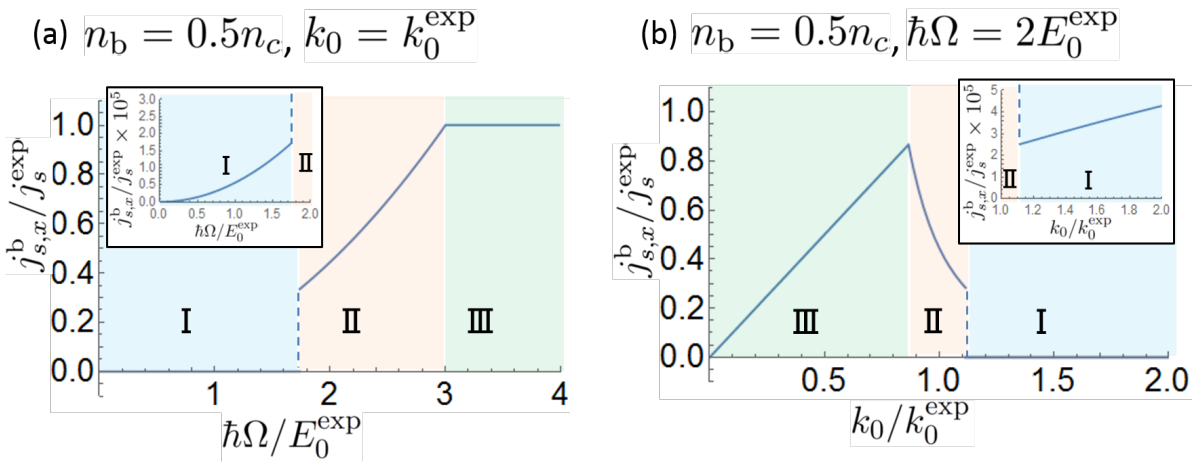

Figure 4.5: Spin current in the SO coupled Bose system. The colors of the lines and Roman numerals indicate the phases of the bosons. Insets are enlarged figures around the phase I and show that the spin current is slightly induced in the phase I. The parameters are $n_{\rm b} = 0.5n_c$, (a) $k_0 = k_0^{\rm exp}$, and (b) $\hbar\Omega = 2E_0^{\rm exp}$. The other parameters are same as in Fig. 4.3.

Next, from Eq. (2.31), the (z-component) spin current is given by

$$\begin{aligned}
\boldsymbol{j}_s &= \tilde{\boldsymbol{j}}_s + \tilde{\boldsymbol{j}}_{sU} \\
\tilde{\boldsymbol{j}}_s &= -\frac{i\hbar}{4m}\left[\left(\nabla\tilde{\psi}^\dagger\right) U\sigma_z U^\dagger\tilde{\psi} - \tilde{\psi}^\dagger U\sigma_z U^\dagger\left(\nabla\tilde{\psi}\right)\right] \\
\tilde{\boldsymbol{j}}_{sU} &= -\frac{i\hbar}{4m}\left\{\tilde{\psi}^\dagger\left[\left(\nabla U\right)\sigma_z U^\dagger - U\sigma_z\left(\nabla U^\dagger\right)\right]\tilde{\psi}\right\}.
\end{aligned}$$

where $\tilde{\boldsymbol{j}}_s$ is the particle current in the unitary tranformed frame and $\tilde{\boldsymbol{j}}_{sU}$ is the additional term by the unitary transformation. Substituting Eqs. (4.9) and (3.10) into this equation, the x-component of the spin current is written as

$$\tilde{j}_{s,x}^{\rm b} = -\frac{\hbar k_1\cos(2\theta)}{2m}n_{\rm b}, \quad \tilde{j}_{sU,x}^{\rm b}(x) = \frac{\hbar k_0}{2m}n^{\rm b}(x).$$

In addition, by using Eq. (4.17) and the relation $\cos(2\theta) = k_1/k_0$, the spin current can be rewritten as

$$\begin{aligned}
j_{s,x}^{\rm b}(x) &= \frac{\hbar n_{\rm b}}{2m}\left\{k_0\left[1 + 2\beta\sin(2\theta)\cos(2k_1x+\phi)\right] - k_1\cos(2\theta)\right\} \\
&= \frac{\hbar k_0 n_{\rm b}}{2m}\sqrt{1-\frac{k_1^2}{k_0^2}}\left[\sqrt{1-\frac{k_1^2}{k_0^2}} + 2\beta\cos(2k_1x+\phi)\right]. \qquad (4.21)
\end{aligned}$$

This equation shows that the spin current is globally induced when $k_1 \neq k_0$ as shown in Fig. 4.5, where we use the normalized parameter $j_s^{\rm exp} = \hbar k_0^{\rm exp} n_{\rm b}/2m$ and show

the mean value because the spin current have a spatial variation only in the phase I. Figure 4.5 shows that the spin current is always induced but it is negligibly small in the phase I. In addition, when Ω or k_0 increase, the spin current increases once, then saturates or decreases. To understand this reason intuitively, we consider the single particle Hamiltonian in the laboratory frame given by

$$h_{\rm so} = \frac{\boldsymbol{p}^2}{2m} + \frac{\hbar\Omega}{2}\left[\sigma_x \cos(2k_0 x - \Delta\omega t) + \sigma_y \sin(2k_0 x - \Delta\omega t)\right] - \frac{\hbar\omega_Z}{2}\sigma_z, \qquad (4.22)$$

where ω_Z is Zeeman shift. This Hamiltonian shows that Ω is the intensity of the spiral magnetic field and k_0 is the parameter expressing the amplitude of the spatial variation. Therefore, when Ω increase or k_0 decrease, the spin of the bosons is well aligned with the spiral magnetic field. On the other hand, when the bosons have a spiral spin structure in x-y plane, the spin current proportional to k_0 is induced as mentioned in Sec. 2.4. As a result, when Ω increase, the bosons well follow the spiral magnetic field and the spin current increases, however, when all the bosons follow the magnetic field completely, the spin current is not increase anymore. In addition, when k_0 increase, the spin current proportional to k_0 is induced, however, the bosons gradually do not follow the spiral magnetic field and the spin current decreases.

Chapter 5

Artificial spin-orbit coupled Fermi system

The artificial spin-orbit (SO) coupled Fermi system has been realized experimentally by using ^{40}K or ^{6}Li degenerate Fermi gases[4, 5]. It is expected that this system can be ued as a simulator of the SO coupled erectron system and a start point of a novel system such as a strong SO couple. Therefore, variety of theoretical and experimental studies on this system have been reported[21, 22, 23, 24, 25, 26, 27].

In this chapter, we analyze the ground state and the spin current in the artificial SO coupled Fermi system. Firstly, we show the ground state pahse diagram and the parameter dependence of the spin current in the SO coupled Fermi system without interaction. Next, we analyze the effect of the weak interaction on the system by using a perturbation theory and show that the effect of the interaction is negligibly small within the experiment.

5.1 Fermi system without interaction

5.1.1 Ground state

Let us consider the SO coupled Fermi gas of $N_{\rm f}$ particles enclosed in a volume V without the interaction. The single-particle Hamiltonian is given by

$$\tilde{h}_{\rm so} = \frac{\boldsymbol{p}^2}{2m} - \frac{\hbar k_0}{m} p_x \sigma_z + \frac{\hbar\Omega}{2}\sigma_x + \frac{\hbar\delta}{2}\sigma_z + E_0, \tag{5.1}$$

where this is the same as Eq. (4.1) and Ω, k_0 and, δ are experimentally tunable parameters. By reminding the discussion in Sec. 4.1, we can find the eigen-energy

$$\epsilon^{\pm}_{\rm so}(\boldsymbol{q}) = \frac{\hbar^2\boldsymbol{q}^2}{2m} + E_0 \pm \sqrt{\left(\frac{\hbar^2}{m}\boldsymbol{q}\cdot\boldsymbol{k}_0 - \frac{\hbar\delta}{2}\right)^2 + \left(\frac{\hbar\Omega}{2}\right)^2}. \tag{5.2}$$

and, the eigen-state

$$\begin{pmatrix}\tilde{\psi}^{+}_{\boldsymbol{q}}\\ \tilde{\psi}^{-}_{\boldsymbol{q}}\end{pmatrix} = \begin{pmatrix}\cos\theta_{q_x} & \sin\theta_{q_x}\\ -\sin\theta_{q_x} & \cos\theta_{q_x}\end{pmatrix}\begin{pmatrix}\tilde{\psi}_{\uparrow,\boldsymbol{q}}\\ \tilde{\psi}_{\downarrow,\boldsymbol{q}}\end{pmatrix}, \tag{5.3}$$

$$\tan\theta_{q_x} = \frac{1}{(\hbar\Omega/2)}\left[\sqrt{\left(\frac{\hbar^2 k_0}{m}q_x - \frac{\hbar\delta}{2}\right)^2 + \left(\frac{\hbar\Omega}{2}\right)^2} + \frac{\hbar^2 k_0}{m}q_x - \frac{\hbar\delta}{2}\right]. \tag{5.4}$$

Since Eq. (5.3) can be rewritten as

$$\begin{pmatrix}\tilde{\psi}_{\uparrow,\boldsymbol{q}}\\ \tilde{\psi}_{\downarrow,\boldsymbol{q}}\end{pmatrix} = \begin{pmatrix}\cos\theta_{q_x} & -\sin\theta_{q_x}\\ \sin\theta_{q_x} & \cos\theta_{q_x}\end{pmatrix}\begin{pmatrix}\tilde{\psi}^{+}_{\boldsymbol{q}}\\ \tilde{\psi}^{-}_{\boldsymbol{q}}\end{pmatrix}, \tag{5.5}$$

the wave function in the non-interacting system in real space can be written as

$$\tilde{\psi}_0(\boldsymbol{r}) = \frac{1}{\sqrt{V}}\sum_{\boldsymbol{q}} e^{i\boldsymbol{q}\cdot\boldsymbol{r}}\tilde{\psi}_{\boldsymbol{q}} = \frac{1}{\sqrt{V}}\sum_{\boldsymbol{q}} e^{i\boldsymbol{q}}\begin{pmatrix}\cos\theta_{q_x}\tilde{\psi}^{+}_{\boldsymbol{q}} - \sin\theta_{q_x}\tilde{\psi}^{-}_{\boldsymbol{q}}\\ \sin\theta_{q_x}\tilde{\psi}^{+}_{\boldsymbol{q}} + \cos\theta_{q_x}\tilde{\psi}^{-}_{\boldsymbol{q}}\end{pmatrix}, \tag{5.6}$$

where $\int d\boldsymbol{r}|\tilde{\psi}_0(\boldsymbol{r})|^2 = N_{\rm f}$. Here, this wave function is in rotational frame and we interested in the properties in the laboratory frame. Therefore, in the following, we use the wave function in the laboratory frame given by

$$\begin{aligned}\psi_0(\boldsymbol{r},t) &= U_2^{\dagger}(x,t)\tilde{\psi}_0(\boldsymbol{r})\\ &= \frac{1}{\sqrt{V}}\sum_{\boldsymbol{q}}\begin{pmatrix}e^{i\left[(\boldsymbol{q}-\boldsymbol{k}_0)\cdot\boldsymbol{r}-(\omega-\frac{\Delta\omega}{2})t\right]}\left[\cos\theta_{q_x}\psi^{+}_{\boldsymbol{q}} - \sin\theta_{q_x}\psi^{-}_{\boldsymbol{q}}\right]\\ e^{i\left[(\boldsymbol{q}+\boldsymbol{k}_0)\cdot\boldsymbol{r}-(\omega+\frac{\Delta\omega}{2})t\right]}\left[\sin\theta_{q_x}\psi^{+}_{\boldsymbol{q}} + \cos\theta_{q_x}\psi^{-}_{\boldsymbol{q}}\right]\end{pmatrix},\end{aligned} \tag{5.7}$$

where we use the unitary matrix (3.10).

The single-particle dispersion is the same as the one of SO coupled Bose system (Fig. 4.1), however, the ground state of the fermions greatly differs from that of the bosons because of the difference of the quantum statistics [4]. When the mean number density of the fermions $n_{\rm f}$ increases at zero temperature, the fermions fill up the energy dispersion up to the Fermi energy and we can classify the ground state into difference of the property of the Fermi sphere as shown in Figs. 5.1(a) and 5.2(a), where Fig. 5.1 is for $\delta = 0$ and Fig. 5.2 is for $\delta \neq 0$. In these figures, we use the normalized paramters $q^0_{\rm F} = (3\pi n_{\rm f})^{\frac{1}{3}}$ and $k_\Omega = (2m\Omega/\hbar)^{\frac{1}{2}}$ and assume that the fermions are ^{40}K. Note that $n_{\rm f} \simeq 6.4\mu{\rm m}^{-3}$ when $q^0_{\rm F}/k_0^{\rm exp} = 1$. The phase diagrams show that the ground states are classified into single Fermi surface (SFS) phase and double Fermi surface (DFS) phases. In addition, Figs. 5.1(b) and 5.2(b) show the relation between Fermi energy $\epsilon_{\rm f}$ and Fermi surface and Fermi surface topologically changes at the phase boundary (Lifshitz transition).

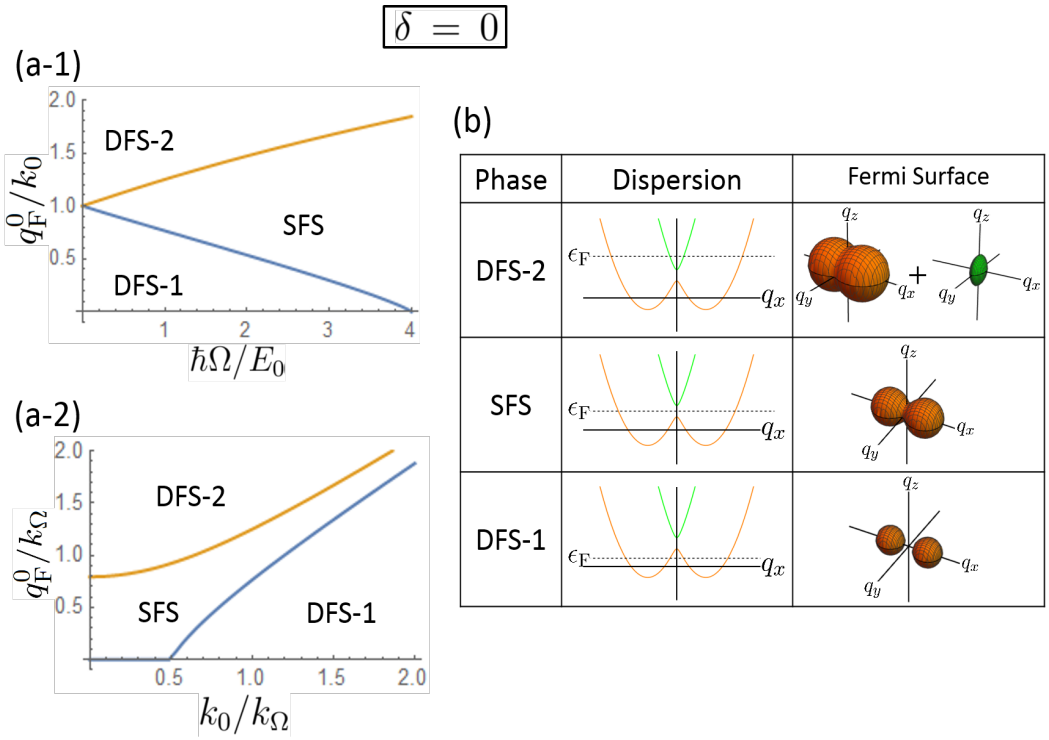

Figure 5.1: (a) Ground state phase diagrams of the SO coupled Fermi system without the interaction for $\delta = 0$. The ground state can be classified by the difference of the Fermi surface such as a single Fermi surface (SFS) and a double Fermi surface (DFS). The parameters are $m = 6.64 \times 10^{-26}$kg, $q_F^0 = (3\pi n_f)^{\frac{1}{3}}$, $k_\Omega = (2m\Omega/\hbar)^{\frac{1}{2}}$, (a-1) $k_0 = k_0^{\rm exp}$, and (a-2) $\hbar\Omega = E_0^{\rm exp}$. (b) Dispersions (5.2) in the q_x direction and Fermi surfaces corresponding to the three phases for $\delta = 0$.

5.1.2 Spin density

In the following, we will calculate the physical quantities of the Fermi system in the laboratory frame. As a beginning, we calculate the density and the spin density. By using Eq. (5.7), the density is given by

$$\left\langle |\psi_0(\boldsymbol{r},t)|^2 \right\rangle = \frac{1}{V}\sum_{\boldsymbol{q}} \left(n_{\boldsymbol{q}}^+ + n_{\boldsymbol{q}}^- \right) = n_{\rm f}, \tag{5.8}$$

where $\langle \cdots \rangle$ means a statistical average and we define Fermi distribution function $n_{\boldsymbol{q}}^{\pm} = \left\langle \left(\psi_{\boldsymbol{q}}^{\pm}\right)^\dagger \psi_{\boldsymbol{q}}^{\pm} \right\rangle$. Equation (5.8) shows that the density is always uniform.

Next, using Eq. (5.7), the spin density per a fermion $\boldsymbol{s}^{\rm f}(\boldsymbol{r},t) = -\left\langle \psi_0^\dagger(\boldsymbol{r},t)\boldsymbol{\sigma}\psi_0(\boldsymbol{r},t) \right\rangle / n_{\rm f}$

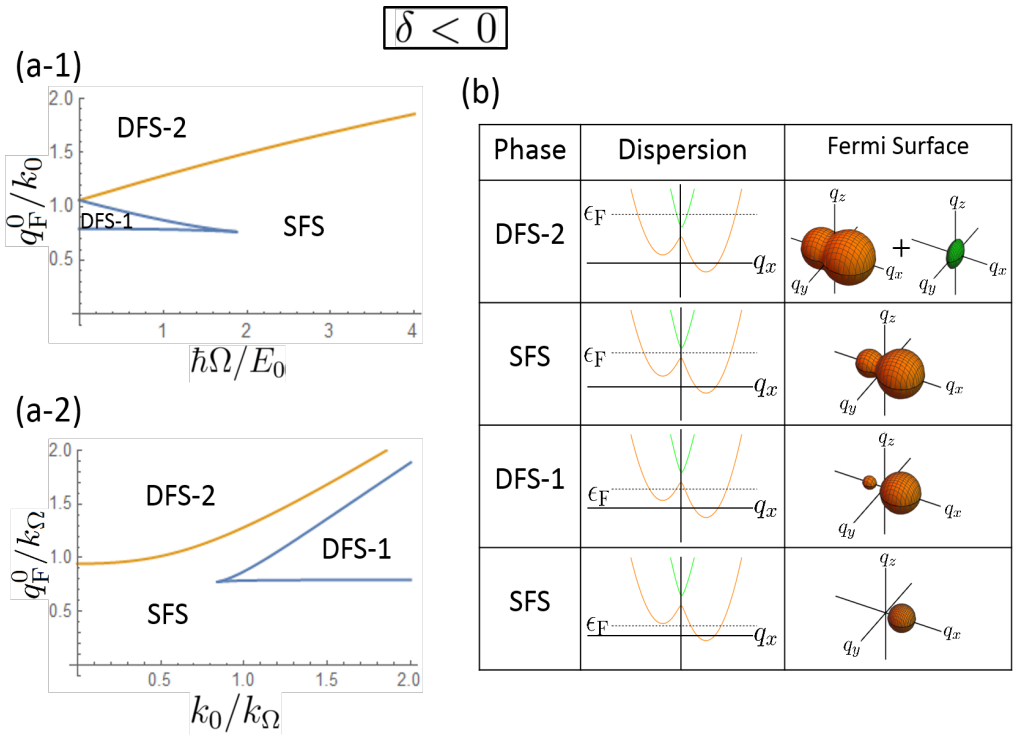

Figure 5.2: (a) Ground state phase diagrams of the SO coupled Fermi system without the interaction for $\delta < 0$. The parameters are (a-1) $\hbar\delta = -E_0$, (a-2) $\delta = -\Omega$, and the other parameters are same as in Fig. 5.1. (b) Dispersions (5.2) in the q_x direction and Fermi surfaces corresponding to the three phases for $\delta < 0$.

can be written as

$$\begin{aligned} s_x^{\rm f}(x,t) &= \frac{1}{n_F V}\sum_{\boldsymbol{q}}\left[\sin(2\theta_{q_x})\left(n_{\boldsymbol{q}}^- - n_{\boldsymbol{q}}^+\right)\right]\cos\Theta = s_p^{\rm f}\cos\Theta, \\ s_y^{\rm f}(x,t) &= \frac{1}{n_F V}\sum_{\boldsymbol{q}}\left[\sin(2\theta_{q_x})\left(n_{\boldsymbol{q}}^- - n_{\boldsymbol{q}}^+\right)\right]\sin\Theta = s_p^{\rm f}\sin\Theta, \\ s_z^{\rm f} &= \frac{1}{n_F V}\sum_{\boldsymbol{q}}\left[\cos(2\theta_{q_x})\left(n_{\boldsymbol{q}}^- - n_{\boldsymbol{q}}^+\right)\right], \end{aligned} \tag{5.9}$$

where $\Theta = \Theta(x,t) = 2k_0 x - \Delta\omega t$ and we define

$$s_p^{\rm f} = \frac{1}{n_F V}\sum_{\boldsymbol{q}}\left[\sin(2\theta_{q_x})\left(n_{\boldsymbol{q}}^+ - n_{\boldsymbol{q}}^-\right)\right].$$

Note that we can find

$$\sin(2\theta_{q_x}) = \frac{\frac{\hbar\Omega}{2}}{\sqrt{\left(\frac{\hbar^2 k_0}{m}q_x - \frac{\hbar\delta}{2}\right)^2 + \left(\frac{\hbar\Omega}{2}\right)^2}}, \quad \cos(2\theta_{q_x}) = \frac{\frac{\hbar^2 k_0}{m}q_x - \frac{\hbar\delta}{2}}{\sqrt{\left(\frac{\hbar^2 k_0}{m}q_x - \frac{\hbar\delta}{2}\right)^2 + \left(\frac{\hbar\Omega}{2}\right)^2}},$$

from Eq. (5.4). By using the replacement $\sum_{\boldsymbol{q}} = \frac{V}{(2\pi)^3}\int d\boldsymbol{q}$ and integrating out Eq. (5.9), we can obtain the spin density as shown in Fig. 5.3. The figure shows that $s_p^{\rm f}$ increases with increasing Ω and decreases with increasing k_0. These phenomena can be explained from the single-particle Hamiltonian in the laboratory frame given by

$$h_{\rm so} = \frac{\boldsymbol{p}^2}{2m} + \frac{\hbar\Omega}{2}\left[\sigma_x\cos(2k_0x - \Delta\omega t) + \sigma_y\sin(2k_0x - \Delta\omega t)\right] - \frac{\hbar\omega_Z}{2}\sigma_z, \qquad (5.10)$$

as mentioned in Sec. 4.2.2. In this equation, the parameters Ω and k_0 correspond to the amplitude of the spiral magnetic field and the spatial variation of the magnetic field, respectively. If the fermion spins follow the spiral magnetic field, the fermions can gain the magnetic interaction energy but lose some kinetic energy. Therefore, when Ω increases, the gain the magnetic interaction energy also increases and, when the pitch π/k_0 decreases, the loss of the kinetic energy increases. These are the reasons of the behavior of $s_p^{\rm f}$. In addition, Fig. 5.3 also shows that the z-spin $s_z^{\rm f}$ is nonzero when the intensity of the magnetic field in z direction δ is nonzero.

5.1.3 Spin current

In this subsection, we analyze the particle and spin current density of the SO coupled fermions without the interaction. By substituting Eq. (5.7) into Eq. (2.9), the particle current can be written as

$$\begin{aligned}\boldsymbol{j}^{\rm f}(\boldsymbol{r}) &= -\frac{i\hbar}{2m}\left\langle\left[\nabla\psi_0^\dagger(\boldsymbol{r})\right]\psi_0(\boldsymbol{r}) - \psi_0^\dagger(\boldsymbol{r})\left[\nabla\psi_0(\boldsymbol{r})\right]\right\rangle \\ &= \frac{\hbar}{mV}\sum_{\boldsymbol{q}}\left[\boldsymbol{q}\left(n_{\boldsymbol{q}}^+ + n_{\boldsymbol{q}}^-\right) + \boldsymbol{k}_0\cos(2\theta_{q_x})\left(n_{\boldsymbol{q}}^+ - n_{\boldsymbol{q}}^-\right)\right]. \qquad (5.11)\end{aligned}$$

By calculating this equation, we can find that it becomes zero. Therefore, the particle current is not induced in the SO coupled Fermi system.

Next, we will calculate the spin current density. Substituting Eq. (5.7) to Eq. (2.18), the spin current density is given by

$$\begin{aligned}\boldsymbol{j}_s^{\rm f}(\boldsymbol{r}) &= -\frac{i\hbar}{2m}\left\langle\left[\nabla\psi_0^\dagger(\boldsymbol{r})\right]\sigma_z\psi_0(\boldsymbol{r}) - \psi_0^\dagger(\boldsymbol{r})\sigma_z\left[\nabla\psi_0(\boldsymbol{r})\right]\right\rangle \\ &= \frac{\hbar}{2mV}\sum_{\boldsymbol{q}}\left[\boldsymbol{q}\cos(2\theta_{q_x})\left(n_{\boldsymbol{q}}^+ - n_{\boldsymbol{q}}^-\right)\right] + \frac{\hbar\boldsymbol{k}_0}{2m}n_{\rm f}. \qquad (5.12)\end{aligned}$$

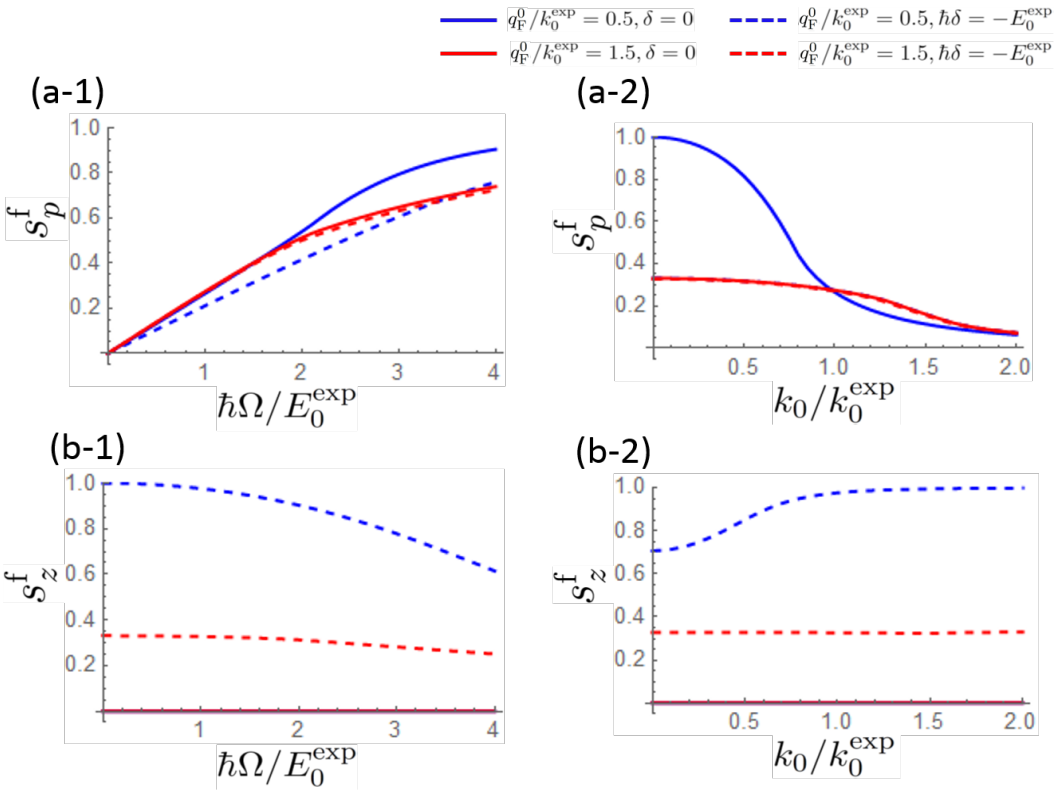

Figure 5.3: (a) Spiral spin density $s_p^{\rm f}$ and (b) z-spin density $s_z^{\rm f}$ in the SO coupled Fermi system without the interaction. The solid lines are for $q_{\rm F}^0/k_0^{\rm exp} = 0.5$ (blue) and for $q_{\rm F}^0/k_0^{\rm exp} = 1.5$ (red) with $\delta = 0$ and the dashed lines are for $q_{\rm F}^0/k_0^{\rm exp} = 0.5$ (blue) and for $q_{\rm F}^0/k_0^{\rm exp} = 1.5$ (red) with $\hbar\delta = -E_0^{\rm exp}$. The parameters are (a-1, b-1) $k_0 = k_0^{\rm exp}$ and (a-2, b-2) $k_\Omega = k_0^{\rm exp}$ and the other parameters are same as in Fig. 5.1.

From this equation, we can find that $j_{s,y}^{\rm f} = j_{s,z}^{\rm f} = 0$ and only $j_{s,x}^{\rm f}$ has a finite value as shown in Fig. 5.4, where we use the normalized parameter $j_s^{\rm exp} = \hbar k_0^{\rm exp} n_{\rm f}/m$. In Figs. 5.4, the spin current increases with increasing Ω and exhibits a peak with increasing k_0. These behaviors are same as that of the SO coupled Bose system and can be understood as mentioned in Sec. 4.2.2. However, the spin current of the fermions changes continuously and smoothly even if the phase transitions occur because of the difference of the quantum statistics.

5.2 Effect of weak interaction on the spin current

We have considered non-interacting Fermi system so far. Then, at the end of this chapter, we show the effect of the weak interaction on the spin current of the SO coupled Fermi system by using a perturbation theory. The Hamiltonian with the

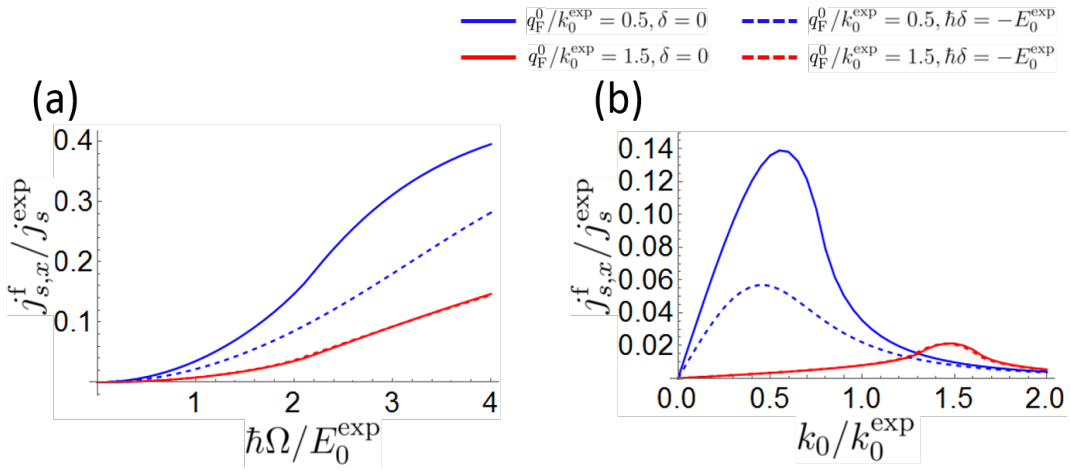

Figure 5.4: Spin current in the SO coupled Fermi system without the interaction. The lines and the parameters are same as in Fig. 5.3.

interaction is given by

$$H = H_0 + H_{\rm int}, \tag{5.13}$$

$$H_0 = \sum_j^{N_F} h_{\rm so}(j), \tag{5.14}$$

$$H_{\rm int} = \int dx \int dx' \psi_\uparrow^\dagger(x)\psi_\downarrow^\dagger(x') \left[u^{\rm ff}\delta(x-x')\right] \psi_\downarrow(x')\psi_\uparrow(x), \tag{5.15}$$

where $x = (\boldsymbol{r}, t)$, $u^{\rm ff}$ is the relevant coupling constants between the different spin channels of the fermions and $N_{\rm F}$ is the number of the fermions. In the following, we assume repulsive interaction ($u^{\rm ff} > 0$) and the interaction energy is weak enough in comparison with the system's typical energy scale. Note that $u^{\rm ff} n_{\rm f}/E_0^{\rm exp} \simeq 10^{-1} \sim 10^{-3}$ in the experiment.

To investigate the effect of the interaction, we use Green functions given by

$$G(x,x') = \begin{pmatrix} G_{\uparrow\uparrow}(x,x') & G_{\uparrow\downarrow}(x,x') \\ G_{\downarrow\uparrow}(x,x') & G_{\downarrow\downarrow}(x,x') \end{pmatrix}, \tag{5.16}$$

$$G_{\alpha\beta}(x,x') = -i\left\langle {\rm T}\left[\psi_{\alpha,{\rm H}}(x)\psi_{\beta,{\rm H}}^\dagger(x')\right]\right\rangle \quad (\alpha,\beta = \uparrow,\downarrow), \tag{5.17}$$

where ${\rm T}[\cdots]$ is the time-order operator and $\psi_{\alpha,{\rm H}}$ is the wave function with spin α in Heisenberg picture. Then, the density can be written as

$$\langle n(\boldsymbol{r},t)\rangle = \left\langle \psi_{\rm H}^\dagger(\boldsymbol{r},t)\psi_{\rm H}(\boldsymbol{r},t)\right\rangle = -\left\langle {\rm T}\left[\psi_{\rm H}(\boldsymbol{r},t)\psi_{\rm H}^\dagger(\boldsymbol{r},t^+)\right]\right\rangle = -i{\rm Tr}\left[G(\boldsymbol{r}t,\boldsymbol{r},t^+)\right], \tag{5.18}$$

where $t^+ = t + \eta$ and η is a positive infinitesimal quantity. In the same way, the spin density and the spin current can be written as

$$\langle \boldsymbol{s}(\boldsymbol{r},t)\rangle = -i\mathrm{Tr}\left[\boldsymbol{\sigma}G(\boldsymbol{r}t,\boldsymbol{r}t^+)\right], \tag{5.19}$$

$$\langle \boldsymbol{j}_s(\boldsymbol{r},t)\rangle = -\frac{\hbar\left(\nabla-\nabla'\right)}{2m}\mathrm{Tr}\left[\sigma_z G(\boldsymbol{r}'t,\boldsymbol{r}t^+)\right]\Big|_{\boldsymbol{r}'\to\boldsymbol{r}}. \tag{5.20}$$

When the interaction can be regarded as a perturbation, Green function can be written as[63]

$$G(x,x') \simeq G^{(0)}(x,x') + G^{(1)}(x,x'), \tag{5.21}$$

where the zeroth- and first-order Green functions are given by

$$G^{(0)}_{\alpha\beta}(x,x') = -i\left\langle \mathrm{T}\left[\psi^{(0)}_{\alpha,\mathrm{H}}(x)\psi^{(0)\dagger}_{\beta,\mathrm{H}}(x')\right]\right\rangle, \tag{5.22}$$

$$G^{(1)}_{\alpha\beta}(x,x') = -\frac{u^{\mathrm{ff}}}{\hbar}\int dx_1\int dx_2\delta(x_1-x_2)\sum_{\gamma=\uparrow,\downarrow}\Big[-G^{(0)}_{\alpha\gamma}(x,x_1)G^{(0)}_{\bar{\gamma}\bar{\gamma}}(x_2,x_2)G^{(0)}_{\gamma\beta}(x_1,x') + G^{(0)}_{\alpha\gamma}(x,x_1)G^{(0)}_{\gamma\bar{\gamma}}(x_1,x_2)G^{(0)}_{\bar{\gamma}\beta}(x_2,x')\Big]. \tag{5.23}$$

In these equations, $\psi^{(0)}_{\alpha,\mathrm{H}}(x)$ is the wave function of the fermions with spin α and no interaction and $\bar{\gamma}$ denotes an opposite spin of γ. In Eqs. (5.18), (5.19), and (5.20), all Green functions are formed by $G(\boldsymbol{r}'t,\boldsymbol{r}t^+)$ and it can be rewritten as

$$G_{\alpha\beta}(\boldsymbol{r}'t,\boldsymbol{r}t^+) = -i\left\langle \mathrm{T}\left[\psi_{\alpha,\mathrm{H}}(\boldsymbol{r}',t)\psi^\dagger_{\beta,\mathrm{H}}(\boldsymbol{r},t^+)\right]\right\rangle = i\left\langle \psi^\dagger_{\beta,\mathrm{H}}(\boldsymbol{r},t^+)\psi_{\alpha,\mathrm{H}}(\boldsymbol{r}',t)\right\rangle. \tag{5.24}$$

Therefore, by substituting Eq. (5.7) into Eq. (5.22), the zeroth-order Green functions can be written as

$$\begin{aligned}
G^{(0)}_{\uparrow\uparrow}(\boldsymbol{r}'t,\boldsymbol{r}t^+) &= \frac{i}{V}\sum_{\boldsymbol{q}} e^{i(\boldsymbol{q}+\boldsymbol{k}_0)\cdot(\boldsymbol{r}-\boldsymbol{r}')}\left(\cos^2\theta_{q_x}n^+_{\boldsymbol{q}} + \sin^2\theta_{q_x}n^-_{\boldsymbol{q}}\right),\\
G^{(0)}_{\downarrow\downarrow}(\boldsymbol{r}'t,\boldsymbol{r}t^+) &= \frac{i}{V}\sum_{\boldsymbol{q}} e^{i(\boldsymbol{q}-\boldsymbol{k}_0)\cdot(\boldsymbol{r}-\boldsymbol{r}')}\left(\sin^2\theta_{q_x}n^+_{\boldsymbol{q}} + \cos^2\theta_{q_x}n^-_{\boldsymbol{q}}\right),\\
G^{(0)}_{\uparrow\downarrow}(\boldsymbol{r}'t,\boldsymbol{r}t^+) &= \frac{i}{V}\sum_{\boldsymbol{q}} e^{i\boldsymbol{q}\cdot(\boldsymbol{r}-\boldsymbol{r}')-i\boldsymbol{k}_0\cdot(\boldsymbol{r}+\boldsymbol{r}')}\sin\theta_{q_x}\cos\theta_{q_x}\left(n^+_{\boldsymbol{q}} - n^-_{\boldsymbol{q}}\right),\\
G^{(0)}_{\downarrow\uparrow}(\boldsymbol{r}'t,\boldsymbol{r}t^+) &= \frac{i}{V}\sum_{\boldsymbol{q}} e^{i\boldsymbol{q}\cdot(\boldsymbol{r}-\boldsymbol{r}')+i\boldsymbol{k}_0\cdot(\boldsymbol{r}+\boldsymbol{r}')}\sin\theta_{q_x}\cos\theta_{q_x}\left(n^+_{\boldsymbol{q}} - n^-_{\boldsymbol{q}}\right).
\end{aligned}$$

By using these zeroth-order Green functions and Eq. (5.23), the first-order term of the density is given by

$$n^{(1)} = -i\mathrm{Tr}\left[G^{(1)}(\boldsymbol{r}t, \boldsymbol{r}, t^+)\right] = \frac{u^{\mathrm{ff}}}{2\hbar V^2}\left[\left(\sum_{\boldsymbol{q}} F^0_{\boldsymbol{q}}\right)^2 - \sum_{\boldsymbol{q}_1,\boldsymbol{q}_2} n_{\boldsymbol{q}_1} F^-_{\boldsymbol{q}_2}\right],$$

where we define

$$F^0_{\boldsymbol{q}} = \left(n^-_{\boldsymbol{q}} - n^+_{\boldsymbol{q}}\right)\cos\left(2\theta_{q_x}\right), \quad F^\pm_{\boldsymbol{q}} = n^\pm_{\boldsymbol{q}} + n^\mp_{\boldsymbol{q}}\cos^2\left(2\theta_{q_x}\right),$$

and $n_{\boldsymbol{q}} = n^-_{\boldsymbol{q}} + n^+_{\boldsymbol{q}}$. In the same way, from Eqs. (5.19) and (5.20), the first-order terms of the spin density and the spin current are given by

$$\begin{aligned}
s_x^{\mathrm{f}(1)} &= s_p^{\mathrm{f}(1)}\cos\Theta, \quad s_y^{\mathrm{f}(1)} = s_p^{\mathrm{f}(1)}\sin\Theta, \\
s_z^{\mathrm{f}(1)} &= \frac{u^{\mathrm{ff}}}{2\hbar n_{\mathrm{f}} V^2}\sum_{\boldsymbol{q}_1,\boldsymbol{q}_2}\left(n_{\boldsymbol{q}_1}F^0_{\boldsymbol{q}_2} - F^+_{\boldsymbol{q}_1}F^0_{\boldsymbol{q}_2}\right), \\
\boldsymbol{j}_s^{\mathrm{f}(1)} &= \frac{u^{\mathrm{ff}}}{2mV^2}\sum_{\boldsymbol{q}_1,\boldsymbol{q}_2}\left[n_{\boldsymbol{q}_1}\left(\boldsymbol{k}_0F^+_{\boldsymbol{q}_2} - \boldsymbol{q}F^0_{\boldsymbol{q}_2}\right) + \left(\boldsymbol{q}_1F^+_{\boldsymbol{q}_1} - \boldsymbol{k}_0F^0_{\boldsymbol{q}_1}\right)F^0_{\boldsymbol{q}_2}\right],
\end{aligned}$$

where $s_p^{\mathrm{f}(1)}$ is the first-order term of the spiral spin density [1)]. These equations show that the interaction does not cause a new time-space variation and only the amplitude of the physical quantities changes in the system. As a result, we can obtain the first-order effect of the interaction on the physical quantities as shown in Fig. 5.5. Note that $u^{\mathrm{ff}}n_{\mathrm{f}}/E_0^{\mathrm{exp}} \simeq 3.4\times10^{-3}$ when $q^0_{\mathrm{F}}/k_0^{\mathrm{exp}} = 0.5$ ($n_{\mathrm{f}} \simeq 0.8\mu\mathrm{m}^{-3}$) and $u^{\mathrm{ff}}n_{\mathrm{f}}/E_0^{\mathrm{exp}} \simeq 9.1\times10^{-2}$ when $q^0_{\mathrm{F}}/k_0^{\mathrm{exp}} = 1.5$ ($n_{\mathrm{f}} \simeq 22\mu\mathrm{m}^{-3}$). In Fig. 5.5, the physical quantities change complicatedly and it is difficult to understand these properties intuitively. However, the results show the important facts that the effect of the interaction on the system is negligibly small within the experimental parameters.

[1)] The concrete form of $s_p^{\mathrm{f}(1)}$ is given by

$$\begin{aligned}
s_p^{\mathrm{f}(1)} = \frac{u^{\mathrm{ff}}}{\hbar n_{\mathrm{f}} V^2}\sum_{\boldsymbol{q}_1,\boldsymbol{q}_2}\Big\{ &-\Big[\left(n^-_{\boldsymbol{q}_1} - n^+_{\boldsymbol{q}_1}\right)^2\cos^2\theta_{q_{1x}}\sin^2\theta_{q_{1x}} + \left(n^-_{\boldsymbol{q}_1-2\boldsymbol{k}_0}\cos^2\theta_{q_{1x}-2k_0} + n^+_{\boldsymbol{q}_1-2\boldsymbol{k}_0}\sin^2\theta_{q_{1x}-2k_0}\right) \\
&\times\left(n^+_{\boldsymbol{q}_1+2\boldsymbol{k}_0}\cos^2\theta_{q_{1x}+2k_0} + n^-_{\boldsymbol{q}_1+2\boldsymbol{k}_0}\sin^2\theta_{q_{1x}+2k_0}\right)\Big]\left(n^-_{\boldsymbol{q}_2} - n^+_{\boldsymbol{q}_2}\right)\cos\theta_{q_{2x}}\sin\theta_{q_{2x}} \\
&+\left(n^-_{\boldsymbol{q}_1-\boldsymbol{k}_0}\cos^2\theta_{q_{1x}-k_0} + n^+_{\boldsymbol{q}_1-\boldsymbol{k}_0}\sin^2\theta_{q_{1x}-k_0}\right)\left(n^-_{\boldsymbol{q}_1+\boldsymbol{k}_0} - n^+_{\boldsymbol{q}_1+\boldsymbol{k}_0}\right)\cos\theta_{q_{1x}+k_0}\sin\theta_{q_{1x}+k_0} \\
&\times\left(n^+_{\boldsymbol{q}_2}\cos^2\theta_{q_2} + n^-_{\boldsymbol{q}_2}\sin^2\theta_{q_2}\right) + \left(n^+_{\boldsymbol{q}_1+\boldsymbol{k}_0}\cos^2\theta_{q_{1x}+k_0} + n^-_{\boldsymbol{q}_1+\boldsymbol{k}_0}\sin^2\theta_{q_{1x}+k_0}\right) \\
&\times\left(n^-_{\boldsymbol{q}_1-\boldsymbol{k}_0} - n^+_{\boldsymbol{q}_1-\boldsymbol{k}_0}\right)\cos\theta_{q_{1x}-k_0}\sin\theta_{q_{1x}-k_0}\left(n^-_{\boldsymbol{q}_2}\cos^2\theta_{q_2} + n^+_{\boldsymbol{q}_2}\sin^2\theta_{q_2}\right)\Big\}.
\end{aligned}$$

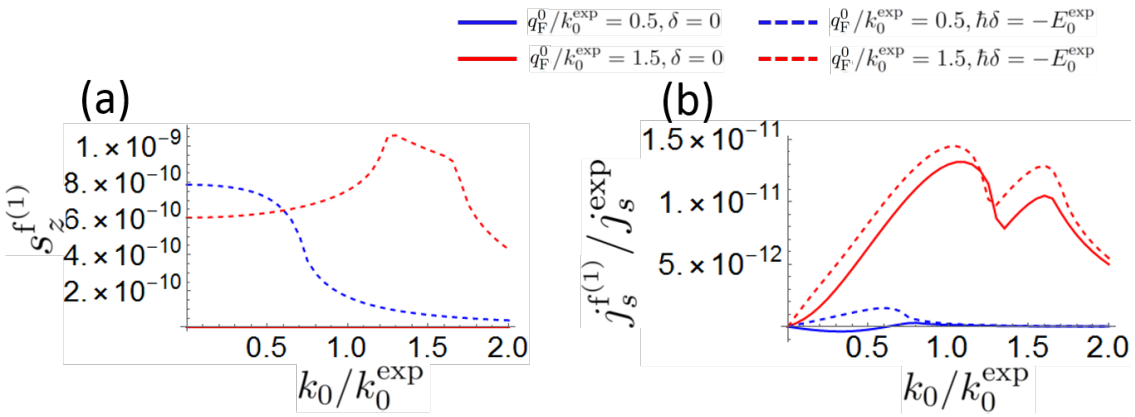

Figure 5.5: First-order terms of (a) the z-spin density and (b) the spin current for $u^{\rm ff} = 4\pi\hbar^2(105a_B)/m$ [64]. The lines and the parameters are same as in Figs. 5.3.

Chapter 6

Artificial spin-orbit coupled Bose-Fermi mixture

In the above chapters, we have analyzed the SO coupled Bose and Fermi systems. As a result, we could find that the spin density have a spiral structure and the spin current is induced in these systems. In addition, the behaviors of the bosons and the fermions were different in spite of the system described by the same single-particle Hamiltonian. On the other hand, the progress of cold atom experiments has realized a Bose-Fermi mixtures by using alkali atoms such as ^{7}Li and ^{6}Li or ^{87}Rb and ^{40}K [28, 29, 30]. The Bose-Fermi mixtures where atoms of different quantum statistics coexist could have a variety of aspects and have been studied from different viewpoint[31, 32, 33, 34]. From these facts, we can expect the appearance of a novel phenomenon in the SO coupled Bose-Fermi mixture.

In this chapter, we show the ground state phase diagram and the spin current of the fermions in the mixture of the fermions and the SO coupled bosons[66, 67, 53, 52]. In Sec. 6.1, the ground state phase diagram of the bosons is shown in the mixture without the Bose-Fermi spin interaction by using the variational method and the tight-binding approximation[66, 67]. Next, in Sec. 6.2, we present the ground state phase diagram and the spin current in the mixture with the Bose-Fermi spin interaction[53].

6.1 Bose-Fermi mixture without Bose-Fermi spin interaction

6.1.1 Model and method

Let us consider a mixture of a spin-1/2 fermions and SO coupled spin-1/2 bosons without Bose-Fermi spin interaction. The total Hamiltonian H is given by

$$H = H^{\mathrm{b}} + H_0^{\mathrm{f}} + H^{\mathrm{bf}}, \tag{6.1}$$

$$H^{\mathrm{b}} = \sum_{j=1}^{N_{\mathrm{b}}} \tilde{h}_{\mathrm{so}}^{\mathrm{b}}(j) + \frac{1}{2}\sum_{\alpha,\,\beta}\int d\boldsymbol{r}\; u_{\alpha\beta}^{\mathrm{bb}} n_\alpha^{\mathrm{b}}(\boldsymbol{r}) n_\beta^{\mathrm{b}}(\boldsymbol{r}), \tag{6.2}$$

$$H_0^{\mathrm{f}} = \sum_{\alpha}\sum_{j=1}^{N_f} \tilde{h}_\alpha^{\mathrm{f}}(j), \tag{6.3}$$

$$H^{\mathrm{bf}} = \sum_{\alpha,\,\beta}\int d\boldsymbol{r}\; u_{\alpha\beta}^{\mathrm{bf}} n_\alpha^{\mathrm{b}}(\boldsymbol{r}) n_\beta^{\mathrm{f}}(\boldsymbol{r}), \tag{6.4}$$

where the superscripts b and f indicate boson and fermion, respectively, and α and β ($=\uparrow,\downarrow$) are the spin indices. $N^{\mathrm{b(f)}}$ is the number of bosons (fermions), $n_\alpha^{\mathrm{b(f)}}(\boldsymbol{r})$ is the number density of bosons (fermions) with spin α, and $u^{\mathrm{bb(f)}}$ are the boson-boson (boson-fermion) interactions. The Bose Hamiltonian (6.2) is the same as Eq. (4.7). Equation (6.3) expresses the Fermi Hamiltonian without the interaction where $\tilde{h}_\alpha^{\mathrm{f}} = \boldsymbol{p}_\alpha^2/2m_{\mathrm{f}}$ is the single-particle Hamiltonian for spin α and H^{bf} is the Bose-Fermi interaction Hamiltonian. For simplicity, we assume that the bosons and the fermions have the same mass ($m_{\mathrm{b}} = m_{\mathrm{f}} = m$), $\delta = 0$, $u_{\uparrow\uparrow}^{\mathrm{bb}} = u_{\downarrow\downarrow}^{\mathrm{bb}} = u_0^{\mathrm{bb}} > u_{\uparrow\downarrow}^{\mathrm{bb}}$, $u_{\uparrow\uparrow}^{\mathrm{bf}} = u_{\downarrow\downarrow}^{\mathrm{bf}} = u_0^{\mathrm{bf}} \geq u_{\uparrow\downarrow}^{\mathrm{bf}}$, and the number of the fermions is much smaller than that of the bosons. Under these assumptions, we will show the ground state phase diagram of the SO coupled bosons in the Bose-Fermi mixture by using a variational method and tight-binding approximation.

Since we assumed the weak Bose-Fermi interaction and the number of the fermions is small, it is expected that we can use the same analysis of the Bose system as Sec. 4.2. Therefore, we employ the same variational wave function (4.9) for the bosons. Substituting Eq. (4.9) to Eq. (6.4) and using Eq. (6.3), we can find the single-particle Hamiltonian of the fermion with spin α including the Bose-Fermi interactions:

$$h_{\sigma,\mathrm{tot}}^{\mathrm{f}} = h_\sigma^{\mathrm{f}} + U_1^{\mathrm{bf}} + U(\alpha,\theta)\cos(2k_1 x + \phi) + \sigma\alpha U_2^{\mathrm{bf}}\cos(2\theta), \tag{6.5}$$

where we define

$$U_1^{\mathrm{bf}} = \frac{u_0^{\mathrm{bf}} + u_{\uparrow\downarrow}^{\mathrm{bf}}}{2} n_{\mathrm{b}}, \quad U_2^{\mathrm{bf}} = \frac{u_0^{\mathrm{bf}} - u_{\uparrow\downarrow}^{\mathrm{bf}}}{2} n_{\mathrm{b}}, \quad U(\alpha,\theta) = U_1^{\mathrm{bf}}\sin(2\theta)\sqrt{1-\alpha^2},$$

and $\alpha = |C_+|^2 - |C_-|^2$. When $\alpha = \pm 1$, we have $U(\pm 1, \theta) = 0$ and the energy per fermion with spin α is given by

$$\epsilon^{\rm f}_{\sigma,\alpha=\pm 1}(\boldsymbol{q};\alpha,\theta) = \frac{\hbar^2 \boldsymbol{q}^2}{2m} + U_1^{\rm bf} + \sigma\alpha U_2^{\rm bf}\cos(2\theta). \tag{6.6}$$

When $\alpha \neq \pm 1$, we have the periodic potential term in Eq. (6.5) and use tight-binding approximation to calculate the energy. In the approximation, the Hamiltonian (6.5) becomes

$$\begin{aligned} h^{\rm f}_{\sigma,\rm tot} \simeq & \sum_{i,\boldsymbol{q}_\perp} \Big\{ -J(k_1,\alpha,\theta)(a^\dagger_{i,\sigma,\boldsymbol{q}_\perp} a_{i+1,\sigma,\boldsymbol{q}_\perp} + a^\dagger_{i+1,\sigma,\boldsymbol{q}_\perp} a_{i,\sigma,\boldsymbol{q}_\perp}) \\ & + \left[\frac{\hbar^2 \boldsymbol{q}_\perp^2}{2m} + U_1^{\rm bf} - |U(\alpha,\theta)| + \sigma\alpha U_2^{\rm bf}\cos(2\theta) \right] a^\dagger_{i,\sigma,\boldsymbol{q}_\perp} a_{i,\sigma,\boldsymbol{q}_\perp} \Big\}, \end{aligned} \tag{6.7}$$

where $\boldsymbol{q}_\perp = (q_y, q_z)$, $a_{\alpha,i,\boldsymbol{q}_\perp}$ ($a^\dagger_{\alpha,i,\boldsymbol{q}_\perp}$) is the annihilation (creation) operator of a fermion with spin α and momentum $\boldsymbol{q}_\perp$ at site i on the x axis, and $J(k_1,\alpha,\theta)$ is the hopping parameter in the x direction. In the limit $U(\alpha,\theta) \gg E_1(k_1) = \hbar^2 k_1^2/(2m)$, the hopping parameter can be approximately obtained from the lowest band of the 1D Mathieu equation[65] as

$$J(k_1,\alpha,\theta) = \frac{4E_1(k_1)}{\sqrt{\pi}} \left(\frac{|U(\alpha,\theta)|}{E_1(k_1)} \right)^{\frac{3}{4}} \exp\left[-2 \left(\frac{|U(\alpha,\theta)|}{E_1(k_1)} \right)^{\frac{1}{2}} \right]. \tag{6.8}$$

The detail of the derivation of Eqs. (6.7) and (6.8) is shown in appendix C. Under the present conditions, the eigen-energy of the Hamiltonian (6.7) is provided by

$$\begin{aligned} \epsilon^{\rm f}_{\sigma,\alpha\neq\pm 1}(\boldsymbol{q};k_1,\alpha,\theta) = & \frac{\hbar^2 \boldsymbol{q}_\perp^2}{2m} + U_1^{\rm bf} - |U(\alpha,\theta)| \\ & + \sigma\alpha U_2^{\rm bf}\cos(2\theta) - 2J(k_1,\alpha,\theta)\cos\left(\frac{\pi q_x}{k_1}\right). \end{aligned} \tag{6.9}$$

The energy difference between Eqs. (6.6) and (6.9) is given by $\hbar^2 q_x^2/(2m) - |U(\alpha,\theta)| - 2J(k_1,\alpha,\theta)\cos(\pi q_x/k_1)$, which depends only on the strength of the Bose-Fermi interactions, not on the sign of the interactions. This result comes from the fact that, for repulsive the Bose-Fermi interactions, the fermions are located in the valleys of the periodic potential and, for attractive interactions, the fermions are in the peaks of the periodic potential in the tight-binding approximation. Since these two situations are equivalent to each other energetically, the resulting energy is independent of the sign of the Bose-Fermi interactions. We therefore assume $u_0^{\rm bf}, u_{\uparrow\downarrow}^{\rm bf} > 0$ in the followings without loss of generality.

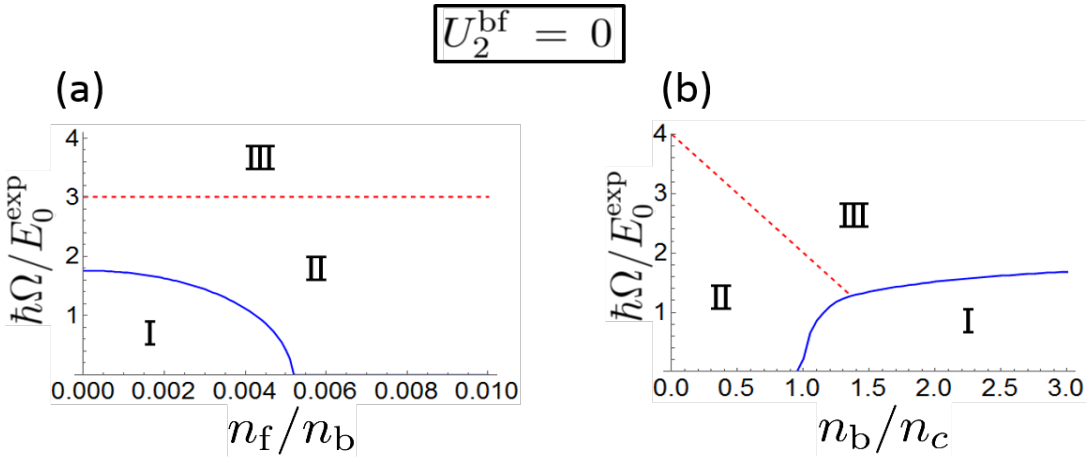

Figure 6.1: Ground state phase diagrams of the bosons in the SO coupled Bose-Fermi mixture with $U_2^{\rm bf} = 0$ ($u_{\uparrow\downarrow}^{\rm bf} = u_0^{\rm bf}$) at zero temperature. The solid and dashed lines represent the first- and second-order phase boundaries, respectively. The parameters are $u_0^{\rm bf} = u_0^{\rm bb}$, (a) $n_{\rm b} = 0.5n_c$, and (b)$n_{\rm f} = 0.01n_c$. The other parameters are same as in Fig. 4.3.

6.1.2 Ground state phase diagram

From Eqs. (6.6), (6.9), and the Bose energy (4.10), we can obtain the total energy of the SO coupled Bose-Fermi mixture as a function of the variational parameters. Minimizing the energy with respect to the variational parameters, we obtain the ground state phase diagram of the boson in the SO coupled Bose-Fermi mixture. In the following, we consider the phase diagram for two cases, $U_2^{\rm bf} = 0$ and $U_2^{\rm bf} > 0$.

Firstly, we consider the case of $U_2^{\rm bf} = 0$ ($u_0^{\rm bf} = u_{\uparrow\downarrow}^{\rm bf}$) [66]. In this case, we can obtain the ground state phase diagram of the bosons as shown in Fig. 6.1, where we use the mean number density of the fermions $n_{\rm f} = N_{\rm f}/V$. The figures show that even a small number of the fermions ($n_{\rm f}/n_{\rm b} < 0.01$) have a significant influence on the ground state property of the bosons. This is because all the bosons take two degenerated states (phase I) or a single state (phases II and III) having a low energy while the fermions, even if the number is small, fill up the energy dispersion up to the Fermi energy and take a relatively large energy. Note that, from these facts, we can find that the effect of the fermions on the bosons becomes smaller when $n_{\rm b}$ is small even if the ratio of $n_{\rm b}$ to $n_{\rm f}$ is the same as in the Fig. 6.1. This can be confirmed in the next section.

In the phase diagrams, one can also see that there is a phase transition from the phase I to II as the number of the fermions increases. In the phase II, the bosons have a uniform density and the fermions interacting with the bosons can also have a uniform density which is energetically favorable to the fermions. In the phase I, on the other hand, the bosons have a modulated density and the Bose-Fermi

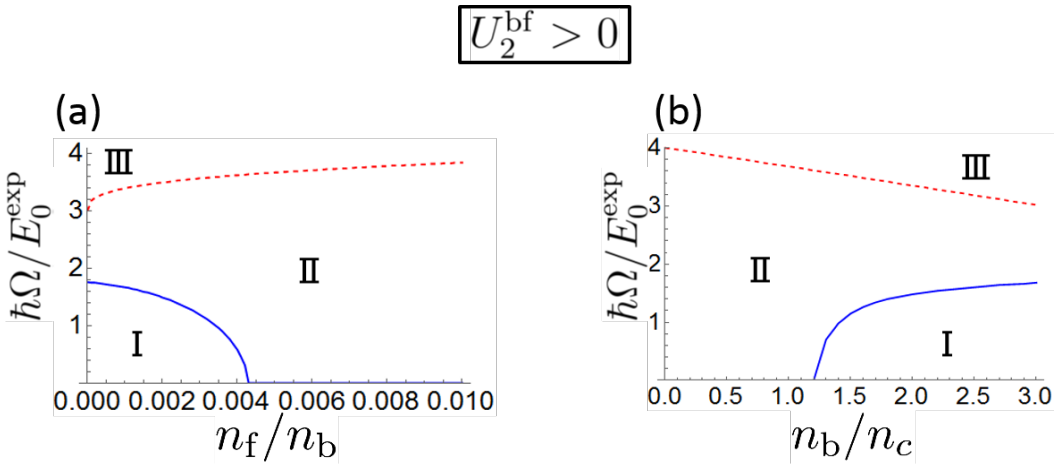

Figure 6.2: Ground state phase diagrams of the bosons in the SO coupled Bose-Fermi mixture with $U_2^{\rm bf} \sim 0.11 U_1^{\rm bf} (u_{\uparrow\downarrow}^{\rm bf}/u_0^{\rm bf} = 0.8)$ at zero temperature. The solid and dashed lines represent the first- and second-order phase boundaries, respectively. The parameters except $U_2^{\rm bf}$ are same as in Fig. 6.1.

interactions destroy the uniformity of the fermion density. Therefore the bosons can take the phase I when $n_{\rm f}$ is relatively small but have to take the phase II when $n_{\rm f}$ becomes larger in order to lower the fermion energy. In addition, the transition line between the phase II and the phase III, the straight dashed line in the figures, is not dependent on the number of the fermions because Eq. (6.6) is the same in the phase II and III when $U_2^{\rm bf} = 0$.

Secondly, we consider the case of $U_2^{\rm bf} > 0$ ($u_0^{\rm bf} > u_{\uparrow\downarrow}^{\rm bf}$) [67]. In this case, we can obtain the phase diagram as shown in Fig. 6.2. By comparing Figs. 6.1 and 6.2, we can find that the parameter $U_2^{\rm bf}$ enlarges the area of the phase II. This reason can be understood as follows. The energetic profit by the increase $U_2^{\rm bf}$ ($\propto u_0^{\rm bf} - u_{\uparrow\downarrow}^{\rm bf}$) is larger when there is imbalance between the number of the spin-up and spin-down particles. This imbalance exists only in the phase II, which is therefore preferred to the phase I or III for finite $U_2^{\rm bf}$.

In the above calculation, the tight-binding approximation was employed. However, the approximation is not appropriate in some areas of the phase diagram. In particular, the condition $U(\alpha, \theta) \gg E_1(k_1)$ that the hopping parameter (6.8) can be used is not satisfied near the origin of the phase diagram. In these parameter areas it is necessary to solve the Mathieu equation given by Eqs. (6.3) numerically and (6.4) or to use the other approximation.

6.2 Bose-Fermi mixture with Bose-Fermi spin interaction

As shown in the following, we can regard the magnetization (spin) of the bosons as the effective magnetic field acting on the fermions in a Bose-Fermi mixture with a Bose-Fermi spin interaction. Since the spin current is induced by a spatial variation of the magnetic field, if the bosons have a spiral magnetization, it is expected to induce the spin current of the fermions in the mixture. Therefore, in this section, we analyze the SO coupled Bose-Fermi mixture with Bose-Fermi spin interaction[53].

6.2.1 Model and Method

We use the following Hamiltonian in the rotation frame:

$$H = H^{\mathrm{b}} + H^{\mathrm{f}} + H_{\mathrm{P}}^{\mathrm{bf}} + H_{\mathrm{S}}^{\mathrm{bf}}, \tag{6.10}$$

$$H^{\mathrm{b}} = \sum_{j=1}^{N^{\mathrm{b}}} \tilde{h}_{\mathrm{so}}^{\mathrm{b}}(j) + \frac{1}{2}\sum_{\alpha,\,\beta}\int d\boldsymbol{r}\; u_{\alpha\beta}^{\mathrm{bb}} n_{\alpha}^{\mathrm{b}}(\boldsymbol{r}) n_{\beta}^{\mathrm{b}}(\boldsymbol{r}), \tag{6.11}$$

$$H^{\mathrm{f}} = \sum_{j=1}^{N^{\mathrm{f}}} \tilde{h}^{\mathrm{f}}(j), \tag{6.12}$$

$$H_{\mathrm{p}}^{\mathrm{bf}} = u_{\mathrm{p}}^{\mathrm{bf}} \int d\boldsymbol{r}\; n^{\mathrm{b}}(\boldsymbol{r}) n^{\mathrm{f}}(\boldsymbol{r}), \tag{6.13}$$

$$H_{\mathrm{s}}^{\mathrm{bf}} = \frac{u_{\mathrm{s}}^{\mathrm{bf}}}{4} \int d\boldsymbol{r}\; \tilde{\psi}^{\mathrm{f}}(\boldsymbol{r})^{\dagger} \left[\tilde{\boldsymbol{m}}^{\mathrm{b}}(\boldsymbol{r})\cdot\boldsymbol{\sigma}\right] \tilde{\psi}^{\mathrm{f}}(\boldsymbol{r}). \tag{6.14}$$

The Bose Hamiltonian H^{b} is the same as Eq. (4.7). Equation (6.12) expresses the Fermi Hamiltonian in the rotation frame where $\tilde{h}^{\mathrm{f}} = (\boldsymbol{p} - \hbar\boldsymbol{k}_0\sigma_z)^2/(2m_{\mathrm{f}})$ is the kinetic energy of a fermion, where $\boldsymbol{k}_0 = (k_0, 0, 0)$ and we assume that the Zeeman effect on the fermions is the same as the effect on the bosons and $\delta = 0$. The Hamiltonians $H_{\mathrm{p}}^{\mathrm{bf}}$ and $H_{\mathrm{s}}^{\mathrm{bf}}$ are the Bose-Fermi particle and spin interaction Hamiltonians with interaction strengths $u_{\mathrm{p}}^{\mathrm{bf}}$ and $u_{\mathrm{s}}^{\mathrm{bf}}$, respectively, $\tilde{\psi}^{\mathrm{f}}(\boldsymbol{r}) = (\tilde{\psi}_{\uparrow}^{\mathrm{f}}(\boldsymbol{r}), \tilde{\psi}_{\downarrow}^{\mathrm{f}}(\boldsymbol{r}))^T$ is the annihilation operator of the fermions, and $\tilde{\boldsymbol{m}}^{\mathrm{b}}(\boldsymbol{r})$ is the magnetization density of the bosons [1)]. In what follows, $\tilde{\boldsymbol{m}}^{\mathrm{b}}(\boldsymbol{r})$ is treated as a classical field at zero temperature because of the macroscopic occupation of the bosons in a single-particle state.

As in the previous section, we assume that the bosons and fermions have the same mass, $m_{\mathrm{b}} = m_{\mathrm{f}} = m$, $\delta = 0$, and the number of fermions is much smaller than that of bosons, $N^{\mathrm{f}} \ll N^{\mathrm{b}}$. In addition, we choose the interaction strengths as $u_{\uparrow\uparrow}^{\mathrm{bb}} = u_{\downarrow\downarrow}^{\mathrm{bb}} = u_0^{\mathrm{bb}} > u_{\uparrow\downarrow}^{\mathrm{bb}}$ and $u_{\mathrm{p}}^{\mathrm{bf}} = u_{\mathrm{s}}^{\mathrm{bf}} = u_0^{\mathrm{bb}}$ and assume that they are weak enough in comparison with the system's typical energy scale. Under these assumptions, we employ the same variational wave function (4.9) for the bosons. From Eqs.

[1)] To derive Eq. (6.14), we use the ralarion $\psi^{\mathrm{f}}(\boldsymbol{r},t)^{\dagger}\left[\boldsymbol{m}^{\mathrm{b}}(\boldsymbol{r},t)\cdot\boldsymbol{\sigma}\right]\psi^{\mathrm{f}}(\boldsymbol{r},t) = \tilde{\psi}^{\mathrm{f}}(\boldsymbol{r})^{\dagger}\left[\tilde{\boldsymbol{m}}^{\mathrm{b}}(\boldsymbol{r})\cdot\boldsymbol{\sigma}\right]\tilde{\psi}^{\mathrm{f}}(\boldsymbol{r})$, where $\psi^{\mathrm{f}}(\boldsymbol{r},t) = U_2^{\dagger}(x,t)\tilde{\psi}^{\mathrm{f}}(\boldsymbol{r})$. It can be found from Eqs. (3.10), (4.18), and (4.19).

(4.9), (6.13), (6.14), and (6.12), the single-fermion Hamiltonian with the Bose-Fermi interactions can be written as

$$\tilde{h}^{\mathrm{f+bf}} = \frac{\hbar^2(i\nabla + \boldsymbol{k}_0\sigma_z)^2}{2m} + u_{\mathrm{p}}^{\mathrm{bf}} n^{\mathrm{b}}(x) + \frac{u_{\mathrm{s}}^{\mathrm{bf}}}{4}\tilde{\boldsymbol{m}}^{\mathrm{b}}(x)\cdot\boldsymbol{\sigma}, \tag{6.15}$$

where, from Eqs. (4.17) and (4.18), the number density and the magnetization of the bosons are given by

$$n^{\mathrm{b}}(x) = |\tilde{\psi}^{\mathrm{b}}(x)|^2 = n_{\mathrm{b}}\left[1 + 2\beta\sin(2\theta)\cos(2k_1x+\phi)\right], \tag{6.16}$$

$$\tilde{\boldsymbol{m}}^{\mathrm{b}}(x) = n_{\mathrm{b}}\begin{pmatrix} -\sin(2\theta) - 2\beta\cos(2k_1x+\phi) \\ 2\beta\cos(2\theta)\sin(2k_1x+\phi) \\ \cos(2\theta)\sqrt{1-4\beta^2} \end{pmatrix}^T. \tag{6.17}$$

Equation (6.15) shows that the bosons produce the effective potential $u_{\mathrm{p}}^{\mathrm{bf}} n^{\mathrm{b}}(x)$ and the effective magnetic field $u_{\mathrm{s}}^{\mathrm{bf}}\tilde{\boldsymbol{m}}^{\mathrm{b}}(x)/4$ for the fermions.

In the followings, we consider the single-fermion energy for two cases, $\beta = 0$ and $\beta > 0$. When $\beta = 0$, both the Bose density and the Bose magnetization density are uniform and the single-fermion Hamiltonian can be written as

$$\tilde{h}^{\mathrm{f+bf}}_{\beta=0} = \frac{(\boldsymbol{p} - \hbar\boldsymbol{k}_0\sigma_z)^2}{2m} + U_{\mathrm{p}}^{\mathrm{bf}} - U_{\mathrm{s}}^{\mathrm{bf}}\sin(2\theta)\sigma_x + U_{\mathrm{s}}^{\mathrm{bf}}\cos(2\theta)\sigma_z, \tag{6.18}$$

where $U_{\mathrm{p}}^{\mathrm{bf}} = n^{\mathrm{b}}u_{\mathrm{p}}^{\mathrm{bf}}$ and $U_{\mathrm{s}}^{\mathrm{bf}} = n^{\mathrm{b}}u_{\mathrm{s}}^{\mathrm{bf}}/4$. Since this single-particle Hamiltonian has the same from as Eq. (5.1), we can obtain the following single-fermion energy similar to Eq. (5.2):

$$\epsilon^{\mathrm{f+bf}}_{\beta=0,\pm}(\boldsymbol{q}) = \frac{\hbar^2\boldsymbol{q}^2}{2m} + E_0 + U_{\mathrm{p}}^{\mathrm{bf}} \pm \left[\left(\frac{\hbar^2 k_0 q_x}{m} - U_{\mathrm{s}}^{\mathrm{bf}}\cos(2\theta)\right)^2 + \left(U_{\mathrm{s}}^{\mathrm{bf}}\sin(2\theta)\right)^2\right]^{\frac{1}{2}}. \tag{6.19}$$

When $\beta > 0$, on the other hand, since both the density and the magnetization of the bosons have a spatial variation, the single-fermion energy can not be calculated exactly. We therefore focus on a situation where the single-fermion energy can be easily calculated in an approximate way. To find the condition for the approximation, we first remind Eq. (4.15) that the variational parameter of the bosons without the fermions:

$$k_1 = \begin{cases} k_0\sqrt{1 - \left[\dfrac{\hbar\Omega}{4F(\beta)}\right]^2} & (\hbar\Omega \le 4F(\beta)) \\ 0 & (\hbar\Omega > 4F(\beta)) \end{cases}, \tag{6.20}$$

where $F(\beta) = \epsilon_{\boldsymbol{k}_0} + [(6\beta^2-1)u_0^{\mathrm{bb}} + (1-2\beta^2)u_{\uparrow\downarrow}^{\mathrm{bb}}]/4$. This relation shows that $k_1 \sim k_0$ when $\hbar^2\Omega^2 \ll [4F(\beta)]^2$. In the laboratory frame, since the Bose magnetization is

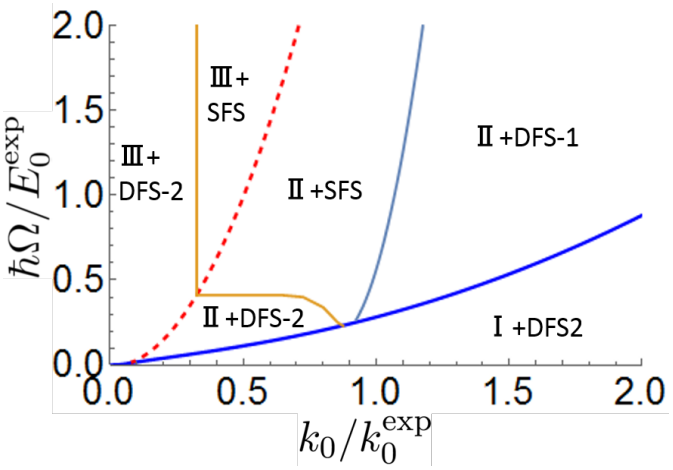

Figure 6.3: Ground-state phase diagram of the Bose-Fermi mixture with Bose-Fermi spin interaction at zero temperature. The parameters are $n_{\rm b} = 10^3\mu{\rm m}^{-3}$, $n_{\rm f} = 10\ \mu{\rm m}^{-3}$, $u_{\rm p}^{\rm bf} = u_{\rm s}^{\rm bf} = u_0^{\rm bb} = 4\pi\hbar^2/m \times 100a_B$, $u_{\uparrow\downarrow}^{\rm bb}/u_0^{\rm bb} \simeq 0.9976$, $m = 1.45 \times 10^{-25}$ kg, $a_{\rm B}$ is the Bohr radius, and $k_0^{\rm exp} = 2\pi\sin(\pi/4)/(804.1){\rm nm}^{-1} \simeq 5.5\mu{\rm m}^{-1}$ and $E_0^{\rm exp} = (\hbar k_0^{\rm exp})^2/(2m)$ are experimental normalized parameters ($k_0^{\rm exp}/q_{\rm F}^0 \sim 0.66$, where $q_{\rm F}^0$ is the Fermi wave number of the Fermi system without the Bose-Fermi spin interaction).

given by Eq. (4.18), Eqs. (6.16) and (4.18) with the relation $\cos(2\theta) = k_1/k_0$ indicates that the density and the magnetization of the bosons have a spatial variation unless $k_1 = k_0$. From these facts, in the laboratory frame, it is obvious that the fermions favor $k_1 = k_0$ to $k_1 < k_0$, because, in the latter case, the potential and the magnetic field have a spatial variation and unfavorable for the fermions. Therefore, we focus on the situation that $\hbar^2\Omega^2 \ll [4F(\beta)]^2$ and assume $k_1 \sim k_0$ and $\theta = 0$ for the case of $\beta > 0$ in what follows. Then the density and the magnetization of the bosons are given by $n_{\beta>0}^{\rm b} \simeq n^{\rm b}$ and

$$\boldsymbol{m}_{\beta>0}^{\rm b}(t) \simeq n^{\rm b}\left(-2\beta\cos(2k_0x+\phi), 2\beta\sin(2k_0x+\phi), \sqrt{1-4\beta^2}\right),$$

respectively, and the single-fermion energy is calculated in the following simple form:

$$\epsilon_{\beta>0,\pm}^{\rm f+bf}(\boldsymbol{q}) = \epsilon_{\boldsymbol{q}} + U_{\rm p}^{\rm bf} \pm U_{\rm s}^{\rm bf}. \tag{6.21}$$

6.2.2 Ground-state phase diagram

From Eqs. (6.19), (6.21), and (4.10), the total energy is provided as a function of the variational parameters. By minimizing the total energy with respect to k_1, θ, and β, we obtain the ground state phase diagram of the Bose-Fermi mixture as shown in Fig. 6.3. In the figure, roman numerals I-III express the phases of the bosons

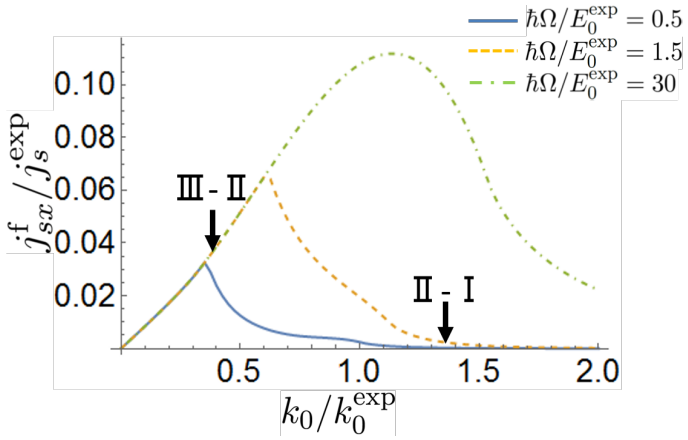

Figure 6.4: Spin current of the fermions in the Bose-Fermi mixture for $\Omega/E_0^{\rm exp} = 0.5$ (blue solid), 1.5 (orange dashed), and 30 (green dot-dashed). The other parameters are the same as in Fig. 6.3. The indicated phase transition points are for $\Omega/E_0^{\rm exp} = 0.5$.

and SFS (single Fermi surface) and DFS (double Fermi surface) express the phases of the fermions indicated in Figs. 4.3 and 5.1.

We should comment on the influence of the fermions on the bosons. In our variational energy calculation, it is shown that the SO coupled bosons can have the same three phases even without the fermions and the introduction of the fermions only causes slight expansion of the areas of the phases I and II in Fig. 6.3. This is because the spatial variation of the Bose magnetization in the laboratory frame, which works as an effective magnetic field on the fermions, is smaller in the phase I than in the phase II and smaller in the phase II than in the phase III. However, since the spatial variation of the magnetization depends on k_0, the fermions hardly affect the I-III and II-III transitions as far as k_0 is small. On the other hand, when Ω is large, the I-II transition occurs at large k_0. However, since the spiral magnetization in the phase II becomes small near the I-II transition line as shown in Fig. 4.4, the fermions hardly affect the I-II transition. From these facts, we can conclude that the fermions have little influence on the Bose phase diagram in our parameter region.

6.2.3 Spin Current

Now we are ready to calculate the spin current of the fermions. By calculating in the same way as in Sec. 5.1.3, we can obtain the spin current in the laboratory frame as shown in Fig. 6.4, where we use the normalized parameter $j_s^{\rm exp} = \hbar k_0^{\rm exp} n_{\rm f}/m$. In Fig. 6.4, the spin current decreases after the III-II phase transition when k_0 increases. As we mentioned in Sec. 4.2, the magnitude of the spatial variation of the magnetization of the bosons, that is the effective magnetic field for the fermions,

is the maximum in the phase III and decreases with increasing k_0 in the phase II, and therefore the spin current begins to decrease as the system goes from the phase III to the phase II. If k_0 increases more, the bosons enter the phase I, where the magnetic field is almost uniform and creates a negligibly small spin current. Figure 6.4 also shows that, when Ω is large (dotted line), the spin current still exhibits a peak even without the phase transition of the bosons. This behavior is the same that we discussed in Sec. 5.1.3.

Chapter 7

Conclusion

We showed the ground state phase diagrams and the spin currents in the spin-orbit (SO) coupled cold atoms for three systems : Bose system, Fermi system, and Bose-Fermi mixture. As a result, our studies newly revealed the ground state of the SO coupled Bose-Fermi mixture and the experimental controllability of the spin currents.

Firstly, in Chaps. 2, we defined a spin current and investigated the conditions to induce the spin current. In addition, we reviewed the experimental methods to realize the artificial SO coupled cold atoms and showed the experimentally controllable parameters in Chap. 3. In Chaps. 4 and 5, we analyzed the ground states and spin currents in the artificial SO coupled Bose and Fermi systems. For these systems, the ground states had already been studied in the previous studies[4, 10, 11], but, the spin currents had not. Therefore, by showing the experimental parameter dependences of the spin currents, we clarified the controllability of the spin current in these systems. In particular, in the SO coupled Bose system, the spin current changes discontinuously and non-smoothly across the phase boundaries, while in the SO coupled Fermi system, the spin current changes continuously and smoothly even at the phase boundaries. In Chap. 6, we also analyzed the ground states and spin currents in the artificial SO coupled Bose-Fermi mixture. The ground states were calculated in the Bose-Fermi mixture with high density or low density of the atoms by using a variational method and some approximations such as tight-binding approximation. For the high density, the fermions have a large influence on the Bose system, while, for the low density, the fermions have little influence although the relative amounts of the bosons and the fermions are comparable in the two cases. In addition, we showed that the spin current of the fermions changes discontinuously and non-smoothly across the phase boundaries of the bosons.

The above results revealed the properties of the novel cold atom system, an SO coupled Bose-Fermi mixture, and the novel controllability of the atoms by the spin current. We hope that these studies will lead to the development of atomtronics and cold atoms in future.

Appendix A

Derivation of the equation (3.1)

To derive Eq. (3.1), we will analyze the system described by Raman coupled five states[68, 69]. As a first step, in Sec. A.1, we derive the effective two-level system from three-level system coupled by Raman lasers. By expanding this discussion, we derive Eq. (3.1) from five-level system coupled by Raman lasers in Sec. A.2.

A.1 Three-level system

Let us consider the three-level system as shown in Fig. A.1, where two lasers with frequency ω_1 and ω_2 couple the states between $|1\rangle$ and $|2\rangle$ and between $|2\rangle$ and $|3\rangle$ respectively and we define the energies of each state E_i $(i = 1, 2, 3)$ and detunes Δ and δ.

Assuming that laser field is given by

$$\boldsymbol{E}_L(t) = \frac{1}{2}\left[\boldsymbol{E}_{L1}e^{-i\omega_1 t} + \boldsymbol{E}_{L2}e^{-i\omega_2 t} + \text{c.c.}\right], \tag{A.1}$$

and the wave function of the three states can be written as

$$\Psi(t) = \begin{pmatrix}\Psi_1\\ \Psi_2\\ \Psi_3\end{pmatrix} = \begin{pmatrix}C_1(t)e^{-i\zeta_1(t)}\\ C_2(t)e^{-i\zeta_2(t)}\\ C_3(t)e^{-i\zeta_3(t)}\end{pmatrix},$$

the electric dipole transition matrix in the system is given by

$$\boldsymbol{d} = \begin{pmatrix}0 & \boldsymbol{d}_{12}^* & 0\\ \boldsymbol{d}_{12} & 0 & \boldsymbol{d}_{23}^*\\ 0 & \boldsymbol{d}_{23} & 0\end{pmatrix}.$$

Then, from Schrödinger equation $i\hbar\partial\Psi/\partial t = (H_0 + \boldsymbol{d}\cdot\boldsymbol{E}_L)\Psi$, we can obtain the differential equation for C_i written as

$$i\hbar\frac{\partial}{\partial t}\begin{pmatrix}C_1\\ C_2\\ C_3\end{pmatrix} = \begin{pmatrix}E_1 - \hbar\dot{\zeta}_1 & \boldsymbol{d}_{12}^*\cdot\boldsymbol{E}_L e^{i(\zeta_1-\zeta_2)} & 0\\ \boldsymbol{d}_{12}\cdot\boldsymbol{E}_L e^{-i(\zeta_1-\zeta_2)} & E_2 - \hbar\dot{\zeta}_2 & \boldsymbol{d}_{23}^*\cdot\boldsymbol{E}_L e^{i(\zeta_2-\zeta_3)}\\ 0 & \boldsymbol{d}_{23}\cdot\boldsymbol{E}_L e^{-i(\zeta_2-\zeta_3)} & E_3 - \hbar\dot{\zeta}_3\end{pmatrix}\begin{pmatrix}C_1\\ C_2\\ C_3\end{pmatrix}, \tag{A.2}$$

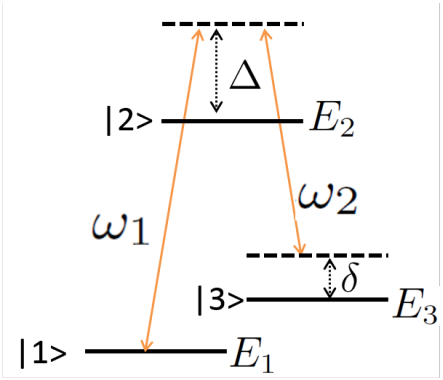

Figure A.1: Raman coupled three states $|1\rangle$, $|2\rangle$, and $|3\rangle$. The three states with the energies E_i $(i = 1, 2, 3)$ are coupled by the Raman lasers with frequencies ω_1 and ω_2, respectively, and Δ and δ are detunes.

where we use the relations $H_0\Psi_i = E_i\Psi_i (i = 1, 2, 3)$ $(E_1 < E_3 < E_2)$.

By substituting Eq. (A.1) into the off-diagonal components in Eq. (A.2), the part depending on e can be written as

$$\begin{aligned} \boldsymbol{E}_L(t)e^{i(\zeta_1-\zeta_2)} &= \frac{1}{2}\left[\boldsymbol{E}_{L1}e^{i(-\omega_1 t+\zeta_1-\zeta_2)} + \boldsymbol{E}_{L2}e^{i(-\omega_2 t+\zeta_1-\zeta_2)}\right. \\ &\quad \left. + \boldsymbol{E}^*_{L1}e^{i(\omega_1 t+\zeta_1-\zeta_2)} + \boldsymbol{E}^*_{L2}e^{i(\omega_2 t+\zeta_1-\zeta_2)}\right]. \end{aligned} \tag{A.3}$$

When $E_1 < E_2$, we can choose $\dot{\zeta}_2 = \dot{\zeta}_1 + \omega_1$. With this choise the exponents in Eq. (A.3) can be written as

$$\begin{aligned} -\omega_1 t + \zeta_1 - \zeta_2 = -2\omega_1 t, \quad -\omega_2 t + \zeta_1 - \zeta_2 = -(\omega_2 + \omega_1)t, \\ \omega_1 t + \zeta_1 - \zeta_2 = 0, \qquad \omega_2 t + \zeta_1 - \zeta_2 = (\omega_2 - \omega_1)t. \end{aligned}$$

If ω_1, ω_2, and $\omega_1 \pm \omega_2$ are larger enough than the typical time scale of the system, we can regard the rapidly oscillating terms as zero. As a result, the equation for C_1 in Eq. (A.2) can be approximately written as

$$i\frac{\partial C_1}{\partial t} \simeq \Delta_1 C_1 + \frac{1}{2}\Omega_1^* C_2,$$

where we define

$$\hbar\Delta_1 = E_1 - \hbar\dot{\zeta}_1, \quad \hbar\Omega_1 = \boldsymbol{d}_{12}\cdot\boldsymbol{E}_{L1}.$$

In the same way, with the choise $\dot{\zeta}_3 = \dot{\zeta}_2 + \omega_2$, we can obtain

$$\begin{aligned} i\frac{\partial C_2}{\partial t} &= \Delta_2 C_2 + \frac{1}{2}\left[\Omega_1 C_1 + \Omega_2^* C_3\right], \\ i\frac{\partial C_3}{\partial t} &= \Delta_3 C_3 + \frac{1}{2}\Omega_2 C_2, \end{aligned}$$

where we also define

$$\hbar\Delta_2 = E_2 - \hbar\dot{\zeta}_2 = E_2 - E_1 - \hbar\omega_1 + \hbar\Delta_1, \quad \hbar\Omega_2 = \boldsymbol{d}_{23}\cdot\boldsymbol{E}_{L2},$$
$$\hbar\Delta_3 = E_3 - \hbar\dot{\zeta}_3 = E_3 - E_1 - \hbar\omega_1 + \hbar\omega_2 + \hbar\Delta_1.$$

Therefore, when $\Delta_1 = 0$, we can obtain the effective differential equations for C_i written as

$$i\hbar\frac{\partial}{\partial t}\begin{pmatrix} C_1 \\ C_2 \\ C_3 \end{pmatrix} = \frac{\hbar}{2}\begin{pmatrix} 2\Delta_1 & \Omega_1^* & 0 \\ \Omega_1 & 2\Delta_2 & \Omega_2^* \\ 0 & \Omega_2 & 2\Delta_3 \end{pmatrix}\begin{pmatrix} C_1 \\ C_2 \\ C_3 \end{pmatrix} = \frac{\hbar}{2}\begin{pmatrix} 0 & \Omega_1^* & 0 \\ \Omega_1 & -2\Delta & \Omega_2^* \\ 0 & \Omega_2 & -2\delta \end{pmatrix}\begin{pmatrix} C_1 \\ C_2 \\ C_3 \end{pmatrix}, \quad \text{(A.4)}$$

where we use the detunes $\Delta = -\Delta_2$ and $\delta = -\Delta_3$ as shown in Fig. A.1.

Assuming a far-detuned Raman process in which $\Delta \gg \Omega_1$, Ω_2, δ, we can approximate $\partial C_2/\partial t \simeq 0$ and obtain the equation $C_2 = (\Omega_1 C_1 + \Omega_2^* C_3)/(2\Delta)$ from Eq. (A.4). At last, we can find the effective differential equation with two-level states

$$i\hbar\frac{\partial}{\partial t}\begin{pmatrix} C_1 \\ C_3 \end{pmatrix} = \hbar\begin{pmatrix} \dfrac{|\Omega_1|^2}{4\Delta} & \dfrac{\Omega_1^*\Omega_2^*}{4\Delta} \\ \dfrac{\Omega_1\Omega_2}{4\Delta} & \dfrac{|\Omega_2|^2}{4\Delta} + \delta \end{pmatrix}\begin{pmatrix} C_1 \\ C_3 \end{pmatrix}.$$

A.2 Five-level system

In this section, we expand the above discussion to the five-level system as shown in Fig. A.2, where two lasers coupled between the states and we redefine the energies of each state E_i and the detunes Δ, δ, and ϵ. Note that δ and ϵ correspond to the detune and the quadratic Zeeman shift in the experiment of the cold atom with the artificial gauge field [51].

Let us write the wave function of the five states as

$$\Psi(t) = \begin{pmatrix} \Psi_1 \\ \Psi_2 \\ \Psi_3 \\ \Psi_4 \\ \Psi_5 \end{pmatrix} = \begin{pmatrix} C_1(t)e^{-i\zeta_1(t)} \\ C_2(t)e^{-i\zeta_2(t)} \\ C_3(t)e^{-i\zeta_3(t)} \\ C_4(t)e^{-i\zeta_4(t)} \\ C_5(t)e^{-i\zeta_5(t)} \end{pmatrix}.$$

Then, we can obtain the differential equation for C_i given by

$$i\hbar\frac{\partial}{\partial t}\begin{pmatrix} C_1 \\ C_2 \\ C_3 \\ C_4 \\ C_5 \end{pmatrix} = \frac{\hbar}{2}\begin{pmatrix} 2\Delta_1 & \Omega_1^* & 0 & 0 & 0 \\ \Omega_1 & 2\Delta_2 & \Omega_2^* & 0 & 0 \\ 0 & \Omega_2 & 2\Delta_3 & \Omega_1^* & 0 \\ 0 & 0 & \Omega_1 & 2\Delta_4 & \Omega_2^* \\ 0 & 0 & 0 & \Omega_2^* & 2\Delta_5 \end{pmatrix}\begin{pmatrix} C_1 \\ C_2 \\ C_3 \\ C_4 \\ C_5 \end{pmatrix}, \quad \text{(A.5)}$$

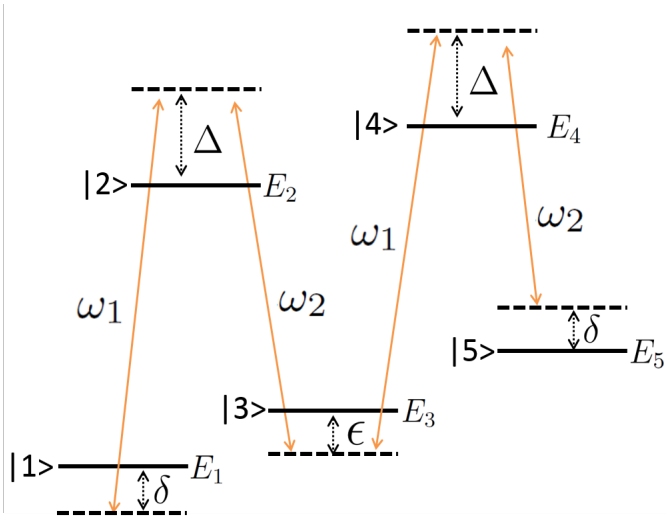

Figure A.2: Raman coupled five states $|1\rangle$, $|2\rangle$, $|3\rangle$, $|4\rangle$, and $|5\rangle$. The five states with the energies E_i $(i = 1, \ldots, 5)$ are coupled by the Raman lasers with frequencies ω_1 and ω_2, respectively, and Δ, δ, and ϵ are detunes.

where we define

$$\begin{aligned}
\hbar\Delta_1 &= 0, \\
\hbar\Delta_2 &= E_2 - E_1 - \hbar\omega_1 + \hbar\Delta_1 = -\Delta - \delta, \\
\hbar\Delta_3 &= E_3 - E_1 - \hbar\omega_1 + \hbar\omega_2 + \hbar\Delta_1 = -\delta + \epsilon, \\
\hbar\Delta_4 &= E_4 - E_3 - \hbar\omega_1 + \hbar\Delta_3 = -\Delta - \delta, \\
\hbar\Delta_5 &= E_5 - E_3 - \hbar\omega_1 + \hbar\omega_2 + \hbar\Delta_3 = -2\delta.
\end{aligned}$$

Assuming a far-detuned Raman process in which $\Delta \gg \Omega_1, \Omega_2, \delta, \epsilon$ and using $\partial C_2/\partial t \simeq 0$ and $\partial C_4/\partial t \simeq 0$, from Eq. (A.5), we can find the equations given by

$$\begin{aligned}
C_2 &= \frac{1}{\Delta + \delta}\left(\Omega_1 C_1 + \Omega_2^* C_3\right) \simeq \frac{1}{\Delta}\left(\Omega_1 C_1 + \Omega_2^* C_3\right), \\
C_4 &= \frac{1}{\Delta + \delta}\left(\Omega_1 C_3 + \Omega_2^* C_5\right) \simeq \frac{1}{\Delta}\left(\Omega_1 C_3 + \Omega_2^* C_5\right).
\end{aligned}$$

Therefore, substituting these equations into Eq. (A.5), we can obtain the effective differential equation with three-level states given by

$$i\hbar\frac{\partial}{\partial t}\begin{pmatrix} C_1 \\ C_3 \\ C_5 \end{pmatrix} = \hbar\begin{pmatrix} \frac{|\Omega_1|^2}{4\Delta} & \frac{\Omega_1^*\Omega_2^*}{4\Delta} & 0 \\ \frac{\Omega_1\Omega_2}{4\Delta} & \frac{|\Omega_1|^2 + |\Omega_2|^2}{4\Delta} + \epsilon - \delta & \frac{\Omega_1^*\Omega_2^*}{4\Delta} \\ 0 & \frac{\Omega_1\Omega_2}{4\Delta} & \frac{|\Omega_2|^2}{4\Delta} - 2\delta \end{pmatrix}\begin{pmatrix} C_1 \\ C_3 \\ C_5 \end{pmatrix}. \qquad \text{(A.6)}$$

By assuming $\Omega_1 = \Omega_2 = \Omega_R e^{ik_0 x}$, the effective Hamiltonian in Eq. (A.6) can be rewritten as

$$\bar{h} = \begin{pmatrix} \dfrac{\boldsymbol{p}^2}{2m} + \hbar\delta & \dfrac{\hbar\Omega}{2} e^{-2ik_0 x} & 0 \\ \dfrac{\hbar\Omega}{2} e^{2ik_0 x} & \dfrac{\boldsymbol{p}^2}{2m} + \epsilon & \dfrac{\hbar\Omega}{2} e^{-2ik_0 x} \\ 0 & \dfrac{\hbar\Omega}{2} e^{2ik_0 x} & \dfrac{\boldsymbol{p}^2}{2m} - \hbar\delta \end{pmatrix}, \tag{A.7}$$

where we define $\Omega = \Omega_R^2/(2\Delta)$ and use $|\Omega_R|^2/(4\Delta) + \epsilon \simeq \epsilon$ because $\Delta \gg \Omega_R, \delta, \epsilon$.

Finally, considering time dependence of Eq. (A.7) in the experiment, we derive Eq. (3.1). In the cold atom experiment, detune δ in Eq. (A.7) is given by $\delta = \Delta\omega - \omega_z$, where $\Delta\omega$ is the frequency difference between Raman lasers and ω_z is first-order Zeeman shift. By using time dependent unitary matrix given by

$$U(t) = \begin{pmatrix} e^{-i\Delta\omega t} & 0 & 0 \\ 0 & 1 & 0 \\ 0 & 0 & e^{i\Delta\omega t} \end{pmatrix},$$

Eq. (A.7) is converted into

$$\begin{aligned} h &= U^\dagger(t)\bar{h}U(t) + i\hbar U(t)\frac{\partial U^\dagger(t)}{\partial t} \\ &= \begin{pmatrix} \dfrac{\boldsymbol{p}^2}{2m} + \hbar\delta & \dfrac{\hbar\Omega}{2} e^{-i(2k_0 x - \Delta\omega t)} & 0 \\ \dfrac{\hbar\Omega}{2} e^{i(2k_0 x - \Delta\omega t)} & \dfrac{\boldsymbol{p}^2}{2m} + \epsilon & \dfrac{\hbar\Omega}{2} e^{-i(2k_0 x - \Delta\omega t)} \\ 0 & \dfrac{\hbar\Omega}{2} e^{i(2k_0 x - \Delta\omega t)} & \dfrac{\boldsymbol{p}^2}{2m} - \hbar\delta \end{pmatrix} + \begin{pmatrix} -\hbar\Delta\omega & 0 & 0 \\ 0 & 1 & 0 \\ 0 & 0 & \hbar\Delta\omega \end{pmatrix} \\ &= \begin{pmatrix} \dfrac{\boldsymbol{p}^2}{2m} - \hbar\omega_z & \dfrac{\hbar\Omega}{2} e^{-i\Theta} & 0 \\ \dfrac{\hbar\Omega}{2} e^{i\Theta} & \dfrac{\boldsymbol{p}^2}{2m} + \epsilon & \dfrac{\hbar\Omega}{2} e^{-i\Theta} \\ 0 & \dfrac{\hbar\Omega}{2} e^{i\Theta} & \dfrac{\boldsymbol{p}^2}{2m} + \hbar\omega_z \end{pmatrix}. \end{aligned}$$

where $\Theta = \Theta(x,t) = 2k_0 x - \Delta\omega t$. Therefore, we can derive Eq. (3.1).

Appendix B

Experimental method to tune the parameters

In the artificial spin-orbit (SO) coupled cold atom, the single-particle Hamiltonian is given by

$$\tilde{h} = \frac{\boldsymbol{p}^2}{2m} - \frac{\hbar k_0}{m} p_x \sigma_z + \frac{\hbar\Omega}{2}\sigma_x + \frac{\hbar\delta}{2}\sigma_z + E_0. \tag{B.1}$$

This equation has three tunable parameters k_0, Ω, and δ in the experiment. In the followings, we show the method to tune these parameters in the experiment [6, 58].

Method to tune Ω by the intensity of the laser

Intensity of the magnetic field in the x direction Ω is the effective amplitude of the Raman coupling given by $\Omega = \Omega_R^2/(2\Delta)$, where Ω_R is Raman coupling strength by two Raman lasers and Δ is the single-photon detune (see appendix A). Since Raman coupling strength Ω_R is proportional to the intensity of Raman laser field, Ω is tuned by the intensity of two Raman lasers.

Method to tune δ by the external magnetic field

Intensity of the magnetic field in the z direction δ is the detune given by $\delta = \Delta\omega - \omega_Z$ in the experiment, where $\Delta\omega$ is the frequency difference between Raman lasers and ω_Z is Zeeman shift. Since Zeeman shift is proportional to the intensity of the external magnetic field, δ is tuned by the external magnetic field. In addition, δ can also be tuned by controlling $\Delta\omega$ dynamically.

Method to tune k_0 by the wave number of the laser

Intensity of the SO coupling k_0 is the projected wave number of the Raman lasers. To understand this fact, we consider the momentum that an atom receives by Raman transition. When an atom is excited by the laser 1 with the laser field $\boldsymbol{E}_{L1}\cos(\boldsymbol{k}_1 \cdot \boldsymbol{r})$ and de-excited by laser 2 with $\boldsymbol{E}_{L2}\cos(\boldsymbol{k}_2 \cdot \boldsymbol{r})$ in the Raman

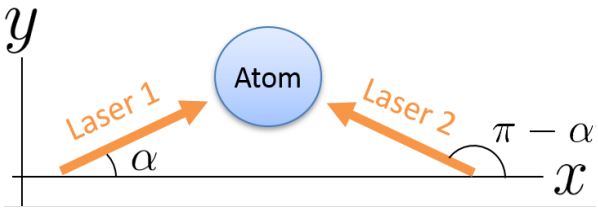

Figure B.1: Configuration of two Raman lasers and an atom.

transition, the atom receives the momentum $\hbar \boldsymbol{k}_1$ by the laser 1 and $-\hbar \boldsymbol{k}_2$ by the laser 2. Assuming $\boldsymbol{k}_1 = \boldsymbol{k}_2$ and the directions of the two Raman lasers are set as shown in Fig. B.1, the total momentum that the atom receives through the Raman transition can be written as $\hbar(\boldsymbol{k}_1 - \boldsymbol{k}_2) = (2\hbar|\boldsymbol{k}_1| \cos\alpha, 0, 0)$. Therefore, we can write as $k_0 = |\boldsymbol{k}_1| \cos\alpha$ and find that k_0 can be tuned by the wave number and the direction of Raman lasers. However, it is difficult to dynamically tune k_0 by using this method and another method is sugested as shown below.

Method to tune k_0 an δ by the intensity of the laser

We show the method to tune k_0 and δ by the intensity of the Raman lasers [58]. Let us consider the Raman laser with the time dependent intensity

$$\Omega = \Omega_0 + \tilde{\Omega} \cos(\omega t), \tag{B.2}$$

where Ω_0 and $\tilde{\Omega}$ are the average value and the modulation amplitude of the intensity and we assume $\hbar\omega$ is much larger than the typical energy scale in the system. Then, by using Eq. (B.2) and the unitary matrix given by

$$U_1(t) = \exp\left(-i\frac{\tilde{\Omega}\sin(\omega t)}{2\omega}\sigma_x\right),$$

Eq. (B.1) is converted into

$$\begin{aligned} h_{\text{eff}} &= U_1^\dagger \tilde{h} U_1 - i\hbar U_1^\dagger \frac{dU_1}{dt} \\ &= \frac{\boldsymbol{p}^2}{2m} + E_0 + \frac{\hbar\Omega_0}{2}\sigma_x \\ &\quad + \left(\frac{\hbar\delta}{2} - \frac{\hbar k_0 p_x}{m}\right)\left\{\cos\left[\frac{\tilde{\Omega}}{\omega}\sin(\omega t)\right]\sigma_z + \sin\left[\frac{\tilde{\Omega}}{\omega}\sin(\omega t)\right]\sigma_y\right\}. \end{aligned} \tag{B.3}$$

Using the standard Bessel function relation

$$\exp\left[i\left(\frac{\tilde{\Omega}}{\omega}\right)\sin(\omega t)\right] = \sum_n J_n\left(\frac{\tilde{\Omega}}{\omega}\right) e^{in\omega t},$$

where

$$J_n(x) = \sum_{m=0}^{\infty} \frac{(-1)^m}{m!\Gamma(m+n+1)} \left(\frac{x}{2}\right)^{2m+n}$$

is the nth Bessel function of the first kind, Eq. (B.3) can be approximately rewritten as

$$\begin{aligned} h_{\text{eff}} &\simeq \frac{\boldsymbol{p}^2}{2m} + \frac{\hbar\Omega_0}{2}\sigma_x + \left(\frac{\hbar\delta}{2} - \frac{\hbar k_0 p_x}{m}\right) J_0\left(\frac{\tilde{\Omega}}{\omega}\right)\sigma_z \\ &= \frac{\boldsymbol{p}^2}{2m} + \frac{\hbar\Omega_0}{2}\sigma_x + \left(\frac{\hbar\delta_{\text{eff}}}{2} - \gamma_{\text{eff}}\, p_x\right)\sigma_z, \end{aligned}$$

where we define the effective detune and intensity of the SO coupling

$$\delta_{\text{eff}} = \delta J_0\left(\frac{\tilde{\Omega}}{\omega}\right), \quad \gamma_{\text{eff}} = \frac{\hbar k_0}{m} J_0\left(\frac{\tilde{\Omega}}{\omega}\right),$$

and ignored higher-order Bessel functions because $\tilde{\Omega} \ll \omega$. Since $J_0(x)$ is monotonically decreasing function when $x \ll 1$, we can tune the detune and intensity of the SO coupling by controlling $\tilde{\Omega}/\omega$.

Appendix C

Tight-binding approximation

By using tight-binding approximation (TBA), we derive Eq. (6.7). In Sec. C.1, we review the TBA in the spin-1/2 Fermi system [70] and, in Sec. C.2, show the method to derive the hopping parameter in TBA[65].

C.1 Tight-binding approximation

Let us consider the system with a spatially periodic potential

$$V(\boldsymbol{r}) = V(\boldsymbol{r} + \boldsymbol{R}),$$

where $\boldsymbol{R}$ is the position vector that characterizes the periodicity. Then, Schrödinger equation is given by

$$\left[-\frac{\hbar^2\nabla^2}{2m} + V(\boldsymbol{r})\right]\psi(\boldsymbol{r}) = \epsilon\psi(\boldsymbol{r}).$$

In this system, we can write the wave function as

$$\psi_{n,\boldsymbol{k}}(\boldsymbol{r}) = e^{i\boldsymbol{k}\cdot\boldsymbol{r}}u_{n,\boldsymbol{k}}(\boldsymbol{r}), \tag{C.1}$$

where n is the quantum number, $\boldsymbol{k}$ is the wave number, and we assume that $u_{n,\boldsymbol{k}}(\boldsymbol{r})$ has a spatially periodicity as

$$u_{n,\boldsymbol{k}}(\boldsymbol{r} + \boldsymbol{R}) = u_{n,\boldsymbol{k}}(\boldsymbol{r}).$$

Here, Eq. (C.1) satisfies the Bloch theorem:

$$\psi_{n,\boldsymbol{k}}(\boldsymbol{r} + \boldsymbol{R}) = e^{i\boldsymbol{k}\cdot(\boldsymbol{r}+\boldsymbol{R})}u_{n,\boldsymbol{k}}(\boldsymbol{r}) = e^{i\boldsymbol{k}\cdot\boldsymbol{R}}\psi_{n,\boldsymbol{k}}(\boldsymbol{r}).$$

When the periodic potential has periodic minima at the position $\boldsymbol{R_i}$ $(i = 1, 2, \cdots, N)$, Eq. (C.1) can be written as

$$\psi_{n,\boldsymbol{k}}(\boldsymbol{r}) \quad = \quad = \frac{1}{N}\sum_{\boldsymbol{i},\boldsymbol{k}'} e^{i(\boldsymbol{k}-\boldsymbol{k}')\cdot\boldsymbol{R_i}}\psi_{n,\boldsymbol{k}'}(\boldsymbol{r}) = \frac{1}{\sqrt{N}}\sum_{\boldsymbol{i}} e^{i\boldsymbol{k}\cdot\boldsymbol{R_i}}w_{n,\boldsymbol{k}}(\boldsymbol{r} - \boldsymbol{R_i}), \tag{C.2}$$

where we use the Wannier function given by

$$w_n(\boldsymbol{r}-\boldsymbol{R_i}) = \frac{1}{\sqrt{N}}\sum_{\boldsymbol{k}}{}' e^{-i\boldsymbol{k}\cdot\boldsymbol{R_i}}\psi_{n,\boldsymbol{k}}(\boldsymbol{r}) = \frac{1}{\sqrt{N}}\sum_{\boldsymbol{k}}{}' e^{i\boldsymbol{k}\cdot(\boldsymbol{r}-\boldsymbol{R_i})}u_{n,\boldsymbol{k}}(\boldsymbol{r}), \tag{C.3}$$

and the summation $\sum'_{\boldsymbol{k}}$ is carried out over $\boldsymbol{k}$ inside the first Brillouin zone.

In the following, we consider the spin-1/2 Fermi system with a lattice potential and interaction. The Hamiltonian is given by

$$\begin{aligned} H &= H_{\rm kin} + H_{\rm int}, \\ H_{\rm kin} &= \int d\boldsymbol{r}\left[\sum_{\sigma=\uparrow,\downarrow}\hat{\psi}^\dagger_\sigma(\boldsymbol{r})\left(\frac{-\hbar^2\nabla^2}{2m}+V_{\rm lat}(\boldsymbol{r})\right)\hat{\psi}_\sigma(\boldsymbol{r})\right], \\ H_{\rm int} &= g\int d\boldsymbol{r}\left[\hat{\psi}^\dagger_\uparrow(\boldsymbol{r})\hat{\psi}^\dagger_\downarrow(\boldsymbol{r})\hat{\psi}_\downarrow(\boldsymbol{r})\hat{\psi}_\uparrow(\boldsymbol{r})\right], \end{aligned} \tag{C.4}$$

where $\hat{\psi}_\sigma(\boldsymbol{r})$ is the field operator with spin σ, $V_{\rm lat}(\boldsymbol{r})$ is the lattice potential with the minima $\boldsymbol{R}_i$, and g is the strength of the interaction. By using Eq. (C.2), we can write $\hat{\psi}_\sigma(\boldsymbol{r})$ as

$$\hat{\psi}_\sigma(\boldsymbol{r}) = \sum_{n,\boldsymbol{k}}\hat{a}'_{\sigma,n,\boldsymbol{k}}\psi_{\sigma,\boldsymbol{k}}(\boldsymbol{r}) = \sum_{n,\boldsymbol{i}}\hat{a}_{\sigma,n,\boldsymbol{i}}w_n(\boldsymbol{r}-\boldsymbol{R_i}),$$

where $\hat{a}'_{\sigma,n,\boldsymbol{k}}$ is annihilation operator and we use

$$\hat{a}_{\sigma,n,\boldsymbol{i}} = \frac{1}{\sqrt{N}}\sum_{\boldsymbol{k}} e^{i\boldsymbol{k}\cdot\boldsymbol{R_i}}\hat{a}'_{\sigma,n,\boldsymbol{k}}. \tag{C.5}$$

By assuming only the lowest energy band is dominant in the system, we can omit the band index n and the field operator can be written as

$$\hat{\psi}_\sigma(\boldsymbol{r}) \simeq \sum_{\boldsymbol{i}}\hat{a}_{\sigma,\boldsymbol{i}}w(\boldsymbol{r}-\boldsymbol{R_i}).$$

From this equation, Eq. (C.4) can be rewritten as

$$H_{\rm kin} = \sum_{\sigma,\boldsymbol{i},\boldsymbol{j}} J_{\boldsymbol{i},\boldsymbol{j}}\hat{a}^\dagger_{\sigma,\boldsymbol{i}}\hat{a}_{\sigma,\boldsymbol{j}}, \quad H_{\rm int} = U\sum_{\boldsymbol{i}}\hat{a}^\dagger_{\uparrow,\boldsymbol{i}}\hat{a}^\dagger_{\downarrow,\boldsymbol{i}}\hat{a}_{\downarrow,\boldsymbol{i}}\hat{a}_{\uparrow,\boldsymbol{i}}, \tag{C.6}$$

where

$$J_{\boldsymbol{i},\boldsymbol{j}} = \int d\boldsymbol{r}\left[w(\boldsymbol{r}-\boldsymbol{R_i})\left(\frac{-\hbar^2\nabla^2}{2m}+V_{\rm lat}(\boldsymbol{r})\right)w(\boldsymbol{r}-\boldsymbol{R_j})\right] \tag{C.7}$$

is the hopping parameter and

$$U = g\int d\boldsymbol{r}w^4(\boldsymbol{r}-\boldsymbol{R_i})$$

is the on-site parameter. Equation (C.6) is TBA Hamiltonian.

Since the single-particle Hamiltonian is given by Eq. (6.5) in our thesis, the Hamiltonian corresponding to Eq. (C.4) can be written as

$$H' = \int d\boldsymbol{r} \left[\sum_{\sigma=\uparrow,\downarrow} \hat{\psi}^\dagger_\sigma(\boldsymbol{r}) \left(\frac{-\hbar^2\nabla^2}{2m} + U_1^{\mathrm{bf}} + \sigma\alpha U_2^{\mathrm{bf}} \cos(2\theta) - |U(\alpha,\theta)| + V'_{\mathrm{lat}}(x) \right) \hat{\psi}_\sigma(\boldsymbol{r}) \right], \tag{C.8}$$

where $V'_{\mathrm{lat}}(x)$ is given by

$$V'_{\mathrm{lat}}(x) = \begin{cases} 2U(\alpha,\theta)\cos^2(k_1 x + \phi/2) & (U(\alpha,\theta) > 0) \\ -2U(\alpha,\theta)\sin^2(k_1 x + \phi/2) & (U(\alpha,\theta) < 0) \end{cases}. \tag{C.9}$$

By using Eq. (C.8) and TBA, we can find the TBA Hamiltonian corresponding to Eq. (C.6), however, the concrete form of the hopping parameter is not provided. Therefore, in the next section, we show the method to derive the approximate hopping parameter (6.8).

C.2 Hopping parameter

Calculating the band width of the lowest energy band by two methods, we show the approximate expression of the hopping parameter J. Firstly, we will calculate the band width from the TBA Hamiltonian. If the particles interact only with the particles at the nearest-neighbor site, the Hamiltonian is given by

$$H_{\mathrm{kin}} = J \sum_{\sigma,\boldsymbol{i}} (\hat{a}^\dagger_{\sigma,\boldsymbol{i}} \hat{a}_{\sigma,\boldsymbol{i}+1} + \hat{a}^\dagger_{\sigma,\boldsymbol{i}+1} \hat{a}_{\sigma,\boldsymbol{i}}), \tag{C.10}$$

where we assume that the hopping parameter does not depend on the site i ($J_{i,i+1} = J$). By using Eq. (C.5), we can find that

$$\hat{a}^\dagger_{\sigma,\boldsymbol{i}} \hat{a}_{\sigma,\boldsymbol{i}+1} = \frac{1}{N} \sum_{\boldsymbol{k},\boldsymbol{k}',\boldsymbol{d}} e^{-i(\boldsymbol{k}-\boldsymbol{k}')\cdot\boldsymbol{R_i}} \hat{a}^\dagger_{\sigma,\boldsymbol{k}} \hat{a}_{\sigma,\boldsymbol{k}'} e^{i\boldsymbol{k}'\cdot\boldsymbol{d}} = \frac{1}{N} \sum_{\boldsymbol{k},\boldsymbol{d}} \hat{a}^\dagger_{\sigma,\boldsymbol{k}} \hat{a}_{\sigma,\boldsymbol{k}} e^{i\boldsymbol{k}\cdot\boldsymbol{d}},$$

where $\boldsymbol{d}$ is the lattice vector and we use the relation $\boldsymbol{R_{i+1}} = \boldsymbol{R_i} + \boldsymbol{d}$. As a result, Eq. (C.10) can be rewritten as

$$\begin{aligned} H_{\mathrm{kin}} &= J \sum_{\sigma,\boldsymbol{i}} \left[\left(\frac{1}{N} \sum_{\boldsymbol{k},\boldsymbol{d}} \hat{a}^\dagger_{\sigma,\boldsymbol{k}} \hat{a}_{\sigma,\boldsymbol{k}} e^{i\boldsymbol{k}\cdot\boldsymbol{d}} \right) + \left(\frac{1}{N} \sum_{\boldsymbol{k},\boldsymbol{d}} \hat{a}^\dagger_{\sigma,\boldsymbol{k}} \hat{a}_{\sigma,\boldsymbol{k}} e^{-i\boldsymbol{k}\cdot\boldsymbol{d}} \right) \right] \\ &= \sum_{\sigma,\boldsymbol{k}} \left[\left\{ \sum_{\boldsymbol{d}} 2J\cos(\boldsymbol{k}\cdot\boldsymbol{d}) \right\} \hat{a}^\dagger_{\sigma,\boldsymbol{k}} \hat{a}_{\sigma,\boldsymbol{k}} \right]. \end{aligned}$$

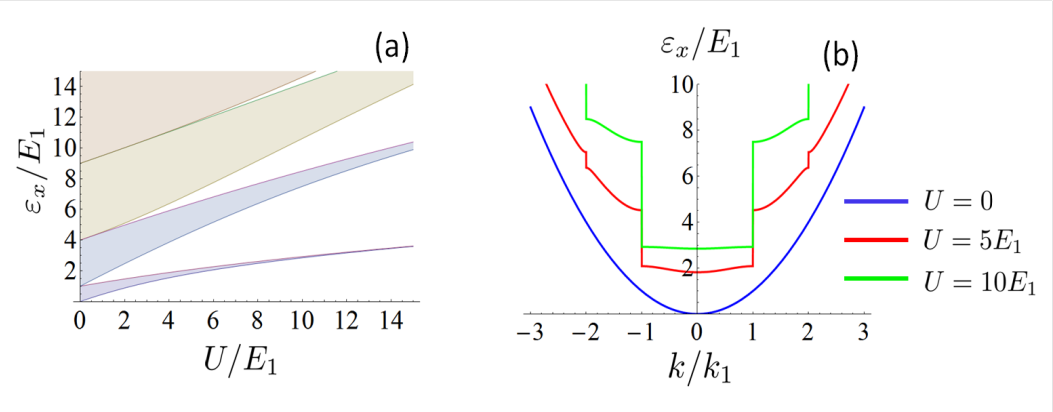

Figure C.1: (a) Eigen energy ε_x and (b) band structure. The band gaps increase with increasing U.

From this equation, we can find that the eigen energy is given by $\sum_{\boldsymbol{d}} 2J\cos(\boldsymbol{k}\cdot\boldsymbol{d})$ and the band width is $4J$.

Secondly, we will calculate the band width from the Mathieu equation. From Eq. (C.8), Schrödinger equation for the the wave function depending on x can be written as

$$\left[-\frac{\hbar^2}{2m}\left(\frac{\partial^2}{\partial x^2}\right) + U\cos^2(k_1 x + \frac{\phi}{2})\right]\psi^{\mathrm{f}}(x) = \varepsilon_x\psi^{\mathrm{f}}(x), \tag{C.11}$$

where $U = 2|U(\alpha,\theta)|$ and ε_x includes all the extra constant terms. When we define that $E_1 = E_1(k_1) = \hbar^2 k_1^2/(2m)$, $q = U/4E_1$, $\lambda = \varepsilon_x/E_1 - 2q$, $z = k_1 x + \phi/2$, and $\Psi(z) = \psi^{\mathrm{f}}(k_1 x + \phi/2)$, Eq. (C.11) can be rewritten as

$$\frac{d^2\Psi(z)}{dz^2} + \{\lambda - 2q\cos(2z)\}\,\Psi(z) = 0.$$

This equation is known as the one-dimentional Mathieu equation. This Mathieu equation can be solved for λ numerically and we can find the eigen-energy ε_x as shown in Fig. C.1(a). In addition, Fig. C.1(b) shows the band structute. It is known that, in the limit $q \to \infty$ ($U \gg E_1$), the width of the lowest energy band is given by [71]

$$\Delta\lambda = 2^5\sqrt{\frac{2}{\pi}}q^{\frac{3}{4}}e^{-4\sqrt{q}}. \tag{C.12}$$

Therefore, the band width of the minimum energy band is given by

$$\Delta\varepsilon_x = E_1\Delta\lambda = E_1 2^5\sqrt{\frac{2}{\pi}}\left(\frac{U}{4E_1}\right)^{3/4}e^{-4\sqrt{U/4E_1}} = \frac{16E_1}{\sqrt{\pi}}\left(\frac{U}{E_1}\right)^{3/4}e^{-2\sqrt{U/E_1}},$$

In conclusion, from Eqs. (C.11) and (C.13), we can find $4J = \Delta\varepsilon_x$ in the limit $q \to \infty (U \gg E_1)$ obtain the following hopping parameter :

$$J(k_1, \alpha, \theta) = \frac{\Delta\varepsilon_x}{4} = \frac{4E_1(k_1)}{\sqrt{\pi}} \left(\frac{2|U(\alpha,\theta)|}{E_1(k_1)} \right)^{\frac{3}{4}} \exp\left[-2 \left(\frac{2|U(\alpha,\theta)|}{E_1(k_1)} \right)^{\frac{1}{2}} \right].$$

Acknowledgments

I would like to show my greatest appreciation to Professor Hiroyuki Mori for his invaluable supports of my Ph.D study. I am deeply grateful to Associate Professor Emiko Arahata and Associate Professor Kazumasa Hattori for her and his fruitful advices. I would like to appreciate all the former and present members of the condensed matter theory group in Tokyo metropolitan university, especially Mr. Somei Suga, Dr. Hideo Kawaguchi, Mr. Yosuke Ono, Mr. Rei Hatsuda, Mr. Kenta Shiina, and Mr. Kota Tsuchikawa for valuable discussions. I was financially supported by JSPS KAKENHI Grant Number JP 17J00717. Finally, special thanks to my family for their supports and understanding.

References

[1] H. Feshbach, "Unified theory of nuclear reactions", Ann. Phys. **19**, 287 (1962).

[2] T. Köhler, K. Goral, and P. S. Julienne, "Production of cold molecules via magnetically tunable Feshbach resonances", Rev. Mod. Phys. **78**, 1311 (2006).

[3] Y.-J. Lin, K. Jiménez-García, and I. B. Spielman, "Spin-orbit-coupled Bose-Einstein condensates", Nature **471**, 83-86 (2011).

[4] P. Wang, Z. Yu, Z. Fu, J. Miao, L. Huang, S. Chai, H. Zhai, and J. Zhang, "Spin-Orbit Coupled Degenerate Fermi Gases", Phys. Rev. Lett. **109**, 095301 (2012).

[5] L. W. Cheuk, A. T. Sommer, Z. Hadzibabic, T. Yefsah, W. S. Bakr, and M. W. Zwierlein, "Spin-Injection Spectroscopy of a Spin-Orbit Coupled Fermi Gas", Phys. Rev. Lett. **109**, 095302 (2012).

[6] Y. Zhang, M. E. Mossman, T. Busch, P. Engels, and C. Zhang, "Properties of spin-orbit coupled Bose-Einstein condensates", Front. Phys. **11**, 118103 (2016).

[7] T. D. Stanescu, B. Anderson, and V. Galitski, "Spin-orbit coupled Bose-Einstein condensates", Phys. Rev. A **78**, 023616 (2008).

[8] C. Wang, C. Gao, C.-M. Jian, and H. Zhai, "Spin-Orbit Coupled Spinor Bose-Einstein Condensates", Phys. Rev. Lett. **105**, 160403 (2010).

[9] T.-L. Ho and S. Zhang, "Bose-Einstein Condensates with Spin-Orbit Interaction", Phys. Rev. Lett. **107**, 150403 (2011).

[10] Y. Li, L. P. Pitaevskii, and S. Stringari, "Quantum Tricriticality and Phase Transitions in Spin-Orbit Coupled Bose-Einstein Condensates", Phys. Rev. Lett. **108**, 225301 (2012).

[11] G. I. Martone, Y. Li, L. P. Pitaevskii, and S. Stringari, "Anisotropic dynamics of a spin-orbit-coupled Bose-Einstein condensate", Phys. Rev. A **86**, 063621 (2012).

[12] M. C. Beeler, R. A. Williams, K. Jiménez-García, L. J. LeBlanc, A. R. Perry, and I. B. Spielman, "The spin Hall effect in a quantum gas", Nature **498**, 201 (2013).

[13] Y. Li, G. I. Martone, L. P. Pitaevskii, and S. Stringari, "Superstripes and the Excitation Spectrum of a Spin-Orbit-Coupled Bose-Einstein Condensate", Phys. Rev. Lett. **110**, 235302 (2013).

[14] X. Zhou, Y. Li, Z. Cai, and C. Wu, "Unconventional states of bosons with the synthetic spinorbit coupling", J. Phys. B **46**, 134001 (2013).

[15] W. Zheng, Z.-Q. Yu, X. Cui, and H. Zhai, "Properties of Bose Gases with Raman-Induced Spin-Orbit Coupling", J. Phys. B **46**, 134007 (2013).

[16] V. E. Lobanov, Y. V. Kartashov, and V. V. Konotop, "Fundamental, Multipole, and Half-Vortex Gap Solitons in Spin-Orbit Coupled Bose-Einstein Condensates", Phys. Rev. Lett. **112**, 180403 (2014).

[17] A. L. Fetter, "Vortex dynamics in spin-orbit-coupled Bose-Einstein condensates", Phys. Rev. A **89**, 023629 (2014).

[18] S.-C. Ji, J.-Y. Zhang, L. Zhang, Z.-D. Du, W. Zheng, Y.-J. Deng, H. Zhai, S. Chen, and J.-W. Pan, "Experimental determination of the finitetemperature phase diagram of a spinorbit coupled Bose gas", Nat. Phys. **10**, 314 (2014).

[19] Z. Wu, L. Zhang, W. Sun, X.-T. Xu, B.-Z. Wang, S.-C. Ji, Y. Deng, S. Chen, X.-J. Liu, J.-W. Pan, "Realization of two-dimensional spin-orbit coupling for Bose-Einstein condensates", Science **354**, 83 (2016).

[20] J.-R. Li, J. Lee, W. Huang, S. Burchesky, B. Shteynas, F. C. Top, A. O. Jamison, and W. Ketterle, "A stripe phase with supersolid properties in spinorbit-coupled BoseEinstein condensates", Nature **543**, 91 (2017).

[21] L. Han and C. A. R. Sá de Melo, "Evolution from BCS to BEC superfluidity in the presence of spin-orbit coupling", Phys. Rev. A **85**, 011606(R) (2012).

[22] R. Wei and E. J. Mueller, "Majorana fermions in one-dimensional spin-orbit-coupled Fermi gases", Phys. Rev. A **86**, 063604 (2012).

[23] Z. Fu, L. Huang, Z. Meng, P. Wang, X.-J. Liu, H. Pu, H. Hu, and J. Zhang, "Radio-frequency spectroscopy of a strongly interacting spin-orbit-coupled Fermi gas", Phys. Rev. A **87**, 053619 (2013).

[24] R. A. Williams, M. C. Beeler, L. J. LeBlanc, K. Jiménez-García, and I. B. Spielman, "Raman-Induced Interactions in a Single-Component Fermi Gas Near an s-Wave Feshbach Resonance", Phys. Rev. Lett. **111**, 095301 (2013).

[25] X.-J. Liu and H. Hu, "Topological Fulde-Ferrell superfluid in spin-orbit-coupled atomic Fermi gases", Phys. Rev. A **88**, 023622 (2013).

[26] C. Chen, "Inhomogeneous Topological Superfluidity in One-Dimensional Spin-Orbit-Coupled Fermi Gases", Phys. Rev. Lett. **111**, 235302 (2013).

[27] N. Q. Burdick, Y. Tang, and B. L. Lev, "Long-Lived Spin-Orbit-Coupled Degenerate Dipolar Fermi Gas", Phys. Rev. X **6**, 031022 (2016).

[28] A. G. Truscott, K. E. Strecker, W. I. McAlexander, G. B. Partridge, and R. G. Hulet, "Observation of Fermi Pressure in a Gas of Trapped Atoms", Science **291**, 2570 (2001).

[29] G. Modugno, G. Roati, F. Riboli, F. Ferlaino, R. J. Brecha, and M. Inguscio, "Collapse of a Degenerate Fermi Gas", Science **297**, 2240 (2002).

[30] Z. Hadzibabic, C. A. Stan, K. Dieckmann, S. Gupta, M.W. Zwierlein, A. Görlitz and W. Ketterle, "Two-Species Mixture of Quantum Degenerate Bose and Fermi Gases", Phys. Rev. Lett. **88**, 160401 (2002).

[31] J. Goldwin, S. Inouye, M. L. Olsen, B. Newman, B. D. DePaola, and D. S. Jin, "Measurement of the interaction strength in a Bose-Fermi mixture with ^{87}Rb and ^{40}K", Phys. Rev. A **70**, 021601(R) (2004).

[32] M. Lewenstein, L. Santos, M. A. Baranov and H. Fehrmann, "Atomic Bose-Fermi Mixtures in an Optical Lattice", Phys. Rev. Lett. **92**, 050401 (2004).

[33] K. Günter, T. Stöferle, H. Moritz, M. Köhl and T. Esslinger, "Bose-Fermi Mixtures in a Three-Dimensional Optical Lattice", Phys. Rev. Lett. **96**, 180402 (2006).

[34] J. M. McNamara, T. Jeltes, A. S. Tychkov, W. Hogervorst and W. Vassen, "Degenerate Bose-Fermi Mixture of Metastable Atoms", Phys. Rev. Lett. **97**, 080404 (2006).

[35] R. A. Pepino, J. Cooper, D. Z. Anderson, and M. J. Holland, "Atomtronic Circuits of Diodes and Transistors", Phys. Rev. Lett. **103**, 140405 (2009).

[36] I. Buluta and F. Nori, "Quantum Simulators", Science **326**, 109 (2009).

[37] M. Fuechsle, J. A. Miwa, S. Mahapatra, H. Ryu, S. Lee, O. Warschkow, L. C. Hollenberg, G. Klimeck, and M. Y. Simmons, "A single-atom transistor"', Nat. Nanotechnol. **7**, 242 (2012).

[38] L. Amico, G. Birkl, M. Boshier, and L. C. Kwek, "Focus on atomtronics-enabled quantum technologies", New J. Phys. **19**, 020201 (2017).

[39] S. A. Wolf, D. D. Awschalom, R. A. Buhrman, J. M. Daughton, S. von Molnár, M. L. Roukes, A. Y. Chtchelkanova, and D. M. Treger, "Spintronics: A Spin-Based Electronics Vision for the Future", Science **294**, 1488 (2001).

[40] I. Žutić, J. Fabian, and S. D. Sarma,, "Spintronics: Fundamentals and applications", Rev. Mod. Phys. **76**, 323 (2004).

[41] D. D. Awschalom and M. E. Flatte, "Challenges for semiconductor spintronics", Nature Phys. **3**, 153 (2007).

[42] L. Bogani and W. Wernsdorfer, "Molecular spintronics using single-molecule magnets", Nature Mat. **7**, 179 (2008).

[43] G. Tatara, *Supintoronikusuriron̄nokiso*(Basics of Spintronics) (Baifukan, 2009) [in Japanese].

[44] S. Kashiwaya, Y. Tanaka, N. Yoshida, and M. R. Beasley, "Spin current in ferromagnet-insulator-superconductor junctions", Phys. Rev. B **60**, 3572 (1999).

[45] S. Murakami, N. Nagaosa, and S. C. Zhang, "Dissipationless Quantum Spin Current at Room Temperature", Science **301**, 1348 (2003).

[46] Y. K. Kato, R. C. Myers, A. C. Gossard and D. D. Awschalom, "Observation of the Spin Hall Effect in Semiconductors", Science **306**, 1910 (2004).

[47] H. Katsura, N. Nagaosa, and A. V. Balatsky, "Spin Current and Magnetoelectric Effect in Noncollinear Magnets",Phys. Rev. Lett. **95**, 057205 (2005).

[48] E. B. Sonin, "Spin currents and spin superfluidity", Adv. Phys. **59**, 181 (2010).

[49] S. Maekawa, H. Adachi, K. Uchida, J. Ieda, and E. Saitoh, "Spin Current: Experimental and Theoretical Aspects", J. Phys. Soc. Jpn. **82**, 102002 (2013).

[50] S. Maekawa, S. O. Valenzuela, E. Saitoh, and T. Kimura, *Spin Current* (Oxford University Press, Oxford, 2012).

[51] Y.-J. Lin, R. L. Compton, A. R. Perry, W. D. Phillips, J. V. Porto, and I. B. Spielman, "Bose-Einstein condensate in a uniform light-induced vector Potential", Phys. Rev. Lett. **102**, 130401 (2009).

[52] R. Sakamoto, Y. Ono, R. Hatsuda, K. Shiina, E. Arahata, and H. Mori, "Analysis of Bose system in spin-orbit coupled Bose-Fermi mixture to induce a spin current of fermions", J. Phys. Conf. Ser. **969** 012014 (2018).

[53] R. Sakamoto, E. Arahata, and H. Mori, "Spin Current of Fermions Induced in SpinOrbit Coupled BoseFermi Mixture", J. Phys. Soc. Jpn. **87**, 074004 (2018).

[54] Y.-J. Lin, R. L. Compton, W. D. Phillips, J. V. Porto, and I. B. Spielman, "Synthetic magnetic fields for ultracold neutral atoms", Nature **462**, 628 (2009).

[55] Y.-J. Lin, R. L. Compton, K. Jiménez-García, J. V. Porto and I. B. Spielman, "A synthetic electric force acting on neutral atoms", Nature Phys. **7**, 531 (2010).

[56] C. L. Kane and E. J. Mele, "Z_2 Topological Order and the Quantum Spin Hall Effect", Phys. Rev. Lett. **95**, 146802 (2005).

[57] D. Hsieh,D. Qian, L. Wray, Y. Xia, Y. S. Hor, R. J. Cava and M. Z. Hasan, "A topological Dirac insulator in a quantum spin Hall phase", Nature **452**, 970 (2008).

[58] Y. Zhang, G. Chen, and C. Zhang, "Tunable Spin-orbit Coupling and Quantum Phase Transition in a Trapped Bose-Einstein Condensate", Sci. Rep. **3**, 1937 (2013).

[59] Y. A. Bychkov and E. I. Rashba, "Oscillatory effects and the magnetic susceptibility of carriers in inversion layers", J. Phys. C **17**, 6039 (1984).

[60] G. Dresselhaus, "Spin-orbit coupling effects in zinc blende structures", Phys. Rev. **100**, 580586 (1955).

[61] J. D. Koralek, C. P. Weber, J. Orenstein, B. A. Bernevig, Shou-Cheng Zhang, S. Mack, and D. D. Awschalom, "Emergence of the persistent spin helix in semiconductor quantum wells", Nature **458**, 610613 (2009).

[62] C. H. L. Quay, T. L. Hughes, J. A. Sulpizio, L. N. Pfeiffer, K.W. Baldwin, K.W.West, D. Goldhaber-Gordon, and R. de Picciotto, "Observation of a one-dimensional spin-orbit gap in a quantum wire", Nature Phys. **6**, 336339 (2010).

[63] A. L. Fetter, J. D. Walecka, *Quantum Theory of Many-Particle Systems* (McGraw-Hill, San Francisco, 1971).

[64] C. Pethick and H. Smith, *Bose-Einstein Condensation in Dilute Gases*, 2nd ed. (Cambridge University Press, Cambridge, England, 2008).

[65] I. Bloch, J. Dalibard, and W. Zwerger, Rev. Mod. Phys. **80**, 885 (2008).

[66] R. Sakamoto, Y. Ono, E. Arahata, and H. Mori, "Ground State of BoseFermi Mixture with SpinOrbit Coupling", J. Phys. Soc. Jpn. **85**, 064401 (2016).

[67] R. Sakamoto, Y. Ono, R. Hatsuda, K. Shiina, E. Arahata, and H. Mori, "Ground State of Bosons in BoseFermi Mixture with SpinOrbit Coupling", J. Phys. Soc. Jpn. **86**, 075003 (2017).

[68] B. W. Shore, *The Theory of Coherent Atomic Excitation* (Wiley, New York, 1990), Vol. 2.

[69] C. Gardiner and P. Zoller, *The Quantum World of Ultra-Cold Atoms and Light Book II: The Physics of Quantum-Optical Devices*, 1st ed. (Imperial College Press, London, 2015).

[70] N. W. Ashcroft and N. D. Mermin, *Solid State Physics*, (Holt, Rinehardt and Winston, New York, 1976).

[71] M. Abramowitz and I. A. Stegun, *Handbook of Mathematical Functions*, (New York, Dover, 1965).